

Targeting mitochondrial glycerol 3-phosphate
dehydrogenase and mitochondrial complex III in
PC-3 prostate cancer cells

Inaugural Dissertation
submitted to the
Faculty of Veterinary Medicine
in partial fulfillment of the requirements
for the PhD-Degree
of the Faculties of Veterinary Medicine and Medicine
of the Justus Liebig University Giessen

by
Di Paola, Floriana Jessica
of
Catania (Italy)

Giessen 2022

From the Institute of Veterinary Physiology and Biochemistry
Director / Chairman Prof. Dr. Rüdiger Gerstberger
of the Faculty of Veterinary Medicine or Medicine of the Justus Liebig University Giessen

First Supervisor and Committee Member: Prof. Sybille Mazurek
Second Supervisor and Committee Member: Prof. Thomas Linn
Committee Members: Prof. Martin Diener, Prof. Leoni Kunz-Schughard

Date of Doctoral Defense: 19.01.2022

Index

1	Summary	1
1.1	English version	1
1.2	German version	3
2	Introduction	5
2.1	Metabolism of cancer cells	5
2.1.1	Glycolysis	5
2.1.1.1	Pyruvate Kinase	7
2.1.2	Glutaminolysis	9
2.1.3	Regeneration of cytosolic NAD ⁺	11
2.1.3.1	Lactate dehydrogenase	12
2.1.3.2	The glycerol 3-phosphate shuttle	13
2.1.3.3	The malate-aspartate shuttle	13
2.1.4	The oxidative phosphorylation (OXPHOS)	14
2.1.4.1	The mitochondrial respiratory chain – Complex III	15
2.2	Reactive Oxygen Species	16
2.2.1	CIII as a source of ROS	17
2.2.2	ROS production by mG3PDH	18
2.2.3	Hypoxia	20
3	Aim of the study	23
4	Materials and Methods	24
4.1	Culture conditions and cell proliferation assays	24
4.2	Glycolytic and glutaminolytic conversion rates	25
4.2.1	Calculation of the metabolic conversion rates	26
4.3	Isoelectric focusing	26
4.3.1	Principle of the method	26
4.3.2	Carrying out the isoelectric focusing	27
4.3.3	Measurement of enzyme activities	28
4.3.4	Calculation of total (V _{max}) enzyme activity	30
4.3.5	Determination of the isoenzymes equipment	30
4.4	Protein quantification	30
4.5	Gel permeation	30
4.5.1	Principle of the method	30
4.5.2	Carrying out the gel permeation	31

4.6	Oxygen consumption and hydrogen peroxide production by high-resolution respirometry	31
4.6.1	Principle of the method.....	31
4.6.1.1	Oxygen consumption	31
4.6.1.2	Hydrogen peroxide production.....	31
4.6.2	Carrying out the oxygen consumption and hydrogen peroxide production measurements	32
4.7	Mass spectrometry	35
4.8	Statistical analysis.....	36
4.8.1	IC ₅₀ – IC ₉₀ – IC ₉₅ values	37
4.8.2	Metabolic conversion rates	37
4.8.3	Intracellular metabolites	38
5	Results	39
5.1	Targeting mitochondrial glycerol 3-phosphate dehydrogenase.....	39
5.1.1	Impact of iGP-1 on PC-3 cell proliferation	39
5.1.2	Impact of iGP-1 on glycolytic and glutaminolytic metabolic conversion rates of PC-3 cells	39
5.1.3	Impact of RH02211 on cell proliferation and metabolism of PC-3 cells	41
5.1.3.1	Impact of RH02211 on cell proliferation of PC-3 cells depending upon oxygen pressure and pyruvate concentration in the medium.....	41
5.1.3.2	Reversibility of RH02211-induced inhibition of PC-3 cell proliferation	42
5.1.3.3	Dose dependent impact of RH02211 on the glycolytic and glutaminolytic conversion rates in pyruvate starved PC-3 cells	43
5.1.3.4	Impact of pyruvate on the glycolytic and glutaminolytic conversion rates of PC-3 cells	44
5.1.3.5	Impact of RH02211 on the glycolytic and glutaminolytic conversion rates depending upon the pyruvate concentration in the medium	45
5.1.3.6	Impact of pyruvate and RH02211 on LDH, MDH and GOT isoenzymes as well as the glycolytic enzyme complex.....	47
5.1.3.7	Impact of RH02211 on the tetramer : dimer ratio of M2-PK in PC-3 cells	49
5.1.3.8	Impact of RH02211 on O ₂ consumption in pyruvate starved and pyruvate supplemented PC-3 cells	50
5.1.3.9	Impact of RH02211 on H ₂ O ₂ production in pyruvate starved and pyruvate supplemented PC-3 cells	50
5.1.3.10	Impact of RH02211 on intracellular metabolites	53
5.2	Targeting mitochondrial CIII in PC-3 prostate cancer cell.....	55
5.2.1.	Impact of mitochondrial complex III inhibitors on PC-3 cell proliferation in presence of 21% and 1.5% oxygen supply.....	55

5.2.2.	Impact of mitochondrial complex III inhibitors on glycolytic and glutaminolytic flux rates in PC-3 cells cultivated in presence of 21% and 1.5% O ₂	57
5.2.3.	Impact of hypoxia on LDH, MDH and GOT isoenzymes as well as the glycolytic enzyme complex.....	62
5.2.4.	Impact of complex III inhibitors on LDH, MDH and GOT isoenzymes as well as the glycolytic enzyme complex.....	63
5.2.5.	Impact of CIII inhibitors on H ₂ O ₂ production in PC-3 cells cultivated at 21% O ₂	64
5.2.6.	Impact of CIII inhibitors on O ₂ consumption in PC-3 cells cultivated at 21% O ₂	65
6	Discussion.....	69
6.1	Metabolism dependency upon cell density.....	69
6.2	Impact of hypoxia on the glycolytic enzyme complex as well as the LDH, MDH and GOT isoenzymes.....	71
6.3	Impact of pyruvate on cell metabolism.....	73
6.4	Impact of mG3PDH targeting on PC-3 prostate cancer cell proliferation and metabolism.....	77
6.5	Impact of mitochondrial CIII inhibitors on PC-3 prostate cancer cell proliferation and metabolism.....	87
7	Conclusions.....	100
8	Abbreviations.....	101
9	List of tables.....	103
10	List of figures.....	104
	References.....	106
	Acknowledgements.....	120

1 Summary

1.1 English version

Cancer is the second main cause of death worldwide. Reactive oxygen species (ROS) play a special role in tumor development and growth. The mitochondrial glycerol 3-phosphate dehydrogenase (mG3PDH) and the mitochondrial complex III (CIII) have a high proportion of cellular ROS production. Due to inadequate blood supply tumors very often are characterized by low oxygen pressure. ROS as well as the oxygen supply regulate the stability of the hypoxic inducing factor (HIF) which induces the expression of key glycolytic (iso)enzymes (i.e. lactate dehydrogenase A (LDHA), pyruvate kinase type M2 (M2-PK)) required for energy production, synthesis of building blocks and cancer cell proliferation. ROS have been shown to induce a dimerization as well as a reduction of M2-PK activity thereby diverting glucose flux towards the synthesis of cell building blocks. In tumor cells besides glycolysis, glutaminolysis is an important pathway to provide energy and metabolic precursors for cell building blocks which are both important in cells with high proliferation rate such as tumor cells. The aim of this study was to investigate the impact of targeting mG3PDH and mitochondrial CIII on cell proliferation and metabolism of PC-3 prostate cancer cells which are characterized by high mG3PDH activity.

The impact of mG3PDH and CIII inhibition on cell proliferation was investigated in presence of 21% O₂ which corresponds to the oxygen concentrations in the air and is used in most of the published cell culture studies as well as in presence of 1.5% O₂ which corresponds to the mean oxygen concentration in a variety of solid tumors. In order to simulate therapy over several days long-term incubation periods (96 hours) of PC-3 cells with the corresponding inhibitors were performed.

In the first part of the study two substances published as inhibitors of mG3PDH (iGP-1 and RH02211) were investigated. mG3PDH together with cytosolic glycerol 3-P dehydrogenase (cG3PDH) is involved in the transfer of hydrogen from cytosolic NADH + H⁺ produced within the cytosolic glyceraldehyde 3-P dehydrogenase (GAPDH) reaction into the mitochondrial electron transport chain in order to restore the cytosolic NAD⁺ for glycolysis. Both iGP-1 and RH02211 induced an inhibition of PC-3 cell proliferation. The RH02211-induced inhibition of cell proliferation was independent upon oxygen supply. The inhibitory effect of both inhibitors on PC-3 cell proliferation was weakened when pyruvate was supplemented into the cultivation medium of the cells suggesting that extracellular pyruvate is an escape mechanism for the inhibition of cell proliferation by both RH02211 and iGP-1. Pyruvate is the substrate via which the LDH oxidizes NADH + H⁺ to NAD⁺. A nutrient medium without supplementation of pyruvate is closer to the physiological pyruvate concentrations in the blood. When cultivated in pyruvate supplemented

medium PC-3 control cells shifted from production of pyruvate to consumption of extracellular pyruvate and glycolytic as well as glutaminolytic conversion rates decreased which points to a severe impact of extracellular pyruvate on the metabolism of the cells. In contrast to the first published description which showed a decrease of H_2O_2 production in pyruvate supplemented PC-3 cells treated for 15 minutes with 1-30 μM RH02211 in our experiments 16 μM RH02211 induced an increase of H_2O_2 production as well as an increase of oxygen consumption independent upon the pyruvate concentration in the medium. Although the H_2O_2 production rates increased together with the glycolytic conversion rates in pyruvate starved RH02211 treated PC-3 cells the tetramer : dimer ratio of M2-PK, the LDH isoenzyme equipment as well as the composition of the glycolytic enzymes were not impaired. In pyruvate supplemented cultivation medium RH02211 did not impair the glycolytic conversion rates. iGP-1 induced an increase of glycolysis and glutaminolysis in pyruvate starved PC-3 cells.

In the second part of the study three different commercially available CIII inhibitors (Antimycin A, Myxothiazol and S3QEL-2) that target CIII by different mode of actions were investigated. All three inhibitors induced a dose dependent inhibition of PC-3 cells proliferation in pyruvate starved medium. The inhibition of cell proliferation by CIII inhibition was weakened by hypoxia when Q_i site was inhibited (AA) but not when CIII Q_o was inhibited (Myx and S3QEL-2). Measurements of metabolic nutrients and products in the cell cultivation supernatants of the cells point to an activation of glycolysis by AA, Myx and S3QEL-2 independently upon oxygen supply. Glutaminolysis was downregulated in AA and Myx treated cells at both 21% and 1.5% O_2 as well as in S3QEL-2 treated cells at 1.5% O_2 but not at 21% O_2 . These results indicate that glucose became the main energetic source for PC-3 cell proliferation when CIII was inhibited. The increase in glycolysis in AA, Myx and S3QEL-2 treated cells was not linked with changes in the activity of the glycolytic enzymes as well as with changes in H_2O_2 production. Both AA and Myx strongly decreased PC-3 cell respiration. In contrast to the first published description which showed no impact of S3QEL-2 on respiration of HEK 293 cells treated for 3 hours with 34 μM S3QEL-2 in our experiments a slight but significant decrease in oxygen consumption was found in presence of 12 μM S3QEL-2. The weaker effect of S3QEL-2 on mitochondrial respiration compared to Myx may be an explanation for the significantly higher IC_{50} values of S3QEL-2 in comparison to Myx for the inhibition of PC-3 cell proliferation.

1.2 German version

Krebs ist weltweit die zweithäufigste Todesursache. Bei der Tumorentstehung und dem Tumorwachstum spielen reaktiven Sauerstoffspezies (ROS) eine besondere Rolle. Einen hohen Anteil an der zellulären ROS-Produktion haben die mitochondriale Glycerin-3-Phosphat-Dehydrogenase (mG3PDH) sowie der mitochondriale Komplex III (CIII). Aufgrund einer häufig unzureichenden Blutversorgung sind Tumoren durch einen niedrigen Sauerstoffdruck gekennzeichnet. Sauerstoffradikale sowie der Sauerstoffdruck regulieren die Stabilität des Transkriptionsfaktors HIF (*Hypoxia Inducible Factor*), welcher u.a. an der Regulation der Expression glykolytischer (Iso)Enzyme, wie der Lactat Dehydrogenase A (LDHA) und der Pyruvatkinase M2 (M2-PK) beteiligt ist. Des Weiteren induzieren ROS eine Dimerisierung und Aktivitätsverminderung des M2-PK-Proteins, welche dazu führen, dass die Zwischenmetabolite der Glycolyse akkumulieren und für die Synthesewege von Zellbausteinen zur Verfügung stehen. Neben der Glycolyse ist in Tumorzellen die Glutaminolyse ein weiterer wichtiger Stoffwechselweg, welcher sowohl Energie als auch metabolische Vorstufen für die Zellbausteine-Synthese bereitstellt.

Das Ziel dieser Studie war es, den Einfluss einer gezielten Hemmung der mG3PDH und des mitochondrialen CIII auf die Zellproliferation und den Stoffwechsel von PC-3-Prostatakarzinom zu untersuchen. PC-3 Zellen zeichnen sich durch eine hohe mG3PDH-Aktivität aus. Die Zellkultur-Experimente wurden in Gegenwart von 21% O₂ und 1,5% Sauerstoff durchgeführt. 1,5% O₂ entspricht dem durchschnittlichen physiologischen Sauerstoffpartialdruck in soliden Tumoren. 21% Sauerstoff ist der Sauerstoffpartialdruck der Luft, welcher in einer Mehrzahl der publizierten Zellkultur-Experimente angewandt wird. Zur Simulation von Therapie-Bedingungen wurden die PC-3 Zellen über einen längeren Zeitraum (96 Stunden) mit den jeweiligen Inhibitoren behandelt.

Im ersten Teil der Studie wurden zwei Substanzen iGP-1 und RH02211, die als Inhibitoren der mG3PDH veröffentlicht wurden, untersucht. Die mitochondriale G3PDH bildet zusammen mit der cytosolischen G3PDH den Glycerol 3-P Shuttle, der am Transfer von glykolytischem Wasserstoff in die Mitochondrien beteiligt ist. Der Glycerol 3-P Shuttle ist neben der LDH und dem Malat-Aspartat-Shuttle ein wichtiger Mechanismus, um NAD⁺ für die Glycolyse zu recyceln. Sowohl iGP-1 als auch RH02211 induzierten eine Hemmung der PC-3-Zellproliferation. Die RH02211-induzierte Hemmung der Zellproliferation war unabhängig vom Sauerstoffangebot. Die hemmende Wirkung beider Inhibitoren auf die Zellproliferation wurde abgeschwächt, wenn dem Kultivierungsmedium der Zellen Pyruvat zugesetzt wurde. Pyruvat ist das Substrat, über welches die LDH NADH + H⁺ zu NAD⁺ oxidiert. Den physiologischen Pyruvat-Konzentrationen im Blut ist ein Nährmedium ohne Pyruvat-Zusatz näher. Die Kultivierung der PC-3 Zellen in Gegenwart von Pyruvat führte zu einschneidenden Veränderungen im Stoffwechsel der Zellen. In Gegenwart

von Pyruvat wechselten die Pyruvat-Umsatzraten von Produktion zu Verbrauch und die Glycolyse- und Glutaminolyse-Umsatzraten nahmen ab. Im Gegensatz zur publizierten Erstbeschreibung von RH02211, in welcher eine Reduzierung der H₂O₂-Produktion in Pyruvat-supplementierten PC-3 Zellen nach dreistündiger Behandlung mit 1 – 30 µM RH02211 gezeigt wurde, fanden wir in unseren Experimenten in Gegenwart von 16 µM RH02211 eine Zunahme der H₂O₂-Produktion und des Sauerstoff-Verbrauchs unabhängig von der Pyruvat-Konzentration im Medium. Obwohl die H₂O₂-Produktionsraten zusammen mit den Umsatzraten der Glycolyse in Pyruvat-gehungerten PC-3 Zellen anstieg, hatte RH02211 keinen Einfluss auf das Tetramer : Dimer-Verhältnis der M2-PK, das Verhältnis der LDH-Isoenzyme und die Zusammensetzung des Glycolyse-Enzym-Komplexes. Im Pyruvat-supplementierten Medium hatte RH02211 keinen Einfluss auf die Glycolyse-Umsatzraten. Die Glutaminolyse wurde durch RH02211 sowohl im Pyruvat-Mangel als auch im Pyruvat-supplementierten Medium gehemmt iGP-1 zeigte in Pyruvat-gehungerten PC-3 Zellen eine Steigerung der Glycolyse und Glutaminolyse.

Im zweiten Teil der Studie wurde die Wirkung von drei kommerziell erhältlichen Hemmstoffen des mitochondrialen CIII auf die Proliferation und den Stoffwechsel der PC-3 Zellen (Antimycin A (AA), Myxothiazol (Myx) und S3QEL-2)), die sich in ihren Wirkmechanismen gegenüber CIII unterscheiden, untersucht. Die Hemmung der PC-3 Zellproliferation durch AA, welches CIII auf der Qi-Seite angreift, wurde durch Hypoxie deutlich abgeschwächt. Dagegen hatte die Sauerstoffkonzentration bei der Hemmung der Zellproliferation mit Myx und S3QEL-2, welche ihren Angriffspunkt auf der Q_o-Seite des CIII haben, nicht beeinflusst. Die Messungen der Stoffwechsel-Umsatzraten in den Nährmedium-Überständen der Zellen ergaben eine Aktivierung der Glykolyse durch AA, Myx und S3QEL-2 unabhängig von den Sauerstoff-Bedingungen. Die Glutaminolyse war in AA- und Myx-behandelten Zellen sowohl in Gegenwart von 21% als auch 1,5% O₂ sowie in S3QEL-2 behandelten Zellen in Gegenwart von 1,5% O₂ herunterreguliert. Diese Ergebnisse weisen darauf hin, dass Glucose die Hauptenergiequelle für die PC-3-Zellen in Gegenwart der drei CIII-Inhibitoren wurde. Der Anstieg der Glykolyse in AA, Myx und S3QEL-2 behandelten PC-3 Zellen war mit keinen Veränderungen in der Aktivität der gemessenen Glykolyse-Enzymen oder Veränderungen der H₂O₂-Produktion verbunden. Sowohl AA als auch Myx induzierten eine deutliche Verringerung des Sauerstoff-Verbrauchs der PC-3-Zellen. Im Gegensatz zur publizierten Erstbeschreibung, die keine Veränderung im Sauerstoff-Verbrauch von HEK 293 Zellen nach dreistündiger Behandlung mit 34 µM S3QEL-2, feststellte, fanden wir in PC-3 Zellen für 12 µM S3QEL-2 eine leichte, aber signifikante Abnahme im Sauerstoffverbrauch. Die im Vergleich zu Myx deutlich schwächere Wirkung von S3QEL-2 auf die mitochondriale Atmung der PC-3 Zellen könnte eine Erklärung für die signifikant höheren IC₅₀-Werte von S3QEL-2 im Vergleich zu Myx für die Hemmung der PC-3-Zellproliferation darstellen.

2 Introduction

2.1 Metabolism of cancer cells

Cancer cell proliferation strongly depends on the coordination of two associated metabolic pathways: glycolysis and glutaminolysis (DeBerardinis and Cheng 2010). Both pathways help to satisfy cancer cells' needs: availability of energy as well as intermediates for macromolecular synthesis (cell building blocks).

Glycolysis is an oxygen independent process that occurs in the cytosol and provides net-ATP in the last reaction step catalyzed by pyruvate kinase. In contrast, the glutaminolytic pathway takes place in the mitochondria and requires molecular oxygen in order to produce ATP via the mitochondrial respiratory chain.

2.1.1 Glycolysis

Glycolysis is an essential metabolic pathway for the catabolic breakdown of glucose to form adenosine triphosphate (ATP). Glycolysis consists of an energy-requiring phase followed by an energy-realising phase. In the first part of the pathway, energy is invested in the form of two ATP and in the second part, four ATP are recovered. The cell converts the absorbed glucose into glucose 6-phosphate (G6P) using a hexokinase (HK) while consuming ATP. The G6P formed can no longer leave the cell and can then flow into either glycogen synthesis (liver, muscle) or the pentose phosphate pathway or can be further isomerized in fructose 6-phosphate (F6P) in glycolysis by glucose 6-phosphate isomerase (GPI). F6P is then phosphorylated to fructose-1, -6-bisphosphate (F-1,6-BP) using phosphofructokinase (PFK) and 1 ATP. F-1,6-BP can be cleaved by the F-1,6-BP aldolase (Aldolase, ALDO) into two three-carbon fragments: glyceraldehyde 3-phosphate (GAP) and dihydroxyacetone phosphate (DHAP). These C3 bodies are isomers, which means that they can be converted into one another by the triose phosphate isomerase (TIM). DHAP can either be reduced to glycerol 3-phosphate using an NAD^+ -dependent glycerol 3-phosphate dehydrogenase and used for the synthesis of triglycerides (storage lipids) and phospholipids (membrane lipids) or converted to GAP using the TIM. The second stage of glucose catabolism comprises reactions through which a net gain of ATP is achieved through the oxidation of one of the triose phosphate compounds formed in the previous step. Thus the aldehyde group of GAP is oxidized by glyceraldehyde 3-phosphate dehydrogenase (GAPDH) and the energy liberated during this oxidation is conserved in the form of a high-energy phosphate compound namely as 1,3-bisphosphoglycerate (1,3-BPG). In this reaction, a reduction equivalent in the form of $\text{NADH} + \text{H}^+$ is obtained and an inorganic phosphate is transferred to the newly

formed carboxyl group. The phosphoglycerate kinase (PGK) now transfers the phosphate group from 1,3-BPG to adenosine diphosphate (ADP), so that the end products of the reaction are ATP and 3-phosphoglycerate (3PG). Then 3PG can either be isomerized to 2-phosphoglycerate (2PG) using the phosphoglycerate mutase (PGM) or serves as an important precursor for the biosynthesis of the amino acids serine, cysteine and glycine. The enzyme enolase removes a molecule of water from 2PG to form phosphoenolpyruvate (PEP). Phosphoenolpyruvate acts as the second source of ATP in glycolysis. The transfer of the phosphate group from PEP to ADP is catalysed by pyruvate kinase (PK). The products are another ATP and pyruvate. This last glycolytic reaction occurs twice for each molecule of glucose entering the glycolytic sequence. Thus, the net yield is two molecules of ATP for each six-carbon sugar. Pyruvate can either be reduced to lactate independently of oxygen in the cytosol or, after transport to the mitochondria, can be converted into CO₂ and water with energy generation (Figure 1).

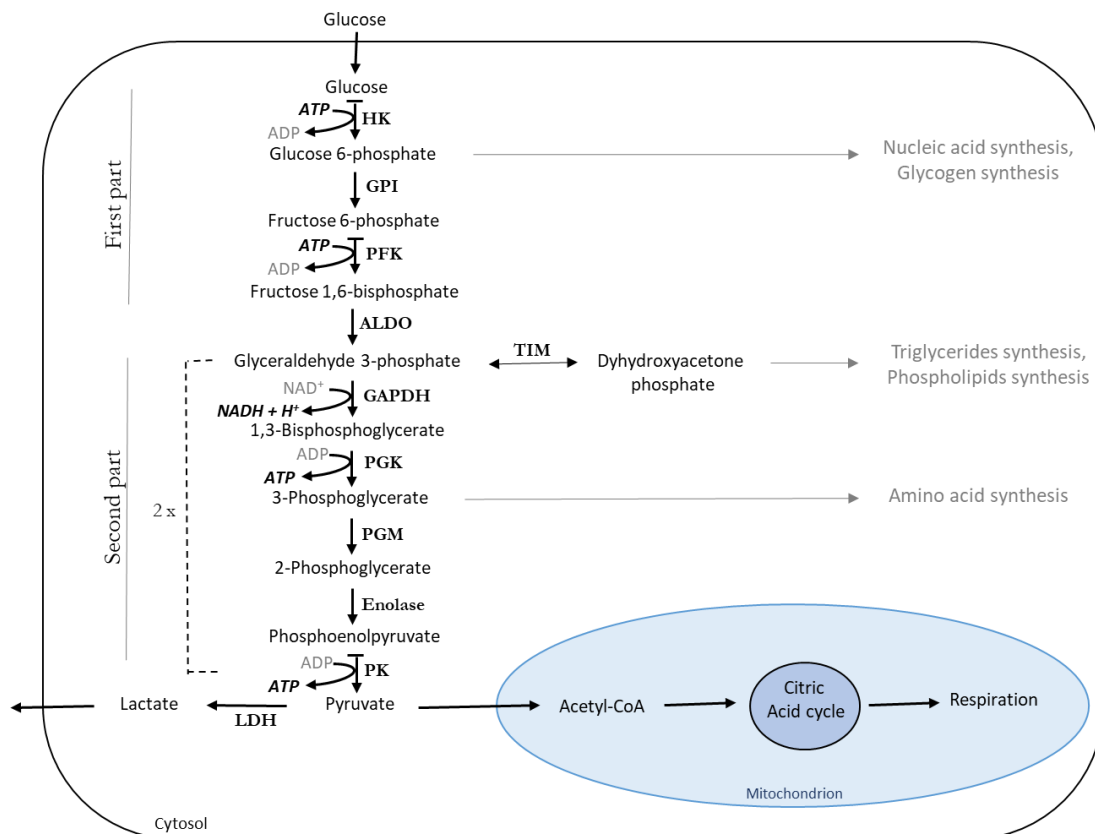


Figure 1. Schematic representation of glycolysis.

ADP: adenosine diphosphate; ALDO: aldolase; ATP: adenosine triphosphate; GAPDH: glyceraldehyde 3-phosphate dehydrogenase; GPI: glucose 6-phosphate isomerase; HK: hexokinase; LDH: lactate dehydrogenase; NAD⁺: nicotinamide adenine dinucleotide; NADH: nicotinamide adenine dinucleotide reduced; PFK: phosphofructokinase; PGM: phosphoglycerate mutase; PGK: phosphoglycerate kinase; PK: pyruvate kinase; TIM: triose phosphate isomerase.

The most intensive studies on the metabolism of proliferating cells have so far been carried out on cancer cells. Cancer cells are characterized by an uncontrolled division behaviour. Otto Heinrich Warburg described the first indications in 1924 that pointed to a change in the metabolism of

cancer cells. Warburg was able to show that cancer cells increasingly convert glucose into lactate even in the presence of oxygen (Warburg 1956). This is a typical behaviour of differentiated tissues and cells under oxygen deficiency conditions (anaerobic glycolysis). For this reason, the increased conversion of glucose to lactate in the presence of oxygen observed in cancer cells was called “aerobic glycolysis”. The conversion of glucose to lactate provides two moles of ATP per mole of glucose, while 32 moles of ATP per mole of glucose are generated by the complete oxygen-dependent degradation of glucose to CO₂ and H₂O via the oxidative phosphorylation (OXPHOS). Due to this reduced energy yield, cancer cells or normally proliferating cells have to convert significantly more glucose than differentiated cells in order to produce a certain amount of energy. Otto Warburg assumed that this aerobic glycolysis of cancer cells could be attributed to a defect in mitochondrial respiration (Warburg 1956).

In addition to ATP, cancer cells require metabolic intermediates that are critical for the biosynthesis of building blocks indispensable for cancer growth and proliferation (Mazurek et al. 2005; DeBerardinis et al. 2008). Adaptation of the metabolism to changes in the energy or cell building block requirement in cancer cells is achieved, among other things, by activating or inhibiting enzymes and changing the isoenzyme equipment of some glycolytic enzymes (Mazurek et al. 1996; Eigenbrodt et al. 1998; Mazurek et al. 2002; Metallo and Vander Heiden 2013). Isoenzymes catalyse the same metabolic reactions but are encoded by different genes and can have different amino acid sequences. They can also be expressed in different organs and organelles and are differently regulated. Pyruvate kinase and lactate dehydrogenase are two important glycolysis enzymes that perform different tasks in cancer cells and differentiated cells.

2.1.1.1 Pyruvate Kinase

Pyruvate kinase (PK), a terminal glycolytic pathway enzyme, catalyses the irreversible phosphorylation reaction between PEP and ADP to yield a molecule of pyruvate and ATP. The PK reaction is responsible for the net energy production of glycolysis, which, in contrast to mitochondrial respiration, is oxygen-independent. In mammals, four different PK tissue-specific isoforms are known, encoded by two different genes: *Pkrf* and *Pkm* (Harada et al. 1978). The *Pkrf* gene encodes the L-PK and R-PK isoforms while M1-PK and M2-PK are encoded by the *Pkm* gene. The PK isoenzyme type R (R-PK) is expressed in erythrocytes while the PK isoenzyme type L (L-PK) is mainly expressed in liver and kidney and it is involved in the gluconeogenesis pathway. M1-PK and M2-PK isoenzymes derive from the alternative splicing of the mutually exclusive exons 9 and 10 of the *Pkm* gene. Out of fifty-six amino acids encoded by exon 9 and exon 10, twenty-two amino acids are different. Therefore, the mature mRNAs that includes either exon 9 (M1-PK) or exon 10 (M2-PK) encodes for two proteins which have the

same size (531 amino acids) but differ for twenty-two amino acids. Despite very similar primary sequences, M1-PK and M2-PK have different tissue-specific expression (Noguchi et al. 1986; Yamada and Noguchi 1999; Prakasam et al. 2018). The expression of the PK isoenzyme type M1 (M1-PK) is characteristic of adult differentiated tissues that require a high-energy supply such as heart, brain and skeletal muscle. The PK isoenzyme type M2 (M2-PK) is mainly expressed in dividing cells with growing anabolic demands (i.e. embryonic cells, normal proliferating cells, stem cells and cancer cell) (Prakasam et al. 2018; Mazurek 2011). The four isoenzymes of PK have a different affinity to its substrate PEP. All four isoenzymes occur in a tetrameric quaternary structure, which means that they consist of four subunits. In contrast to the other PK isoenzymes, M2-PK can also occur in a dimeric form in addition to the tetramer (Figure 2) (Eigenbrodt et al. 1992; Zwerschke et al. 1999).

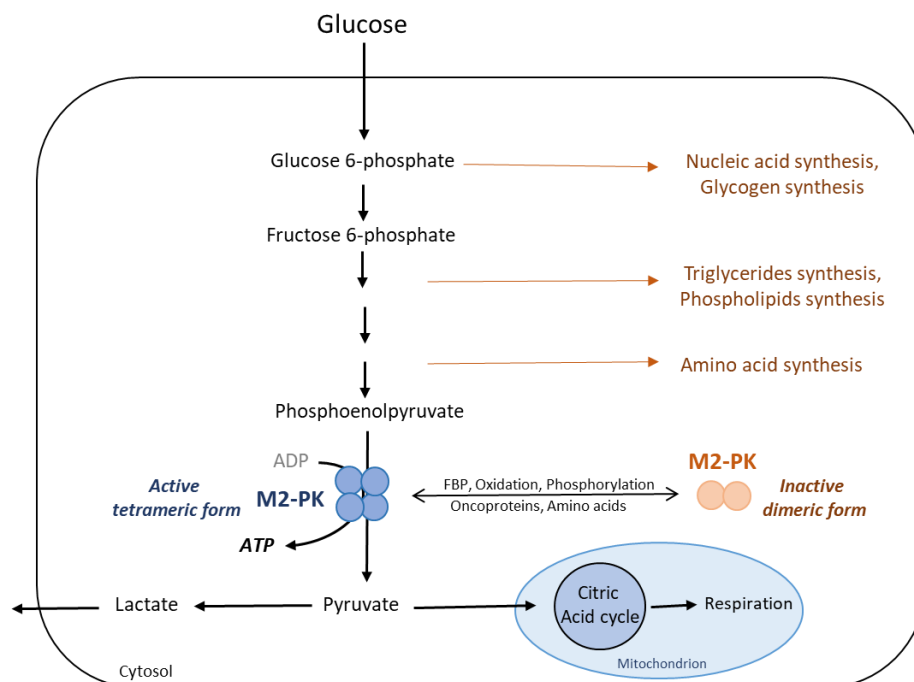


Figure 2 Role of pyruvate kinase isoenzyme type M2 (M2-PK) in glycolysis. Based on Mazurek 2011.

M2-PK has an important regulatory function for the utilization of glucose.

The tetrameric form of M2-PK has a high affinity for the substrate PEP and is highly active under physiological conditions. The dimeric form of M2-PK, on the other hand, has a low affinity for the substrate PEP and is almost inactive under physiological conditions. The ratio between the tetrameric and the dimeric form of the M2-PK (tetramer-dimer ratio) is regulated by the glycolysis intermediate fructose-1,6-bisphosphate (FBP), phosphorylation, oxidation, various amino acids, and by direct interactions with oncoproteins (Figure 2) (Kalaiarasan et al. 2014; Zwerschke et al. 1999; Jurica et al. 1998; Anastasiou et al. 2011; Mazurek 2011).

High concentrations of FBP induce the tetramerization of M2-PK and increase the PEP affinity of PK. Glucose is then converted to lactate until FBP levels drop below a minimum signal level.

This leads to the disassociation of the tetrameric form of M2-PK to the inactive dimeric form. If the proportion of dimeric M2-PK is high, the conversion of PEP to pyruvate is blocked. As consequence, all glycolytic intermediates accumulate above the pyruvate kinase reaction and are available as starting materials for the cell building block synthesis pathways branching off from glycolysis (Eigenbrodt et al. 1997). Therefore, the shift from a highly active tetrameric form to a nearly inactive dimeric form of M2-PK allow proliferating cells to divert glucose into anabolic pathways emanating from glycolysis in order to meet the increased biosynthetic demands of proliferation. Another regulatory mechanism of M2-PK is the oxidation at Cysteine 358. High reactive oxygen species concentrations induced by insulin treatment, hypoxia or addition of hydrogen peroxide into the cultivation medium of cancer cells led to an oxidation of M2-PK, which results in a dissociation of M2-PK to the inactive dimeric form (Brunelle et al. 2005; Anastasiou et al. 2011; Li et al. 2014b; Mohd Askandar Iqbal et al.).

In cancer cells M2-PK is mainly present in the inactive dimeric form. Therefore, less pyruvate is produced by glycolysis and the glycolytic intermediates that accumulate above the PK reaction are then available for cell building blocks synthesis. The tetramer-dimer ratio of the M2-PK can be used to regulate whether glucose is used for energy production or channelled into synthetic processes such as the pentose phosphate pathway (PPP) as well as used for phospholipid and amino acid synthesis, supporting macromolecules biosynthesis and thus cancer cell proliferation. The tetrameric form of M2-PK was found associated with other glycolytic enzymes (hexokinase, lactate dehydrogenase, glyceraldehyde 3-P dehydrogenase, phosphoglycerate kinase, phosphoglyceromutase, enolase) forming the so called *glycolytic enzyme complex* (Mazurek et al. 1996; Mazurek et al. 1999; Mazurek et al. 2005). The association and the close proximity of the glycolytic enzymes within this complex leads to a more effective conversion of glucose to lactate. Therefore, the enzyme composition of the glycolytic enzyme complex regulates the interaction between glycolysis and glutaminolysis (Mazurek et al. 2005).

2.1.2 Glutaminolysis

In analogy to the breakdown of glucose, the oxidation of glutamine is called glutaminolysis. Glutaminolysis takes place in all proliferating cells, such as lymphocytes, enterocytes of the small intestine and especially in cancer cells (Altman et al. 2016; Matés et al. 2020). Glutamine is the most abundant amino acid in blood and muscle and it plays an important role as a carrier of nitrogen, carbon and energy between the organs of the body (Curthoys and Watford 1995). In proliferating cells together with glycolysis, which provides energy and glycolytic intermediates for biosynthetic processes, glutamine is used both for energy generation and as a source of carbon and nitrogen for biomass accumulation. Glutaminolysis creates precursors for fatty acid synthesis as well as

produces starting materials for nucleic acid and serine synthesis through the degradation products glutamate and aspartate. In contrast to glycolysis, which can also be carried out in the absence of oxygen (anaerobic glycolysis), the energy generation in glutaminolysis depends on an adequate supply of oxygen (Le et al. 2012). Through the activity of multiple enzymes, cells convert glutamine into TCA cycle metabolites. In the first reaction step of glutaminolysis, after the absorption of glutamine in the cell, glutamine is deaminated to glutamate and ammonium via glutaminase (GLS/GLS2) (Matés et al. 2020). Glutamate can then be either converted to α -ketoglutarate, which enters the TCA cycle to generate ATP through production of NADH and FADH₂ or excreted by the cells. Glutamate can be converted into α -ketoglutarate via three divergent pathways. The first is via an ammonia-releasing process catalysed by glutamate dehydrogenase (GLDH), while the others are via some non-ammonia producing aminotransferases including glutamate oxaloacetate transaminase (GOT) and glutamate pyruvate transaminase (GPT) (Figure 3). Transaminases promote the generation of nonessential amino acids, including aspartate and alanine. α -ketoglutarate thus generated can serve as an anaplerotic substrate in the TCA cycle being introduced into the TCA cycle and converted to malate via succinyl-CoA, succinate and fumarate. Malate is either metabolized further to oxaloacetate and citrate in the citrate cycle or discharged from the citrate cycle and converted through the malic enzyme reaction to pyruvate and then to lactate (Figure 3). Thus, the lactate produced in cancer cells comes not only from glycolysis, but also from the breakdown of glutamine.

It was shown in cancer cells that the citrate cycle is truncated by high concentrations of reactive oxygen species (ROS) due to an inhibition of the enzyme aconitase which catalyses the conversion of citrate to isocitrate and glutaminolysis therefore only takes place over part of the citrate cycle (Boitier et al. 1995). Due to the truncation of the citrate cycle in cancer cells, the proportion of acetyl-CoA that is introduced into the citrate cycle is low and acetyl-CoA is available for the new synthesis of fatty acids. Furthermore, α -ketoglutarate can also be carboxylated into citrate through isocitrate dehydrogenases (IDHs) for fatty acid synthesis (Ward et al. 2010). Reductive carboxylation seems to be a major source of carbon for lipid synthesis in cancer cells that are hypoxic, have constitutive hypoxia-inducible factor- α (HIF α) stabilization or have mitochondrial defects (Mullen et al. 2011).

The energy yield of glutaminolysis is a guanosine triphosphate (GTP) by direct phosphorylation of GDP, 1.5 ATP by oxidation of FADH₂ and 2.5 ATP per NADH + H⁺, from the α -ketoglutarate dehydrogenase reaction, the malate dehydrogenase reaction and the malate decarboxylase reaction (Figure 3).

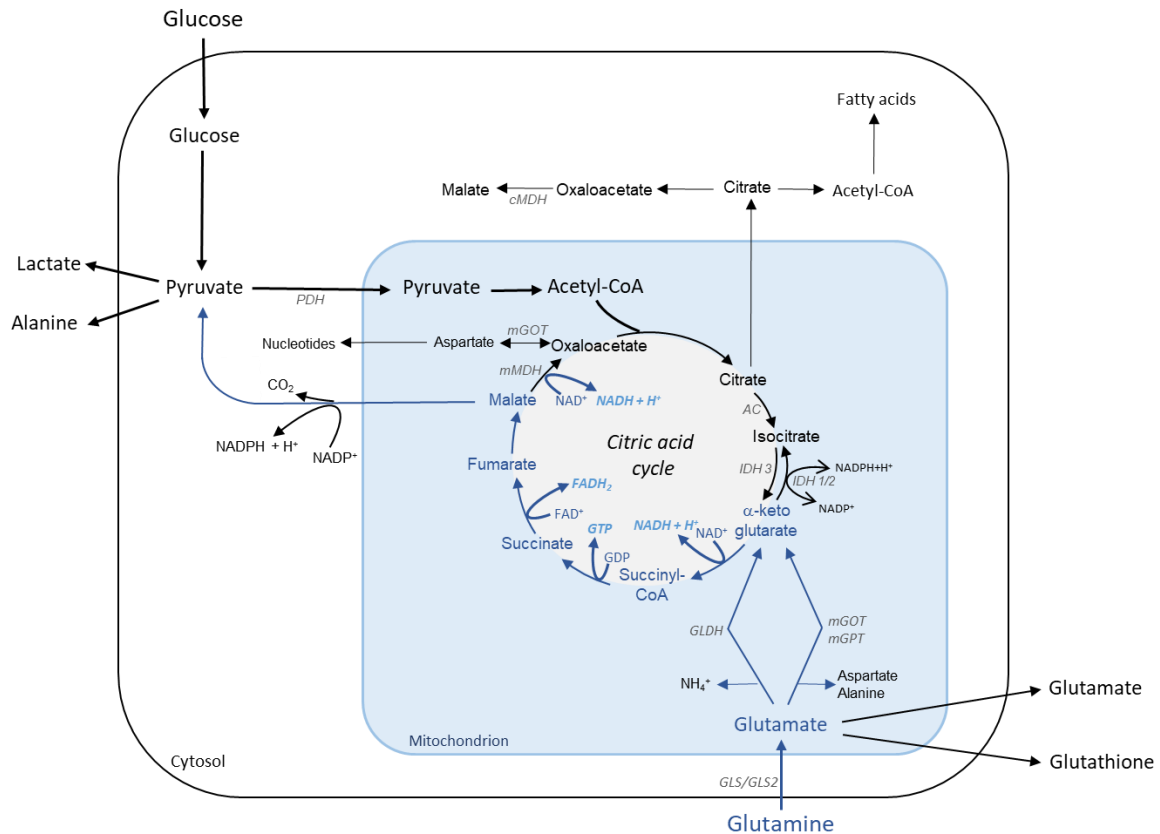


Figure 3. Schematic representation of glutaminolysis. Based on Mazurek 2011.

AC: aconitase; cMDH: cytosolic malate dehydrogenase; mMDH: mitochondrial malate dehydrogenase; FAD⁺: flavin adenine dinucleotide; FADH: flavin adenine dinucleotide reduced; GLDH: glutamate dehydrogenase; GOT: glutamate oxaloacetate transaminase; GDP: guanosine diphosphate; GTP: guanosine triphosphate; mGPT: glutamate pyruvate transaminase; GLS: glutaminase; IDH: isocitrate dehydrogenase; NAD⁺: nicotinamide adenine dinucleotide; NADH: nicotinamide adenine dinucleotide reduced; NADP⁺: nicotinamide adenine dinucleotide phosphate; NADPH: nicotinamide adenine dinucleotide phosphate reduced; PDH: pyruvate dehydrogenase.

2.1.3 Regeneration of cytosolic NAD⁺

Glycolytic metabolism involves the reduction of cytosolic NAD⁺ to NADH + H⁺ at the step catalysed by glyceraldehyde 3-phosphate dehydrogenase. In order to ensure that a high NADH/NAD⁺ ratio does not limit glucose metabolism, especially in cells with high glycolytic rates such as cancer cells, three different mechanisms exist to regenerate cytosolic NAD⁺: the lactate dehydrogenase reaction, the glycerol phosphate shuttle and the malate-aspartate shuttle (Figure 4) (Mary C. McKenna et al. 2006).

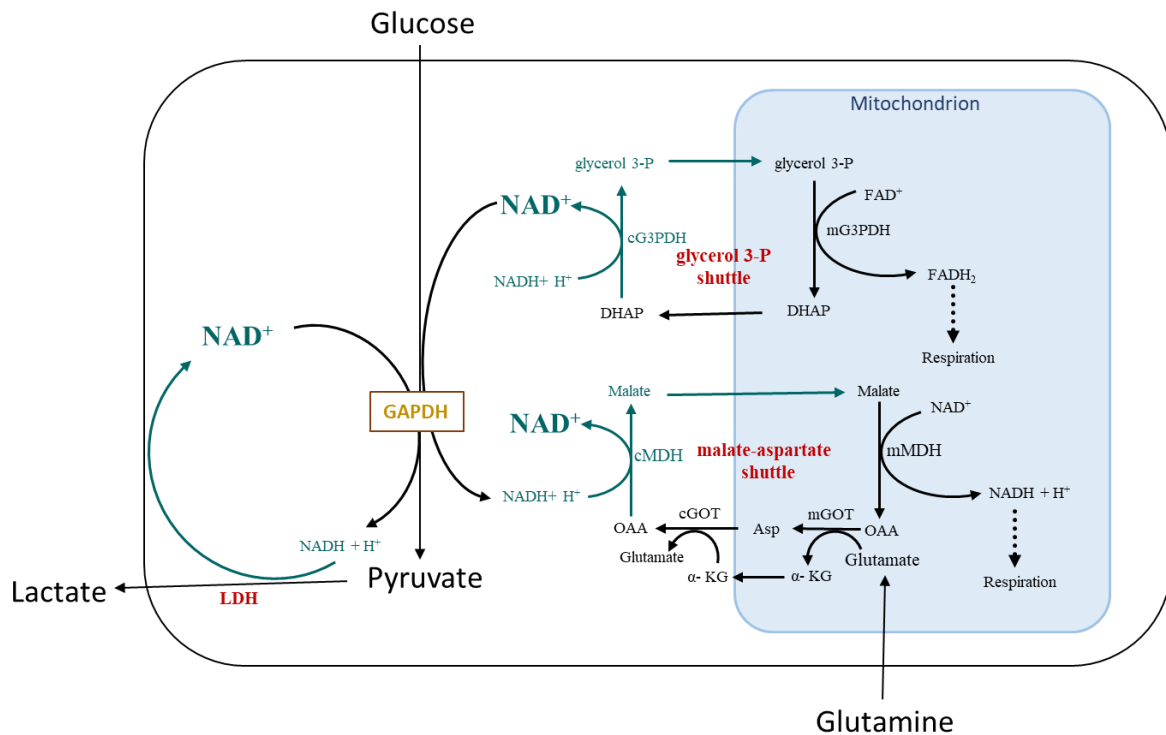


Figure 4. Metabolic scheme of glycolysis with the metabolic reactions involved in the regeneration of cytosolic NAD^+ : lactate dehydrogenase (LDH), glycerol 3-phosphate shuttle and malate-aspartate shuttle.

Modified from Mazurek et al. 1996 and Orr et al. 2014. Asp: aspartate; DHAP: dihydroxyacetone phosphate; FAD^+ : flavin adenine dinucleotide; FADH_2 : flavin adenine dinucleotide reduced; cG3PDH: cytosolic glycerol 3-phosphate dehydrogenase; mG3PDH: mitochondrial glycerol 3-phosphate dehydrogenase; GAPDH: glyceraldehyde 3-phosphate dehydrogenase; cGOT: cytosolic glutamate oxaloacetate transaminase; mGOT: mitochondrial glutamate oxaloacetate transaminase; LDH: lactate dehydrogenase; cMDH: cytosolic malate dehydrogenase; mMDH: mitochondrial malate dehydrogenase; NAD^+ : nicotinamide adenine dinucleotide; NADH : nicotinamide adenine dinucleotide reduced; OAA: oxaloacetate; α -KG: α -ketoglutarate.

2.1.3.1 Lactate dehydrogenase

Lactate dehydrogenase (LDH) is a tetrameric enzyme that catalyses the reversible conversion of pyruvate and $\text{NADH} + \text{H}^+$ to lactate and NAD^+ (Figure 4). There are five different LDH isoenzymes (LDH1-5) which are present in the cytosol of the cell and are composed of different combinations of the subunits M (skeletal muscle type, LDH-A) and H (heart muscle type, LDH-B) (Li et al. 1983). Two of the isoenzymes are homotetramers (LDH1 = H₄ and LDH5 = M₄) and three of the isoenzymes are heterotetramers (LDH2 = H₃M₁; LDH3 = H₂M₂; LDH4 = H₁M₃). The five isoenzymes of LDH show a characteristic tissue-specific distribution. The H-type dominates in tissues with high oxygen consumption, while M-type predominates in tissues with high glycolytic activity (Markert et al. 1975).

In cancer cells as well as in hypoxic conditions it is known that there is a decrease in the H-type with simultaneous overexpression of the M-type of LDH (LDH5) (Feng et al. 2018; Eales et al. 2016). The isoform LDH5 is characterized by a high affinity for the substrate pyruvate (Sumida et al. 1995). Thus, the LDH reaction offers a very effective way to recycle NAD^+ for maintaining the GAPDH reaction and to remove excess hydrogen from the cell.

2.1.3.2 The glycerol 3-phosphate shuttle

The glycerol 3-phosphate shuttle is one of the mechanisms that regenerate cytosolic NAD^+ channelling cytosolic reducing equivalents to the mitochondrial oxidative phosphorylation pathway (Figure 4). In mammalian mitochondria, the glycerol 3-phosphate shuttle links glycolysis, oxidative phosphorylation, and fatty acid metabolism (Mráček et al. 2013). The glycerol 3-phosphate shuttle consists of the soluble NAD^+ -linked cytosolic glycerol 3-phosphate dehydrogenase (cG3PDH) and the membrane bound FAD^+ -linked mitochondrial glycerol-3-phosphate dehydrogenase (mG3PDH). The cG3PDH converts dihydroxyacetone phosphate (DHAP) to glycerol 3-phosphate (G-3-P) via oxidizing one molecule of $\text{NADH} + \text{H}^+$ to NAD^+ (Ansell et al. 1997). G-3-P is then converted back to DHAP by mG3PDH, reducing one molecule of flavin adenine dinucleotide (FAD^+) to FADH_2 , which can then enter into mitochondrial respiration by reducing ubiquinone (coenzyme Q) to ubiquinol (QH_2) and finally generates ATP.

In prostate cancer cells it has been shown that mG3PDH participates in mitochondrial ROS production (Chowdhury et al. 2005).

2.1.3.3 The malate-aspartate shuttle

The enzymes involved in the regeneration of cytosolic NAD^+ through the malate-aspartate shuttles are malate dehydrogenase (MDH) and glutamate oxaloacetate transaminase (GOT) also known as aspartate aminotransferase (AST). Both enzymes exist as cytosolic (cMDH, cGOT) and mitochondrial (mMDH, mGOT) isoenzymes (Figure 4). In addition to the cytosolic and mitochondrial isoform of MDH, another form of mitochondrial MDH occurs. In MCF-7 breast cancer cells, this third form of MDH was identified as the cytosolic precursor of the mitochondrial isoenzyme (Mazurek et al. 1996).

Malate dehydrogenase catalyses the reduction of oxaloacetate to malate using $\text{NADH} + \text{H}^+$ and producing NAD^+ (MDHox). It also catalyses the reaction from malate to oxaloacetate (MDHma) in the reverse direction, consuming NAD^+ and producing $\text{NADH} + \text{H}^+$. Through the malate-aspartate shuttle, the $\text{NADH} + \text{H}^+$ formed in the glycolytic GAPDH reaction can be transferred to oxaloacetate by the cMDH. The resulting malate is then transported into mitochondria where the hydrogen contained in the malate is transferred to NAD^+ using the mMDH. This creates oxaloacetate and $\text{NADH} + \text{H}^+$, which is now available to the respiratory chain. The oxaloacetate formed is used to form aspartate and α -ketoglutarate using glutamate and the mGOT. The aspartate can be transported into the cytosol, where the cGOT can again form glutamate and oxaloacetate from aspartate and α -ketoglutarate (Figure 4).

2.1.4 The oxidative phosphorylation (OXPHOS)

The main role of mitochondria is ATP production through the metabolic process known as oxidative phosphorylation (OXPHOS). Metabolites coming from glycolysis, β -oxidation and TCA cycle are substrates for ATP production. Briefly, pyruvate, end product of glycolysis, is transported into mitochondria and converted to acetyl-CoA by pyruvate dehydrogenase (PDH). On the other hand, fatty acids are oxidized during the β -oxidation to acetyl-CoA entirely within the mitochondria. Then, Acetyl-CoA enters the TCA cycle where it is oxidized, producing CO_2 and the reduced coenzymes $\text{NADH} + \text{H}^+$ and FADH_2 . Reducing equivalents are produced also during glycolysis and β -oxidation (Lenaz and Genova 2009; Szalárdy et al. 2015). The reduced coenzymes donate electrons to the complexes of the respiratory chain embedded within the inner mitochondrial membrane (IMS) (Formosa and Ryan 2018). $\text{NADH} + \text{H}^+$ and FADH_2 provide electrons to the respiratory complex I (CI, NADH dehydrogenase) and complex II (CII, succinate-ubiquinone oxidoreductase) respectively. The electrons are then transported to complex III (CIII, ubiquinol-cytochrome c oxidoreductase) from both complexes via the lipophilic carrier coenzyme Q (CoQ, ubiquinone) and flow through cytochrome c to complex IV (CIV, cytochrome c oxidase) where oxygen, the final electrons acceptor, is reduced to water (Figure 5). During the electron transport, CI, CIII and CIV pump out protons from the matrix across the inner membrane, generating the electrochemical gradient ($\Delta\mu_{\text{H}^+}$), consisting of a proton gradient (ΔpH , alkaline in the matrix side) and an electrical potential ($\Delta\Psi_{\text{m}}$: ~ -180 mV; negative in the matrix) across the membrane (Mitchell 1961). For each NADH molecule oxidized, 10 protons are translocated across the membrane from the matrix to the inner-membrane space by the three respiratory complexes. The electrochemical gradient (also called proton motive force) drives back the protons into matrix via ATP synthase (complex V, CV) inducing conformational changes in the active site of the enzyme and consequently promoting the phosphorylation of ADP to ATP (Wallace and Fan 2010; Sazanov 2015; Szalárdy et al. 2015).

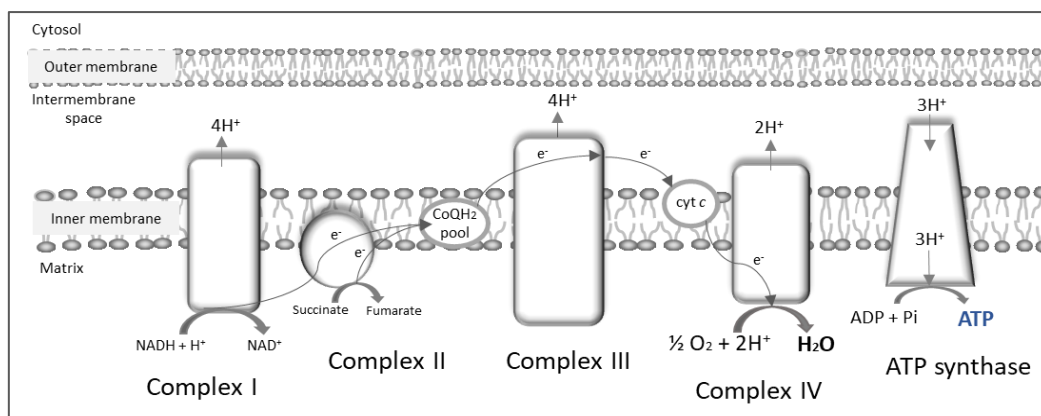


Figure 5. The OXPHOS system consisting of CI, CII, CIII, CIV and the ATP synthase (CV).

ADP: adenosine diphosphate; ATP: adenosine triphosphate; cyt c : cytochrome c ; CoQ: coenzyme Q; NAD^+ : nicotinamide adenine dinucleotide; NADH : nicotinamide adenine dinucleotide reduced.

2.1.4.1 The mitochondrial respiratory chain – Complex III

As introduced in the previous paragraph and shown in Figure 5, four protein complexes embedded within the inner membrane transferring electrons from $\text{NADH} + \text{H}^+$ or FADH_2 to oxygen compose the mitochondrial respiratory chain. The central component of the mitochondrial respiratory chain is CIII (ubiquinol:cytochrome *c* oxidoreductase), which transfers electrons from CoQ to cytochrome *c* generating a proton gradient across the inner membrane (Bénil et al. 2009). CIII was one of the earliest complexes discovered and it was isolated from bovine heart mitochondria in 1962 for the first time (Hatefi et al. 1962). The mammalian CIII is a homodimer enzyme, where each monomer contains 11 subunits, of which only one, cytochrome *b*, is encoded by the mitochondrial genome (Bénil et al. 2009). The catalytic center is formed by three redox subunits: cyt *b*, having two *b*-type haems, a low potential haem b_L and a high potential haem b_H ; cyt *c*₁, containing a *c*-type haem and the iron sulfur protein (Rieske protein, ISP), including a high potential 2Fe–2S iron–sulfur cluster (Figure 6) (Di Xia et al. 2013). The two *b*-type haems of cytochrome *b* are part of the active sites that catalyze opposite reactions: the Q_o site, located near b_L haem and in proximity to the intermembrane space, provides access to lipid-soluble quinol (QH_2) for oxidation, and the Q_i site, situated close to b_H haem and in proximity to the matrix, is involved in the reduction of ubiquinone. Unlike other respiratory complexes, CIII has a quite unique proton extrusion mechanism, since quinol is used to shuttle protons across the membrane via the so called Q-cycle (Mitchell 1976). The Q-cycle requires a quinol oxidation site (Q_o) and a quinone reduction site (Q_i) and the oxidation of two quinol molecules to complete one cycle. In the first half of the Q-cycle, a QH_2 moves into the Q_o site and undergoes oxidation with one electron going to cytochrome *c* via the ISP (2Fe2S) and cytochrome *c*₁ and the other one arriving to Q_i via haems b_L and b_H in order to form a semiquinone radical ($Q^{\cdot-}$) and release two protons into the intermembrane space. In the second half of the Q-cycle, a second QH_2 is oxidized in the same way at the Q_o site, reducing completely the $Q^{\cdot-}$ at Q_i site. The fully reduced QH_2 , upon picking up two protons from the matrix, moves through the membrane to the Q_i site to be oxidized, thus starting the Q-cycle again. As a result of the Q-cycle, four protons are transferred to the intermembrane space, two protons are picked up from the matrix side and effectively only one quinol is oxidized (Figure 6) (Di Xia et al. 2013; Sazanov 2015).

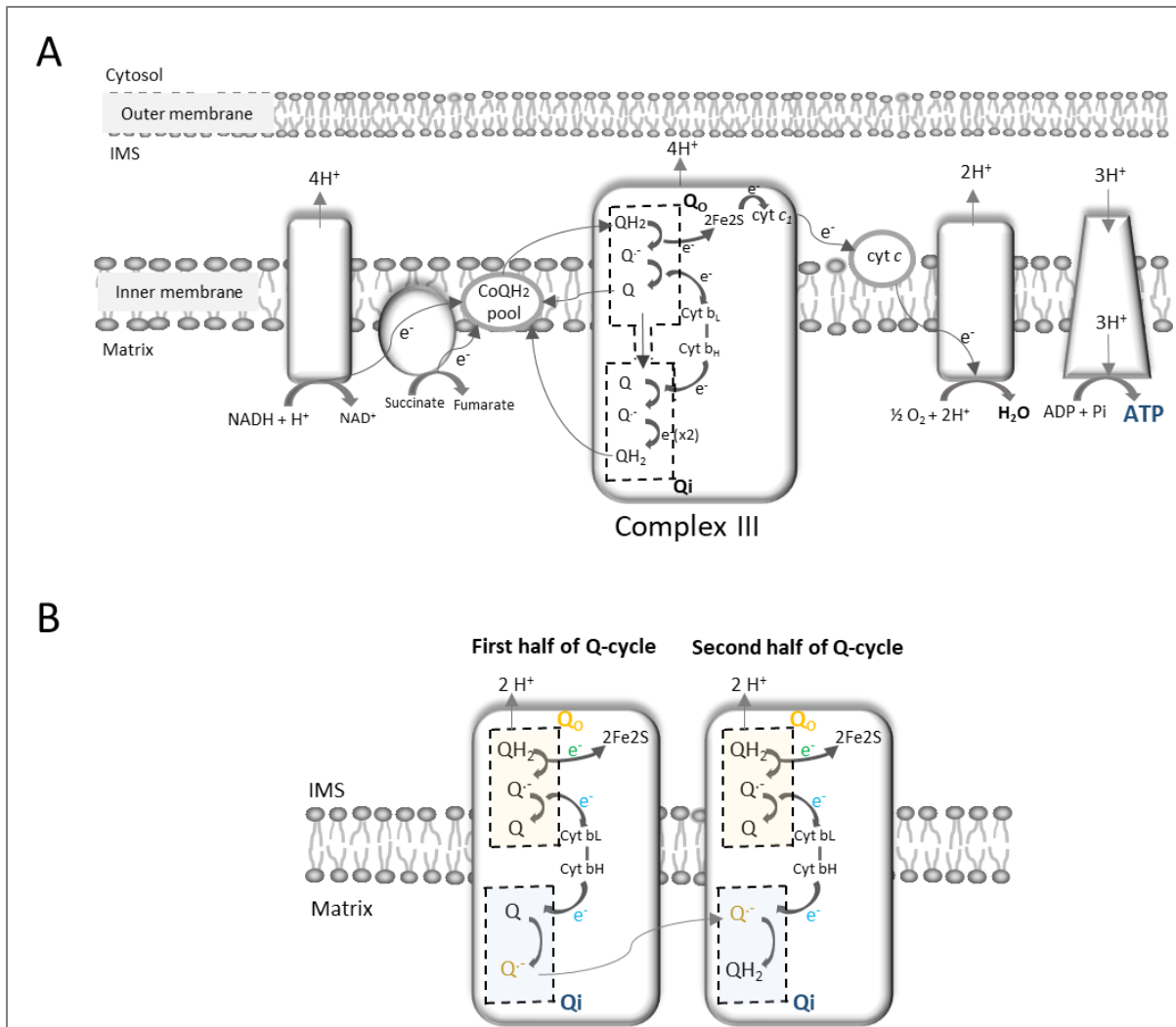


Figure 6. Mitochondrial respiratory chain with a representative scheme of the CIII with the Q-cycle.

A) Schematic representation of the electron flow through the mitochondrial respiratory complexes. The CIII Q-cycle is shown; B) Detailed scheme of the Q-cycle showing the fate of the electrons coming from two successive quinol oxidations. ADP: adenosine diphosphate; ATP: adenosine triphosphate; cyt: cytochrome; CoQ: coenzyme Q; NAD^+ : nicotinamide adenine dinucleotide; NADH : nicotinamide adenine dinucleotide reduced; Q: semiquinone; Q^- : semiquinone radical; QH_2 : quinol.

2.2 Reactive Oxygen Species

It has been observed that cancer cell lines and tumors produce large amount of reactive oxygen species (ROS) promoting tumorigenesis through oxidative DNA damage and subsequent genomic instability (Diebold and Chandel 2016). ROS are a collective term including oxygen derivatives, either radical or non-radical, that are oxidizing agents and/or are easily converted into radicals. If a single electron is supplied to O_2 , the superoxide radical anion $\text{O}_2^{\cdot-}$ is formed. Addition of another electron to $\text{O}_2^{\cdot-}$ gives the peroxide ion, which is a weaker acid and can be protonated to hydrogen peroxide H_2O_2 . Addition of two more electrons splits the molecule producing water H_2O . If one single electron is added to H_2O_2 by a reduced metal ion (e.g., Fe^{2+}), the hydroxyl radical OH^{\cdot} is produced by the Fenton reaction (Genova and Lenaz 2015).

Mitochondria have been recognized as one of the major cellular generators of ROS. In particular, the respiratory CI, CII, and CIII as well as the mG3PDH are known to generate ROS through the

leak of electrons to molecular oxygen (Hamanaka and Chandel 2010; Sena and Chandel 2012). However, while all these sites can deposit $O_2^{\cdot-}$ into the mitochondrial matrix, only site III_{Q_o} (on complex III) and mG3PDH can release $O_2^{\cdot-}$ into the intermembrane space (Miwa et al. 2003; Brand 2010). In order to reach the cytosol, matrix ROS need to cross both the inner and the outer mitochondrial membranes, while ROS released into the intermembrane space only need to cross the outer mitochondrial membrane, and thus they can easily reach the cytosol and exploit their signalling capacity (Sena and Chandel 2012).

2.2.1 CIII as a source of ROS

Within complex III the transfer of electrons from QH_2 to cytochrome *c* is catalyzed by the Q cycle. The formation of superoxide in CIII depends on this peculiar mechanism of electron transfer. Under normal conditions, once the first electron is transferred to the Rieske protein and the $Q^{\cdot-}$ is generated at the site Q_o , $Q^{\cdot-}$ is immediately oxidized by *cyb* b_L to Q (Figure 6). However, when the electron transport is slowed by high membrane potential, the lifetime of Q_o increases and the O_2 dissolved in the membrane can react with the $Q^{\cdot-}$ since O_2 is more soluble in lipid than in water (Thomas et al. 2001; Jezek and Hlavatá 2005). At high membrane potential the delay of the electron transport is due to the trans-membrane organization of the two *b* haems (b_L located to the cytosolic side and b_H closer to the matrix side) on opposing sides of the hydrophobic core of complex III allowing a prolonged occupancy of the $Q^{\cdot-}$ at the Q_o site.

This reaction generates superoxide radical anion ($O_2^{\cdot-}$). The Q_o site is located close to the intermembrane space allowing the release of $O_2^{\cdot-}$ mainly to the cytosolic side (Han et al. 2001). However, about half of $O_2^{\cdot-}$ produced on the complex III is released into the matrix (Muller et al. 2004). Besides Q_o even the Q_i site of complex III, located close to the matrix side, could be able to generate $O_2^{\cdot-}$ since $Q^{\cdot-}$ is produced when *cyt* b_H donates an electron to Q (Figure 6). However, the Q_i site firmly binds and stabilizes $Q^{\cdot-}$ making less likely the reaction with oxygen (Jezek and Hlavatá 2005). A prolongation of the lifetime of $Q^{\cdot-}$ at the Q_o site is also artificially induced by Antimycin A (AA), which is a chemical compound produced by *Streptomyces kitazawensis* (Nakayama et al. 1956) that specifically blocks electron flow from *cyt* b_H to ubiquinone (Q) overlapping partly the quinone reduction site Q_i (Xia et al. 1997). Several studies have shown that AA (2 - 100 μ M) induced $O_2^{\cdot-}$ and H_2O_2 formation in different cell lines after long and short term incubation experiments (15 minutes - 72 hours) carried out at 21% O_2 (Muller et al. 2003; Li et al. 2014a; Dröse and Brandt 2008; Park et al. 2007; Han et al. 2008). Increased levels of $O_2^{\cdot-}$ and H_2O_2 have been reported even when isolated bovine and rat mitochondria as well as human pro-myelocytic leukemia HL-60 cells were treated shortly (up to 6 hours) with 3 – 10 μ M Myxothiazol (Myx) (Starkov and Fiskum 2001). Myx acts at the proximal niche of Q_o and stops the electron flow from ubiquinol (QH_2) to the iron-

sulfur center, and, indirectly, also to cyt b_L (Figure 7A-B) (Xia et al. 1997). During hypoxia (1% - 5% O₂), 1 µg/ml AA increased ROS production and HIF1α in rat liver isolated mitochondria after 30 minutes of treatment, whereas 100 ng/ml Myx decreased ROS production and blocked HIF-1α (Chandel et al. 2000). Accordingly, 100 ng/ml Myx decreased H₂O₂ production levels in micro vessel myocytes measured at 2% O₂ (Waypa Gregory B. et al. 2001).

Recently, novel compounds have been published as suppressors of site III_{Q_o} electron leak (S3QELs) (Figure 7). In isolated rat skeletal muscle mitochondria as well as in primary, immortalized and cancer cells the S3QELs are able to specifically suppress production of superoxide/hydrogen peroxide from site III_{Q_o} without inhibiting the OXPHOS and therefore the energy metabolism (Orr et al. 2015; Fang et al. 2020).

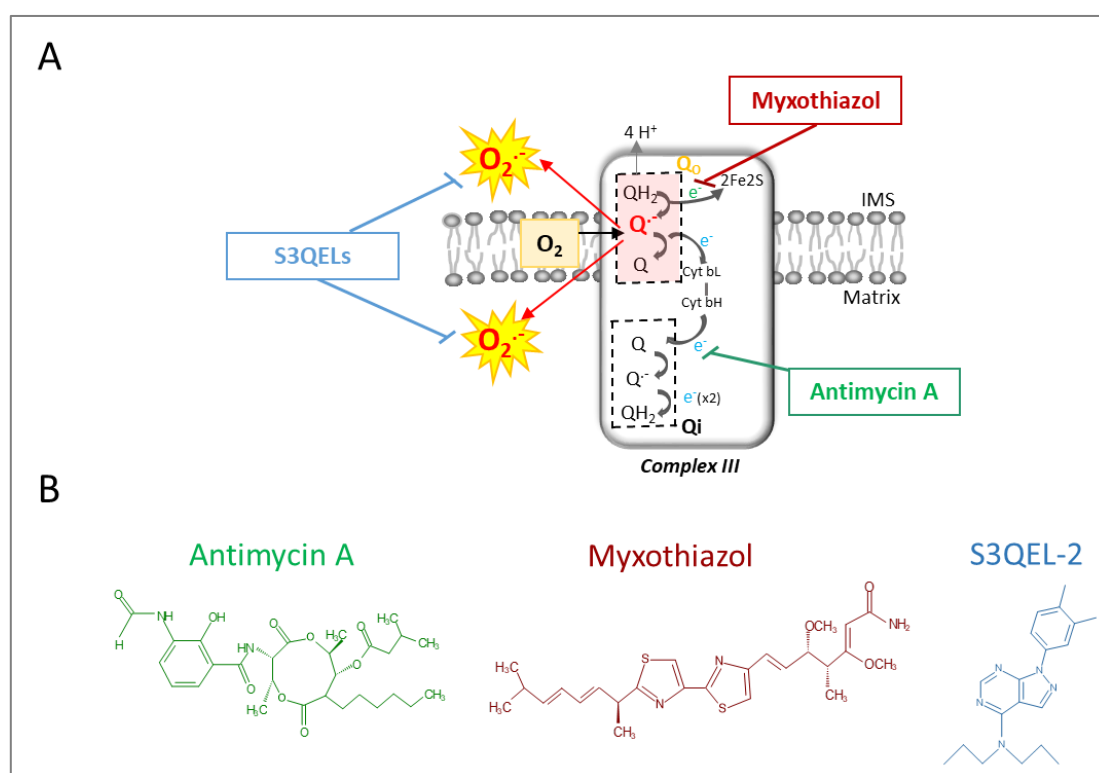


Figure 7. Mitochondrial complex III as source of ROS and target of the inhibitors Antimycin A, Myxothiazol and S3QEL-2. A) Schematic representation of the mechanism through which CIII Q_o site produces ROS. The target site of each inhibitor is shown; B) Molecular structures of the CIII inhibitors. cyt: cytochrome; CoQ: coenzyme Q; Q: semiquinone; Q[•]: semiquinone radical; QH₂: quinol.

2.2.2 ROS production by mG3PDH

mG3PDH is a ubiquinone-linked flavoprotein encoded in the nucleus and located in the outer surface of the mitochondrial inner membrane (Klingenberg 1970). In human the mG3PDH is encoded by the *GPD2* gene located on chromosome 2 (Mráček et al. 2014). The crystal structure of this protein is still unknown. mG3PDH acts in concert with the cG3PDH forming the glycerol 3-phosphate shuttle and it transfers electrons directly from glycerol 3-phosphate to the coenzyme Q within the electron transport chain (Figure 8A). In most mammalian tissues the mG3PDH

activity is low leading to a low glycerol 3-phosphate shuttle activity. However, the glycerol 3-phosphate shuttle is active in tissues that have high glycolytic rates such as thermogenic brown fat, brain and skeletal muscle (Cole et al. 1978; Cottingham and Ragan 1980).

In the pro-oxidative mitochondrial environment, mG3PDH is involved in superoxide anion formation which is then converted to H_2O_2 via superoxide-dismutase. The molecular mechanism of mG3PDH-dependent ROS production is not clear at yet (Mráček et al. 2014).

However, the finding that mG3PDH generates superoxide to both sides of the mitochondrial inner membrane in roughly equal proportions, suggests that the Q-binding site of this enzyme is mainly involved in superoxide production (Figure 8 D) (Mráček et al. 2013; Orr et al. 2012).

Recently, commercial available chemicals (iGP-1 and RH02211) have been proposed as mG3PDH inhibitors displaying an anti-oxidative potency (Figure 8) (Orr et al. 2014; Singh 2014; Hussain et al. 2017; Di Magno et al. 2020). Either iGP-1 (N-(4-(1H-Benzoimidazol-2-yl)-phenyl)-succinamic acid) and RH02211 (2,2-Dimethyl-5-nitro-2H-benzimidazole 1,3-dioxide) have benzimidazole motifs that are essential components for mG3PDH inhibition (Figure 8 B-C). Further, the benzimidazole ring system was proposed to be the best candidate for additional manipulations in order to improve both potency and selectivity of the compounds. In particular, the selectivity of the compounds could be improved by changing or removing the heteroatoms of the imidazole while both potency and selectivity could be improved by adding substituents to the ring system (Orr et al. 2014).

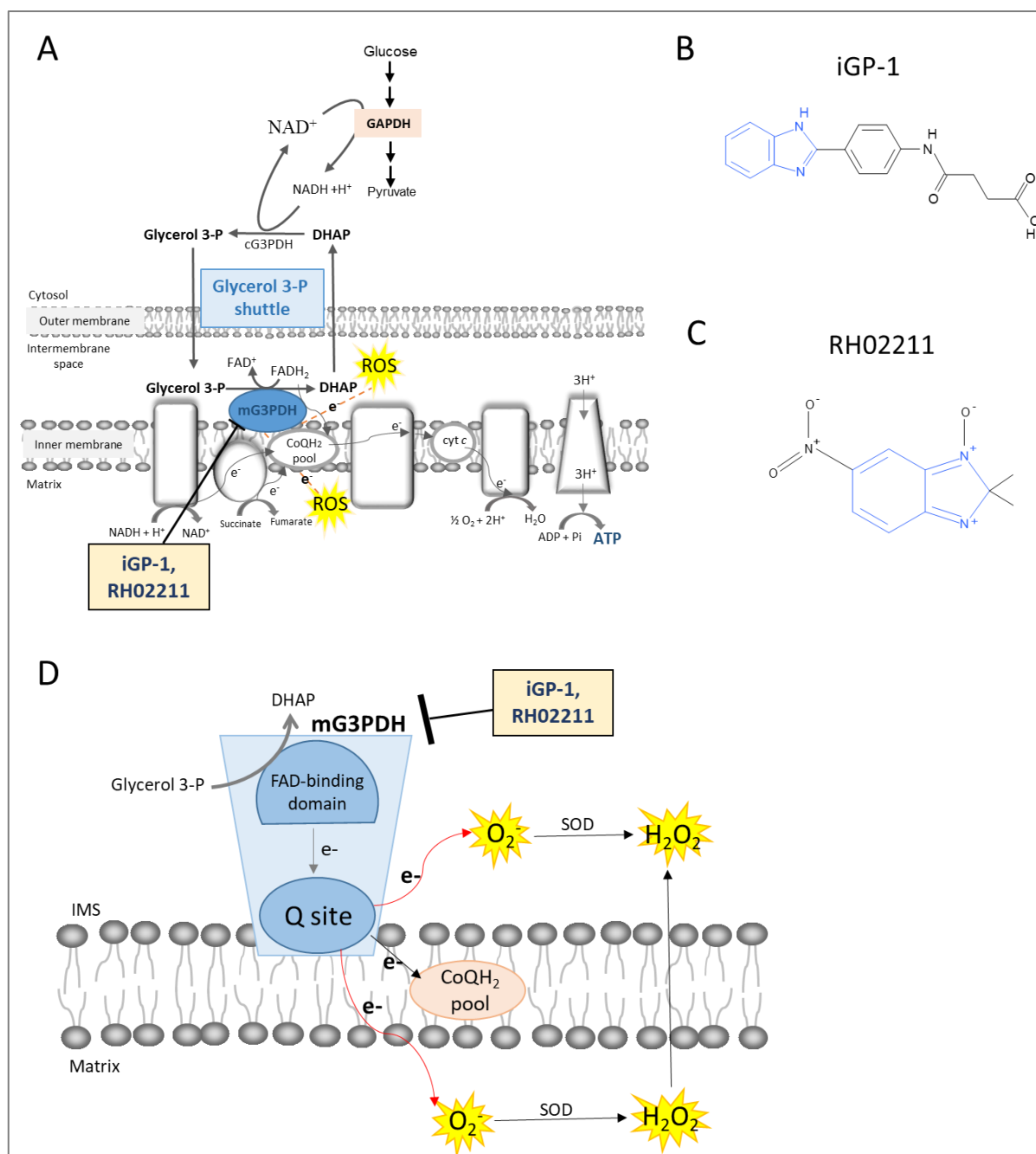


Figure 8. Mitochondrial glycerol 3-phosphate dehydrogenase as source of ROS and target of the inhibitors iGP-1 and RH02211. A) Mitochondrial respiratory chain with the mG3PDH as target of iGP-1 and RH02211; B) and C) Molecular structures of the mG3PDH inhibitors; D) Schematic representation of the mechanism through which mG3PDH produces ROS. The Q-site of the enzyme was proposed as the main ROS production site. Modified from Orr et al. 2012 and Mráček et al. 2013. ADP: adenosine diphosphate; ATP: adenosine triphosphate; cG3PDH: cytosolic glycerol 3-phosphate dehydrogenase; cyt: cytochrome; CoQ: coenzyme Q; DHAP: dihydroxyacetone phosphate; FAD⁺: flavin adenine dinucleotide; FADH₂: flavin adenine dinucleotide reduced; mG3PDH: mitochondrial glycerol 3-phosphate dehydrogenase; NAD⁺: nicotinamide adenine dinucleotide; NADH: nicotinamide adenine dinucleotide reduced; ROS: reactive oxygen species; SOD: superoxide dismutase; Q: semiquinone; Q[•]: semiquinone radical; QH₂: quinol.

2.2.3 Hypoxia

Highly aggressive and rapidly growing solid tumors are characterized by areas with reduced oxygen levels (hypoxic regions) which occur due to inadequate blood supply. Due to the rapid proliferation of cancer cells, the tumor quickly runs out of nutrients and oxygen supply from the normal vasculature and therefore becomes hypoxic (Carmeliet et al. 1998). This leads cancer cells nuclei to

upregulate a number of genes that should help to sustain the supply of oxygen such as erythropoietin which increases the erythrocytes proliferation and the angiogenic factor VEGF which induces the growth of new capillaries (Semenza and Wang 1992). Additional genes upregulated during hypoxia include those involved in the nutrients supply and therefore encoding the glycolytic enzymes and the glucose transporters Glut-1 and Glut-3 (Bunn and Poyton 1996). In hypoxic conditions the induction of all these genes is mediated by hypoxia-inducible factor-1 (HIF-1) which is a heterodimeric protein consisting of HIF-1 α and HIF-1 β subunits (Wang et al. 1995; Wang and Semenza 1995). While HIF-1 β subunit is constitutively expressed, HIF-1 α is regulated by the oxygen concentration. Indeed, under normoxic conditions HIF-1 α is ubiquitinated and degraded via proteasomal degradation due to the binding of the von Hippel-Lindau tumor suppressor protein (VHL) (Salceda and Caro 1997; Maxwell et al. 1999). Only when HIF-1 α is hydroxylated it is bound by VHL. The hydroxylation reaction is mediated by prolyl hydroxylases (PHDs) that need oxygen and α -ketoglutarate as substrates (Epstein et al. 2001). Therefore, under hypoxic conditions, hydroxylation and degradation cannot take place leading to an accumulation of HIF-1 α within the cytosol followed by translocation into the nucleus and dimerization with HIF-1 β , forming the active transcriptional complex HIF-1. To activate target genes, HIF-1 binds the hypoxia-responsive-elements (HRE) in the promoter regions of the genes and induces their expression (Figure 9).

Moreover, proteasomal degradation of HIF-1 α is inhibited by reactive oxygen and nitrogen species (Dewhirst et al. 2008; Semenza 2010a). In hypoxic conditions mitochondrial complex III is one of the major producers of ROS. Superoxide generated at complex III can enter the cytosol via anion channels located in the mitochondrial membranes or they can be dismutated by Mn-superoxide dismutase to H₂O₂ which then diffuse into the cytosol. H₂O₂ activates PI-3 kinases and phosphatases which act upstream of the ubiquitin/proteasome degradation step and lead to HIF-1 α stabilization (Chandel et al. 2000). HIF-1 α plays an important role in the glycolytic switch activating the transcription of genes encoding glucose transporters, glycolytic enzymes (i.e LDHA, M2-PK, PGK, HK) as well as preventing the conversion of pyruvate to acetyl coenzyme A which cannot be conveyed into the OXPHOS pathway (Semenza 2010b). Interestingly, in the nuclei of hypoxic cancer cells, the PHD3-dependent proline hydroxylated M2-PK physically interacts with the HIF-1 α transcription complex and co-regulates its own transcription through a positive feedback loop as well as it promotes HIF-1 transactivation of target glycolytic genes (i.e. Glut-1, LDHA) (Luo et al. 2011; Prakasam et al. 2018). Further, together with glycolysis also the reductive carboxylation of glutamine has been identified as an important metabolic pathway for cells survival in hypoxic conditions. Even if glutamine oxidation is decreased at low oxygen concentrations, HIF-1 and hypoxia promote the reductive carboxylation of glutamine to α -ketoglutarate and citrate,

through the activity of isocitrate dehydrogenase-1 (IDH1), promoting a reverse flux through the TCA cycle and lipogenesis (Metallo et al. 2012; Mullen et al. 2011).

Therefore, the active heterodimer HIF-1 allows cancer cells to not only survive but to continue to proliferate and metastasize even at low oxygen concentrations.

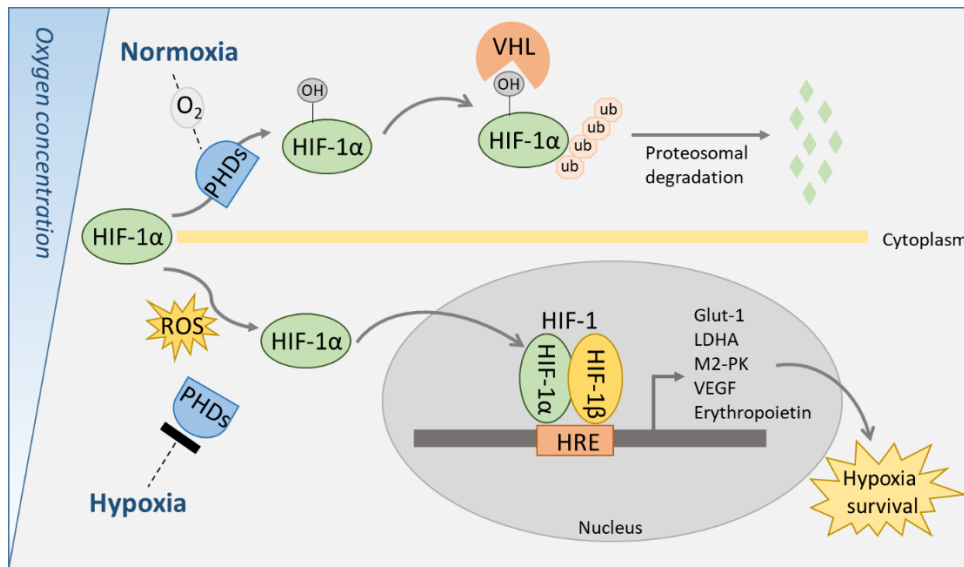


Figure 9. Schematic representation of the oxygen-dependent regulation of the hypoxia inducible factor 1 (HIF-1). Modified from Borsi et al. 2014. Glut-1: glucose transporter 1; HRE: hypoxia-responsive-elements; LDHA: lactate dehydrogenase A; M2-PK: pyruvate kinase M2; PHD: prolyl hydroxylases; ROS: reactive oxygen species; Ub: ubiquitin; VEGF: vascular endothelial growth factor; VHL: von Hippel-Lindau tumor suppressor protein.

3 Aim of the study

Tumor cell proliferation depends upon energy and cell building blocks, such as nucleic acids, amino acids and phospholipids which have to be provided by the metabolism of the cells. In proliferating cells and especially tumor cells the main pathways which meet both metabolic demands are glycolysis and glutaminolysis. Accordingly, most tumors are characterized by high glycolytic and glutaminolytic capacities. Energy production by glycolysis which is located in the cytosol is independent upon oxygen supply. Glutaminolysis recruits reaction steps of the citric acid cycle and partially takes place in the cytosol as well as the mitochondria. In contrast to glycolysis mitochondrial energy regeneration depends upon oxygen. Due to inadequate blood supply tumors very often are characterized by low oxygen pressure (from 0.2 to 4.2 %) (McKeown 2014). The expression of key glycolytic enzymes (i.e LDHA, M2-PK, PGK, HK) is induced by the hypoxic inducing factor 1 (HIF-1). HIF-1 contains a constitutively expressed subunit beta as well as a subunit alpha which is regulated by the oxygen pressure as well as H_2O_2 . Important sources of H_2O_2 are mitochondrial glycerol 3-phosphate dehydrogenase (mG3PDH) and mitochondrial complex III (CIII).

The aim of the present study was to investigate the impact of mG3PDH and CIII targeting on cell proliferation and metabolism of PC-3 prostate cancer cells. PC-3 cells are characterized by high mG3PDH activity (Chowdhury et al. 2005). As part of the glycerol 3-P shuttle mG3PDH is involved in the recycling of cytosolic NAD^+ , which is necessary to maintain high glycolytic conversion rates. In a first step the impact of two different published mG3PDH inhibitors (Orr et al. 2014; Singh 2014) and three different complex III inhibitors with different mode of actions (Orr et al. 2015; Xia et al. 1997) on the cell proliferation of PC-3 cells was investigated dependent upon oxygen supply. Furthermore, in the case of the mG3PDH inhibitors, the impact of extracellular pyruvate was taken under consideration since the conversion of pyruvate to lactate is another important mechanism to recycle cytosolic NAD^+ . Cancer patients are usually subject to cycling treatments that last several hours/days. In order to reproduce treatment protocols used in clinical settings, the effects of long incubation periods (96 hours) of PC-3 cells with the corresponding inhibitor were evaluated. Next IC_{50} and IC_{90} concentrations of the inhibitors were used to investigate the impact of the respective inhibitors on:

- Glycolytic and glutaminolytic conversion rates in the cell culture supernatants of the cells;
- Glycolytic isoenzyme equipment;
- Glycolytic enzyme complex;
- Oxygen consumption and H_2O_2 production;
- Intracellular metabolites.

4 Materials and Methods

4.1 Culture conditions and cell proliferation assays

The prostate cancer cell line PC-3 was purchased from CLS Cell Line Service GmbH, Eppelheim, Germany. The cells were cultured in DMEM-A14430 medium supplemented with 10% (v/v) fetal bovine serum (FBS superior from Biochrome, Berlin Germany), 15 mM glucose, 2 mM glutamine, 1% (v/v) streptomycin and penicillin (Gibco, Life Technologies, Paisley, UK) as well as 0.022 mM phenol red (Sigma-Aldrich, München, Germany). Since pyruvate in the medium may be an escape mechanism in the experiments with mG3PDH inhibitors, the experiments with the mG3PDH inhibitor RH02211 were carried out with and without pyruvate supplementation in the DMEM medium. In the experiments with pyruvate supplementation (pyruvate supplemented cells), the final pyruvate concentration in the medium was 2 mM. In the experiments without pyruvate supplementation (pyruvate starved cells), we determined a pyruvate concentration of 0.015 mM within the medium, which originated from the supplemented FBS.

The cells were cultured at 5% CO₂ at both 21% and 1.5% O₂ (In VivO₂, Baker Ruskinn, Sanford, Maine, USA). Compliance with the correct culture conditions was controlled in all experiments by the recordings of the hypoxic chamber.

All individual experiments were started with three days of pre-cultivation at 21% or 1.5% O₂ respectively without inhibitors. Thereafter, the cells were passaged under the respective oxygen condition. For the proliferation assays increasing concentrations of the respective inhibitors were supplemented into the medium at the time point of cell passage (Figure 10). Control cells were supplemented with DMSO for iGP-1, RH02211, Myxothiazol and S3QEL-2 treatments and with Ethanol for Antimycin A treatment. DMSO and Ethanol concentrations corresponded to the DMSO and Ethanol concentrations in the approaches with the highest drug concentrations. After 96 hours the vital cells were counted in presence of Trypan Blue (Sigma-Aldrich Chemie, München, Germany) by a cell counter (Countess II FL – Thermo Fisher Scientific - Life Technologies, Waltham, USA).

Sources of supply of the inhibitors used: iGP-1 (order no.: 530655, Merck, Sigma-Aldrich Chemie, München, Germany), RH02211 (order no.: RH02211SC, Thermo-Fisher Scientific, Schwerte, Germany), Antimycin A (order no.: A8674, Sigma-Aldrich Chemie, München, Germany), Myxothiazol (order no.: T5580, Sigma-Aldrich Chemie, München, Germany) and S3QEL-2 (order no.: Cay18556-25, Cayman Chemical, Biomol, Hamburg, Germany).

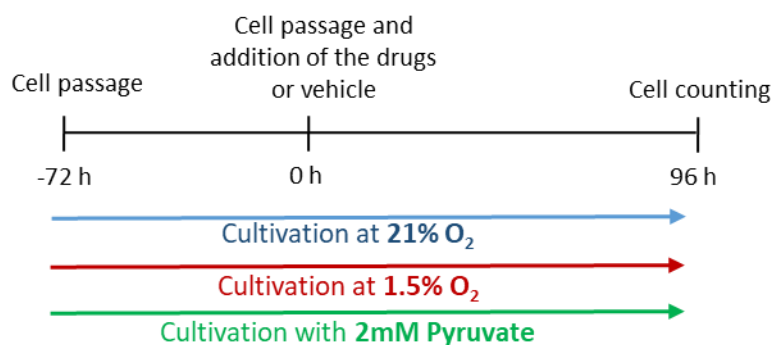


Figure 10. Cell cultivation scheme.

In the approaches with mG3PDH inhibitors cells were cultivated at 21% and 1.5% O₂ in the presence of 0.015 mM pyruvate (pyruvate starved cells) and in the presence of 2 mM pyruvate (pyruvate supplemented cells). In the approaches with complex III inhibitors cells were cultivated at 21% and 1.5% O₂ without pyruvate supplementation.

4.2 Glycolytic and glutaminolytic conversion rates

At the beginning of the test series, 20,000 cells were seeded in exactly one milliliter of cultivation medium on four 24-well plates (one plate/24 hours). In order to determine metabolic conversion rates, the cell culture supernatants were collected every 24 hours and immediately frozen at -80°C (Figure 11). The cells were removed from the wells with Gibco® Trypsin/EDTA (Gibco, Life Technologies, Paisley, UK) and counted in the presence of trypan blue with a cell counter (Countess II FL – Thermo Fisher Scientific - Life Technologies, Waltham, USA).

For determination of the metabolic rates the frozen medium supernatants were heated for 15 min at 95 °C and subsequently centrifuged at 8000 x g for 5 min. Lactate, pyruvate, alanine, serine, glutamine, and glutamate conversion rates (Table 1) were measured according to Bergmeyer 1974 as well as glucose rates were measured using a commercially available test (Diasys Greiner, Flacht, Germany). The concentrations of all metabolites were determined photometrically at a wavelength of 340 nm and 37 °C using the Respons® 920 bench top clinical analyzer (Diasys Greiner, Flacht, Germany).

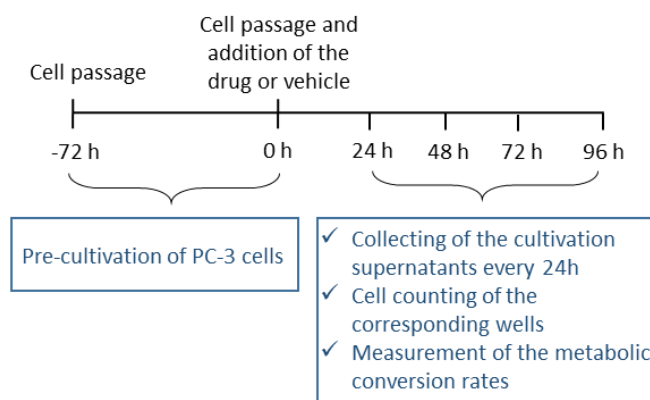


Figure 11. Design of the flux experiments.

Table 1. List of enzymatic reactions used to determine the metabolites concentrations.

G6PDH: glucose 6-phosphate dehydrogenase; GLDH: glutamate dehydrogenase; GPT: glutamate-pyruvate transaminase; HK: hexokinase; LDH: lactate dehydrogenase.

Glucose + ATP $\xrightarrow{\text{HK, MgCl}_2}$ Glucose 6-phosphate + ADP	
Glucose 6-phosphate + NAD ⁺ $\xrightarrow{\text{G-6P-DH}}$ Gluconate 6-phosphate + NADH+H ⁺	
Lactate + NAD ⁺ + Hydrazine $\xrightarrow{\text{LDH}}$ Pyruvate-Hydrazone + NADH+H ⁺ + H ₂ O	
Pyruvate + NADH + H ⁺ $\xrightarrow{\text{LDH}}$ Lactate + NAD ⁺	
Glutamate + H ₂ O + NAD ⁺ $\xrightarrow{\text{GLDH}}$ 2-Oxoglutarate + NADH+H ⁺ + NH ₄ ⁺	
Glutamine + H ₂ O $\xrightarrow{\text{Glutaminase}}$ Glutamate + NH ₃	
Glutamate + H ₂ O + NAD ⁺ $\xrightarrow{\text{GLDH}}$ 2-Oxoglutarate + NADH+H ⁺ + NH ₄ ⁺	
Serine $\xrightarrow{\text{Periodate}}$ Glyoxylate + Formaldehyde	
Glyoxylate + NADH + H ⁺ $\xrightarrow{\text{GLDH}}$ Glycolate + NAD ⁺	
Alanine + 2-Oxoglutarate $\xrightarrow{\text{GPT}}$ Pyruvate + Glutamate	
Pyruvate + NADH + H ⁺ $\xrightarrow{\text{LDH}}$ Lactate + NAD ⁺	

4.2.1 Calculation of the metabolic conversion rates

The conversion rates of each metabolite were determined taking into consideration the incubation time (24 hours), the mean cell density (given in 10⁴ cells) and the incubation volume/well (1 ml). The rates could then be calculated using the following formula:

$$\frac{\text{nmol}}{h \cdot 10^4 \text{ cells}} = \left(\frac{\bar{x}_{\text{metabolite } tx} \left(\frac{\mu\text{mol}}{\text{ml}} \right) - x_{i \text{ } tx+24} \left(\frac{\mu\text{mol}}{\text{ml}} \right)}{24 (h) \cdot \overline{\text{CD}} (10^4 \text{ cells})} \right) \cdot 1 \text{ ml} \cdot 1000$$

$\bar{x}_{\text{metabolite } tx}$ = mean value of the corresponding metabolite concentration at time point x of cultivation (X = 24 or 48 or 72 hours)

$x_{i \text{ } tx+24}$ = metabolite concentration after tx hours of cultivation + 24

$\overline{\text{CD}}$ = mean cell density, $(\text{CD}_{tx} + \overline{\text{CD}}_{tx-24})/2$

The factor 1000 refers to the conversion from μmol to nmol.

4.3 Isoelectric focusing

4.3.1 Principle of the method

Isoelectric focusing (IEF) is an electrophoretic technique which separates proteins that differ in their isoelectric point (pI). The pI is specific for each protein and it is defined as the pH at which the protein has a net neutral charge state. By applying a high voltage proteins migrate, according to their charge, in the direction of the anode or cathode through a pH gradient established with a mixture of carrier ampholytes, which in turn align themselves in the electrical field according to

their pI. As each protein of the cell extracts reaches the position where the pH is equal to its pI, it precipitates. At the beginning of the focusing, the high current flow (about 20 mA) indicates the active migration and alignment of the carrier ampholytes and proteins. Once all ampholytes and proteins precipitate, at the end of the focusing, the current flow drops to approximately 1 mA (Burgaud et al. 1992; Stekhoven et al. 2008). The IEF technique is also used to study the association of proteins within a complex, since the proteins charge changes when they are associated with other proteins (Mazurek et al. 1996).

4.3.2 Carrying out the isoelectric focusing

1.5×10^6 cells were seeded in 15 cm culture dishes. One day after passage the mitochondrial CIII and the mG3PDH inhibitors were supplemented into the medium. Control cells were mock-treated with the corresponding vehicle concentration (DMSO or Ethanol). After two additional cultivation days in the presence of the inhibitors or vehicles, cells were extracted as following. Once the cultivation medium was removed, the adherently cells were washed with cold PBS and frozen at $-80\text{ }^{\circ}\text{C}$ for 1 hour. Thereafter, the cells were scraped in a homogenization buffer containing 10 mM Tris, 1mM EDTA- Na_4 , 1 mM NaF and 1 mM mercaptoethanole, pH 7.4. Using a pistil-glass homogenizer it was obtained a cell suspension which was then centrifuged for twenty minutes at 47,000 g and $4\text{ }^{\circ}\text{C}$. The cytosolic extract (supernatant) was then frozen at $-80\text{ }^{\circ}\text{C}$.

The IEF was carried out with a linear gradient of glycerin (60 to 0% (v/v)) and ampholytes (pI 3.5 - 10.5) (Table 2). The column was run at 400 V for the first hour and 1,200 V for the remainder of 23 h with $4\text{ }^{\circ}\text{C}$ cooling water. When all proteins had reached their isoelectric point (current flow about 1 mA), the content of the column was collected in 1.5 ml fractions via a peristaltic pump. The isoelectric points of the proteins were determined by measuring the pH values in the individual fractions. In the fractions enzyme activities were measured using the Respons® 920 bench top clinical analyzer.

Table 2. Composition of the solutions used for the IEF (Rauschenbach 2017).

Solutions	Composition	Function
Anode solution	150 ml Glycerine; 3.45 ml 85% (v/v) ortho-phosphoric acid; MilliQ water up to 250 ml	Establishes contact with the column anode wire. The glycerol content of the anode solution was 60%.
Intermediate solution	2.75 ml Glycerine; 29 µl Ampholyte pH 4-7; 56 µl Ampholyte pH 3-10; 56 µl Ampholyte pH 6-8; 84 µl Ampholyte pH 8.0-10.5; MilliQ water up to 5 ml	Prevents direct contact of the sample proteins with the acidic anode solution and thus denaturation of the proteins. The glycerol content of the intermediate solution was 55%.
Heavy solution	20 ml Glycerine; 260 µl Ampholyte pH 4-7; 500 µl Ampholyte pH 3-10; 500 µl Ampholyte pH 6-8; 750 µl Ampholyte pH 8.0-10.5; Sample (volume depending upon cells number) x ml; MilliQ water up to 41 ml	Using a gradient mixer, the heavy ampholyte solution containing glycerin was mixed with the light ampholytic solution without glycerin and slowly layered over the intermediate solution. Then the final glycerol gradient was between 48% and 24%.
Light solution	260 µl Ampholyte pH 4-7; 500 µl Ampholyte pH 3-10; 500 µl Ampholyte pH 6-8; 750 µl Ampholyte pH 8.0-10.5; MilliQ water up to 40 ml	
Cathode solution	750 µl Ampholyte pH 8.0-10.5; MilliQ water up to 7.5 ml	Makes contact with the cathode wire of the column. The glycerol content of the anode solution was 0%.

4.3.3 Measurement of enzyme activities

The enzyme activities (Table 3) were measured photometrically at a wavelength of 340 nm and 37 °C using the Respons® 920 bench top clinical analyzer (Diasys Greiner, Flacht, Germany) according to Bergmeyer 1974.

Table 3. List of enzymatic reactions used to measure enzyme activities.

ADP: adenosine diphosphate; ATP: adenosine triphosphate; DHAP: dihydroxyacetone phosphate; dTDP: deoxythymidine diphosphate; dTTP: deoxythymidine triphosphate; GAP: glyceraldehyde 3-phosphate; GAPDH: glyceraldehyde 3-phosphate dehydrogenase; G3PDH: glycerol 3-phosphate dehydrogenase; GOT: glutamate oxaloacetate transaminase; LDH: lactate dehydrogenase; MDH: malate dehydrogenase; NAD⁺: nicotinamide adenine dinucleotide; NADH: nicotinamide adenine dinucleotide reduced; NDPK: nucleoside-diphosphate kinase; PEP: phosphoenolpyruvate; PGM: phosphoglycerate mutase; PGK: phosphoglycerate kinase; PK: pyruvate kinase; TIM: triose-phosphate isomerase.

Aldolase:	$\text{Fructose 1,6-bisphosphate} + \text{H}_2\text{O} \xrightarrow{\text{Aldolase}} \text{GAP} + \text{DAPH}$ $\text{GAP} \xrightarrow{\text{TIM}} \text{DAPH}$ $2 \text{ DAPH} + 2 \text{ NADH} + \text{H}^+ \xrightarrow{\text{G3PDH}} \text{Glycerol 3-P} + 2 \text{ NAD}^+$
GAPDH:	$3\text{-Phosphoglycerate} + \text{ATP} \xrightarrow{\text{PGK}} 1,3\text{-Bisphosphoglycerate} + \text{ADP}$ $1,3\text{-Bisphosphoglycerate} + \text{NADH} + \text{H}^+ \xrightarrow{\text{GAPDH}} \text{GAP} + \text{NAD}^+ + \text{Phosphate}$
GOT:	$2\text{-Oxoglutarate} + \text{Aspartate} \xrightarrow{\text{GOT}} \text{Glutamate} + \text{Oxaloacetate}$ $\text{Oxaloacetate} + \text{NADH} + \text{H}^+ \xrightarrow{\text{MDH}} \text{Malate} + \text{NAD}^+$
LDH:	$\text{Pyruvate} + \text{NADH} + \text{H}^+ \xrightarrow{\text{LDH}} \text{Lactate} + \text{NAD}^+$
MDH_(ox):	$\text{Oxaloacetate} + \text{NADH} + \text{H}^+ \xrightarrow{\text{MDH}_{(ox)}} \text{Malate} + \text{NAD}^+$
MDH_(ma):	$\text{Malate} + \text{NAD}^+ \xrightarrow{\text{MDH}_{(ma)}} \text{Oxaloacetate} + \text{NADH} + \text{H}^+$
NDPK:	$\text{dTDP} + \text{ATP} \xrightarrow{\text{NDPK}} \text{dTTP} + \text{ADP}$ $\text{ADP} + \text{PEP} \xrightarrow{\text{PK}} \text{ATP} + \text{Pyruvate}$ $\text{Pyruvate} + \text{NADH} + \text{H}^+ \xrightarrow{\text{LDH}} \text{Lactate} + \text{NAD}^+$
PGK:	$3\text{-Phosphoglycerate} + \text{ATP} \xrightarrow{\text{PGK}} 1,3\text{-Bisphosphoglycerate} + \text{ADP}$ $1,3\text{-Bisphosphoglycerate} + \text{NADH} + \text{H}^+ \xrightarrow{\text{GAPDH}} \text{GAP} + \text{NAD}^+ + \text{Phosphate}$
PGM:	$3\text{-Phosphoglycerate} \xrightarrow{\text{PGM}} 2\text{-Phosphoglycerate}$ $2\text{-Phosphoglycerate} \xrightarrow{\text{Enolase}} \text{PEP} + \text{H}_2\text{O}$ $\text{PEP} + \text{ADP} \xrightarrow{\text{PK}} \text{Pyruvate} + \text{ATP}$ $\text{Pyruvate} + \text{NADH} + \text{H}^+ \xrightarrow{\text{LDH}} \text{Lactate} + \text{NAD}^+$
PK:	$\text{PEP} + \text{ADP} \xrightarrow{\text{PK}} \text{Pyruvate} + \text{ATP}$ $\text{Pyruvate} + \text{NADH} + \text{H}^+ \xrightarrow{\text{LDH}} \text{Lactate} + \text{NAD}^+$

4.3.4 Calculation of total (Vmax) enzyme activity

The activities of the complete cell extracts were determined as volume activities (Unit/ml) at 340 nm and 37 °C using the Respos® 920 bench top clinical analyzer (Diasys Greiner, Flacht, Germany). Thereafter, the total enzyme activity (Vmax) was determined normalizing the complete cell extract activity with the sample volume and the cell number loaded into the IEF column using the following formula:

$$v_{max} \left(\frac{\text{Unit}}{10^6 \text{ cells}} \right) = \left(\frac{\text{enzyme activity of the total extract} \left(\frac{\text{Unit}}{\text{ml}} \right) * \text{volume loaded into the column (ml)}}{\text{cells applied} (10^6)} \right)$$

4.3.5 Determination of the isoenzymes equipment

The isoenzymes equipment of the enzymes with several expressed isoforms was determined by the comparison each other of the sum of the single peak areas (AUC = Area Under the Curve). The AUC is given in %.

4.4 Protein quantification

The colorimetric biuret assay was used to quantify the protein concentration in the total cell extracts (Gornall et al. 1949). The principle of this technique, specific for peptides and proteins, is based on the formation of a purple complex when substances with two or more peptide bonds reacts with Cu^{2+} ions in an alkaline solution. The absorbance produced is proportional to the protein concentration and can be measured photometrically at 546 nm. The quantification was carried out using Respos 920 bench top clinical analyser at 37 °C.

4.5 Gel permeation

4.5.1 Principle of the method

Gel Filtration or Gel Permeation Chromatography is a size exclusion chromatography, a technique in which the separation of components is based on the difference in molecular weight or size. The column used (HiLoad 26/60 Superdex 200 prep grade from GE Healthcare Bio-Sciences AB, Uppsala, Sweden) is made up of a composite matrix of dextran and highly cross-linked agarose used as stationary phase, while an elution buffer (composition details in section 4.5.2) was used as mobile phase. The basis of the separation is that the molecules of the samples were pumped through the microporous of the column and the molecules above a certain size are totally excluded from the pores, while smaller molecules access the interior of the pores partly or wholly. The flow of the mobile phase hence will cause larger molecules to pass through the column unhindered, without penetrating the gel matrix, whereas smaller molecules will be retarded according to their penetration of the gel.

4.5.2 Carrying out the gel permeation

Cells were prepared as described in the above section 4.3.2 except that the lysis and elution buffer contained 100 mM Na_2HPO_4 / NaH_2PO_4 buffer, 0.2 % (v/v) methanol, 1 mM sodium fluoride (NaF), 10% (v/v) glycerine, 50 mM sodium chloride (NaCl), 1 mM 1,4-dithiothreitol (DTT), 1 mM ϵ -aminocaproic acid, 0.2 mM phenylmethylsulfonylfluoride (PMSF) and 1 mM mercaptoethanol according to (Mazurek et al. 1996). The homogenates were passed over a gel permeation column (HiLoad 26/60 Superdex 200 prep grade from GE Healthcare Bio-Sciences AB, Uppsala, Sweden). The elution rate was 1.5 mL/min. Pyruvate kinase activities were measured using Respos® 920 bench top clinical analyzer from Diasys Greiner, Frick, Germany at a wavelength of 340 nm and 37 ° C. Details about enzymes measurement and protein quantification can be found in the above sections 4.3.3 and 4.4.

4.6 Oxygen consumption and hydrogen peroxide production by high-resolution respirometry

4.6.1 Principle of the method

4.6.1.1 Oxygen consumption

High-resolution respirometry (HRR) through the O2k-FluoRespirometer (Oroboros Instruments, Innsbruck, Austria) allows to monitor in a closed chamber the oxygen consumed by a biological sample over time. The principle of the method is polarography, the oxygen concentration is measured by a Clark type polarographic oxygen sensor (POS). The POS consists of a gold cathode, a silver/silver chloride anode and a KCl electrolyte reservoir separated from the analyte by a 25 μm O_2 - permeant membrane that excludes ions and other potential reductants. With application of a polarization voltage (0.8 V) between anode and cathode when oxygen is consumed a current [A] is obtained as an amperometric signal, which is converted to a voltage [V] (raw signal). Indeed, the dissolved O_2 diffuses through the membrane from the stirred medium, containing the biological sample, to the cathode where it is reduced to water by electrons, yielding a hydroxide that forms KOH. The resulting Cl^- is drawn to the anode where it precipitates with silver to form AgCl. This system provides a current which is proportional to O_2 partial pressure. The latter is converted to oxygen concentration, knowing the oxygen solubility in the experimental medium used (Gnaiger 2008). The oxygen flux per volume and flow per cell [$\text{amol} \times \text{s}^{-1} \times \text{cell}^{-1}$] are calculated from the O_2 concentration time-derivative real-time by the software DatLab 7.4.

4.6.1.2 Hydrogen peroxide production

In HRR the hydrogen peroxide production is measured by the combination of the O2k-FluoRespirometer with the Amplex UltraRed method. The use of Amplex UltraRed in HRR allows

to simultaneously measure the respiration and the H₂O₂ flux. In the presence of horseradish peroxidase, the Amplex UltraRed reagent reacts in a 1:1 stoichiometry with H₂O₂ to produce the red fluorescent compound resorufin. The change of emitted fluorescence intensity is directly proportional to the concentration of the H₂O₂ produced. Insertion of fluorescence sensors (Smart Fluo-Sensor Green) through the front window of the O2k-glass chambers permits to measure hydrogen peroxide production by an amperometric method. The Smart Fluo-Sensor Green is composed by an excitation LED filter (wavelength 525 nm) and a photodiode with an emission filter (wavelength 587 nm, red) which converts the absorbed light into electrical current. The fluorescence slope [mV/s] is automatically calculated by the software DatLab 7.4 from the raw fluorescence signal [V] of the resorufin. A background H₂O₂ calibration together with several H₂O₂ titrations are necessary to check the sensitivity to H₂O₂ of the Amplex UltraRed assay that changes during the experiment. SOD is used to dismutate superoxide into H₂O₂, which can be measured by the assay. The iron chelator DTPA is also included in the medium to avoid ROS production related to contaminating iron (Krumshnabel et al. 2015; Komlódi et al. 2018).

4.6.2 Carrying out the oxygen consumption and hydrogen peroxide production measurements

Cells were cultivated for 96 hours in the presence of the respective inhibitor (mG3PDH inhibitor RH02211, complex III inhibitors Antimycin A, Myxothiazol or S3QEL-2) and as well as with the corresponding vehicles (DMSO or Ethanol). Thereafter, PC-3 cells were trypsinized, counted (Countess II FL – Thermo Fisher Scientific - Life Technologies, Waltham, USA) and re-suspended in PBS. To measure O₂ consumption and H₂O₂ production, the O2k-FluoRespirometer (Oroboros Instruments, Innsbruck, Austria) was used. $0.7 \cdot 10^6$ cells/ml were added into in the O2k chambers containing 2 ml of mitochondrial respiration medium (MiR05-Kit from Oroboros Instruments, Innsbruck, Austria) which contained 15 μ M diethylenetriaminepentaacetic acid (DTPA), 5 U/ml superoxide dismutase, 1 U/ml horseradish peroxidase. During the measurements, the oxygen concentration within the chambers was kept between 30 and 60 μ M. At the beginning of the measurements, the oxygen concentration within the chambers was lowered with N₂ gas, while re-oxygenation of the chambers during the measurements was done by opening the O2k stoppers. The following final concentrations of the chemicals were used to measure oxygen consumption and H₂O₂ production: 10 μ M Amplex UltraRed, 0.5 μ M rotenone, 10 mM glycerophosphate, 10 mM succinate, 2.5 mM adenosine diphosphate (ADP), 10 μ g/ml digitonin, 15 nM oligomycin, 1-3 μ M CCCP, 2.5 μ M antimycin A. The corresponding inhibitor/vehicle concentrations used during the 96 hours of incubation were also titrated into the O2k chambers at the beginning of each measurement in order to keep the same inhibitory/control conditions also during the

measurements. At the end of the measurements, higher inhibitors concentrations than those titrated at the beginning of each measurement were added at the experimental chambers containing the control samples as well as the treated cells, which also received a further titration of the inhibitors completing 30 μM RH02211, 10 nM AA, 10 nM Myx or 30 μM S3QEL-2 respectively. The O2k-Software DatLab 7, specifically developed for HRR with the O2k-FluoRespirometer, was used for data acquisition and analysis.

Description of the respiratory states (Figure 12 A) (Gnaiger 2020).

ROUTINE: Routine Respiration (ROUTINE) in living cells is the physiological coupled state controlled by cellular energy demand, energy turnover and the degree of coupling to phosphorylation. In cell culture media ROUTINE is supported by exogenous substrates while in media without energy substrates, ROUTINE depends on endogenous substrates of the cells. ROUTINE respiration was measured directly after the placement of 0.7×10^6 cells/ml into in the O2k chambers containing mitochondrial respiration medium (MiR05-Kit) but no exogenous substrates.

ROX: Residual Oxygen Consumption (ROX) is the respiration due to oxidative side reactions remaining after inhibition of the electron transfer-pathway, achieved by titration of Rotenone (inhibitor of the mitochondrial CI) to living cells, or Antimycin A (CIII inhibitor) to permeabilized cells. All mitochondrial respiratory states were corrected using ROX as the baseline state.

OXPHOS: The OXPHOS state (from oxidative phosphorylation) is characterized by the oxidation of reduced fuel substrate (i.e. glycerophosphate or succinate) by electron transfer to oxygen, coupled to the phosphorylation of ADP to ATP. The OXPHOS state provides a measure of the respiratory capacity of mitochondria at saturating concentrations of ADP, inorganic phosphate, oxygen, and defined reduced substrates. In the protocol used, the OXPHOS state started when digitonin was titrated into the O2k chambers in the presence of ADP and either glycerophosphate or succinate as substrate. Digitonin is a mild detergent that permeabilizes plasma membranes selectively due to their high cholesterol content, whereas mitochondrial membranes with lower cholesterol content were not affected with this concentration. The optimum digitonin concentration (10 $\mu\text{g}/\text{ml}$) required to PC-3 cells plasma membrane permeabilization was determined by a separate respirometric protocol.

LEAK: LEAK state (from proton leak) is a respiratory state that arises by oligomycin induced inhibition of ATP synthase which is due to a blocking of proton channels which are necessary for the phosphorylation of ADP to ATP. In this non-phosphorylating resting state, the electrochemical

proton gradient increases to a maximum, thus also decreasing respiration. 15 nM oligomycin was used as optimal concentration able to induce the LEAK state in permeabilized PC-3 cells.

ET: The electron transfer state (ET) is the result of an experimentally induced uncoupling of the electron transport and ADP-phosphorylation at maximal stimulation of the respiration chain. In our experiments carbonyl cyanide m-chlorophenyl hydrazine (CCCP) was used as uncoupler and titrated in concentrations from 1 – 3 μM .

H₂O₂ flux measurements in OXPHOS, LEAK and ET states (Figure 12 B)

O₂ and H₂O₂ fluxes were measured simultaneously by following the titration steps of the protocol described in section 4.6.2. This protocol allows to measure H₂O₂ fluxes in permeabilized cells, therefore H₂O₂ production rates were measured in OXPHOS, LEAK and ET states (ROUTINE and ROX states as well as the RH02211 titration are included in figure 11 B only to show the complete titration steps of the protocol).

H₂O₂ fluxes may be influenced by the mitochondrial (mt) membrane potential, which can be tested since it varies among the different respiratory states. After addition of the fuel substrates (i.e. glycerophosphate or succinate), the addition of ADP in permeabilized cells partially depolarises the mt-membrane leading to the decrease of the H₂O₂ flux. Thereafter oligomycin, which induces a LEAK state by inhibiting ATP synthase, hyperpolarises the mt-membrane which can result in increased H₂O₂ production. Finally, the addition of the uncoupler CCCP, a protonophore, decreases the mt-membrane potential-linked H₂O₂ generation due to the dissipation of the electrochemical proton gradient.

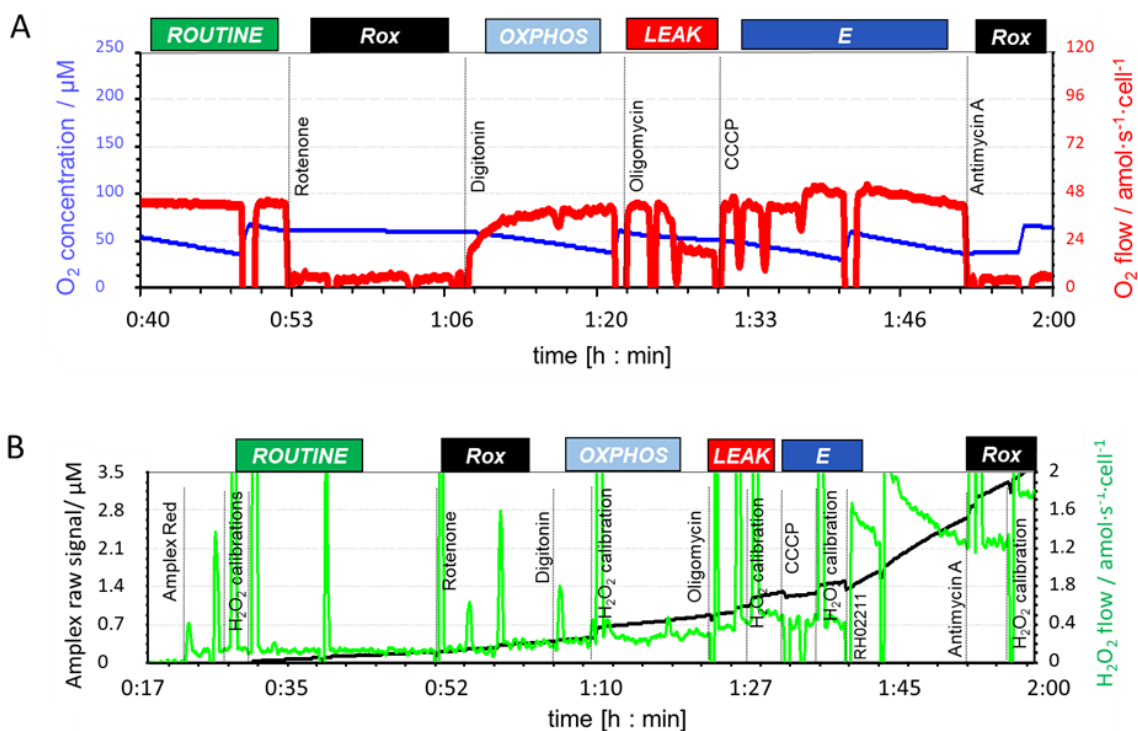


Figure 12. Representative traces of PC-3 cells using the O2k-FluoRespirometer. A) Changes in the oxygen flow (red line) through the different respiratory states (upper boxes). The oxygen concentration is also shown (blue line); B) Changes in the H₂O₂ flow (green line) through the different respiratory states. The Amplex raw signal (black line) is also shown.

4.7 Mass spectrometry

PC-3 cells were passaged and cultivated as described in chapter 4.1. For intracellular metabolite measurements 2×10^5 cells were seeded in 6-well plates. One day after passage $7 \mu\text{M}$ RH02211 were supplemented into the medium. Control cells were mock-treated with 0.0035% DMSO. Three wells from each condition were used to estimate cell number after incubation as well as at time point of cell extraction. Intracellular metabolites were extracted after 24 hours of incubation with $7 \mu\text{M}$ RH02211 as well as with 0.0035% DMSO. To extract intracellular metabolites, cell plates were placed on wet ice and washed twice with cold PBS. Thereafter the cell plates were placed on dry ice and $200 \mu\text{L}$ of MEB/ 10^6 cells was added to each well. After 15 minutes of incubation on dry ice, the cells were scraped. Intracellular fractions were incubated in a thermomixer at max speed for 15 minutes at $4 \text{ }^\circ\text{C}$ and then incubated for 1 hour at $-20 \text{ }^\circ\text{C}$. Proteins were then pelleted by centrifuging samples at 13000 rpm for 10 minutes at $4 \text{ }^\circ\text{C}$ and supernatants were transferred into glass vials and stored at $-80 \text{ }^\circ\text{C}$ until further analysis.

The determination of the intracellular metabolite concentrations by LC-MS was performed at the Medical Research Council Cancer Unit, University of Cambridge, Hutchison/MRC Research Centre, Box 197, Cambridge CB2 0XZ, United Kingdom.

LC-MS chromatographic separation of metabolites was achieved using a Millipore Sequant ZIC-pHILIC analytical column ($5 \mu\text{m}$, $2.1 \times 150 \text{ mm}$) equipped with a $2.1 \times 20 \text{ mm}$ guard column

(both 5 mm particle size) with a binary solvent system. Solvent A was 20 mM ammonium carbonate, 0.05% ammonium hydroxide; Solvent B was acetonitrile. The column oven and autosampler tray were held at 40 °C and 4 °C, respectively. The chromatographic gradient was run at a flow rate of 0.200 mL/min as follows: 0–2 min: 80% B; 2–17 min: linear gradient from 80% B to 20% B; 17–17.1 min: linear gradient from 20% B to 80% B; 17.1–22.5 min: hold at 80% B. Samples were randomized and analyzed with LC–MS in a blinded manner with an injection volume of 5 µL. Pooled samples were generated from an equal mixture of all individual samples and analyzed interspersed at regular intervals within sample sequence as a quality control.

Metabolites were measured with a Thermo Scientific Q Exactive Hybrid Quadrupole-Orbitrap Mass spectrometer (HRMS) coupled to a Dionex Ultimate 3000 UHPLC. The mass spectrometer was operated in full-scan, polarity-switching mode, with the spray voltage set to +4.5 kV/-3.5 kV, the heated capillary held at 320 °C, and the auxiliary gas heater held at 280 °C. The sheath gas flow was set to 25 units, the auxiliary gas flow was set to 15 units, and the sweep gas flow was set to 0 unit. HRMS data acquisition was performed in a range of $m/z = 70–900$, with the resolution set at 70,000, the AGC target at 1×10^6 , and the maximum injection time (Max IT) at 120 ms. Metabolite identities were confirmed using two parameters: (1) precursor ion m/z was matched within 5 ppm of theoretical mass predicted by the chemical formula; (2) the retention time of metabolites was within 5% of the retention time of a purified standard run with the same chromatographic method. Chromatogram review and peak area integration were performed using the Thermo Fisher software Tracefinder 5.0 and the peak area for each detected metabolite was normalized against the total ion count (TIC) of that sample to correct any variations introduced from sample handling through instrument analysis. The normalized areas were used as variables for further statistical data analysis.

4.8 Statistical analysis

The statistical analysis for comparison of IC_{50} and IC_{95} values for inhibition of cell proliferation as well as the flux measurements was performed in cooperation with Dr. Klaus Failing, the official statistician of the Faculty of Veterinary Medicine Giessen using (Dixon 1993).

The statistical analysis for evaluating the impact of extracellular pyruvate on cell proliferation was performed by the Student's t-test with Mann-Whitney test using GraphPad Prism 9 (San Diego, CA, USA). Unpaired Student's t-test was performed by using GraphPad Prism 9 to evaluate the significance of total enzymes activities (V_{max}) as well as of the composition of the isoenzyme equipment (AUC). The statistical analysis for O_2 consumption and H_2O_2 production measurements was performed in cooperation with Oroboros Instruments, Innsbruck, Austria. The O_2 consumption and H_2O_2 production results correspond to the median values with interquartile

range. The data were analyzed using GraphPad Prism 8 (San Diego, CA, USA). The Student's t-test with Mann-Whitney test was used for non-parametrical data analysis.

4.8.1 IC_{50} – IC_{90} – IC_{95} values

AA and Myx. A logistic equation model incorporating a baseline was fitted to the proliferation data by non-linear regression using the logarithm of the drug doses as the independent variable (program BMDPAR). The resulting equation was solved for the desired cell number reduction. By the maximum likelihood method an estimate and asymptotic standard error of the interesting parameter $\log(IC_{50})$ was determined. Additionally, the 95% confidence limits of $\log IC_{50}$ and $\log IC_{95}$ were computed. Then the statistical comparison of the estimated values between drugs resp. normoxia vs. hypoxia was done by the asymptotic u-test. In the last step of the computation the logarithmic confidence limits were retransformed to the original dose scale.

RH02211 with 0.015 mM pyruvate. A logistic equation model incorporating a baseline was fitted to the proliferation data using the square root transformation of the drug doses as the independent variable (program BMDPAR). The resulting equation was solved for the desired cell number reduction. By the maximum likelihood method an estimate and asymptotic standard error of the interesting parameter was determined. Then the statistical comparison of the estimated values between drugs resp. normoxia vs. hypoxia was done by the asymptotic u-test.

S3QEL-2 and RH02211 with 2 mM pyruvate. A logistic equation model via non-linear regression method was fitted to the proliferation data. In this case, both, the incorporation of a baseline as well as transformation of the drug dose were not necessary to get a good fit of the model to the data. Again, the resulting equation was solved for the desired cell number reduction. By the maximum likelihood method an estimate and asymptotic standard error of the interesting parameters was determined.

Then the statistical comparison of the estimated values between drugs resp. normoxia vs. hypoxia was done by the asymptotic u-test.

4.8.2 Metabolic conversion rates

Due the dependencies upon cell density of the metabolic conversion rates, the values of the controls and treated cells were adjusted to the global mean cell density (except by three groups comparison for RH02211) using one way analysis of covariance (ANCOVA) either using a linear model (original values used) or an exponential model (logarithmic transformed data used in the analysis). ANCOVA tests the homogeneity of the slopes and the cell number dependency as well as the differences between adjusted means. In cases where the slopes were not statistically different, the result of the test of differences between adjusted means out of the ANCOVA was used. In

such cases where the slopes were significantly different, the adjustment at the same mean cell density was done by application of individual slopes. For comparison of two groups, t-Tests were performed, using the manually adjusted values (resulting by differing slopes). For comparison of three groups (for RH02211, comparison between control, 7 μ M and 16 μ M with correction to the mean cell density of 16 μ M) one-way ANOVA (analysis of variance) + Tukey Test were carried out.

4.8.3 Intracellular metabolites

The statistical analysis for evaluating the impact of RH02211 on intracellular PC-3 cells metabolites was performed by Wilcoxon Test using the statistical software package SAS 9.4 (SAS® Institute Inc. 2013). The Wilcoxon Test was performed since the data did not show a normal distribution and it was not possible to find an appropriate transformation in order to fit a normal distribution. The data are shown as median with minimal and maximal values.

The significance level was set to $p < 0.05$.

5 Results

5.1 Targeting mitochondrial glycerol 3-phosphate dehydrogenase

Two commercially available substances iGP-1 and RH02211, published as mG3PDH inhibitors (Singh 2014; Orr et al. 2014), have been tested on PC-3 prostate cancer cell proliferation and metabolism.

5.1.1 Impact of iGP-1 on PC-3 cell proliferation

The effect of iGP-1 was tested on PC-3 cells proliferation in the presence of 21% O₂ and 0.015 mM pyruvate within the cultivation media (low pyruvate cultivation conditions = pyruvate starved cells). After an incubation time of 96 hours the iGP-1 induced an about 45% inhibition of cell proliferation which was independent upon the inhibitor dosage (100 – 400 μM) (Figure 13).

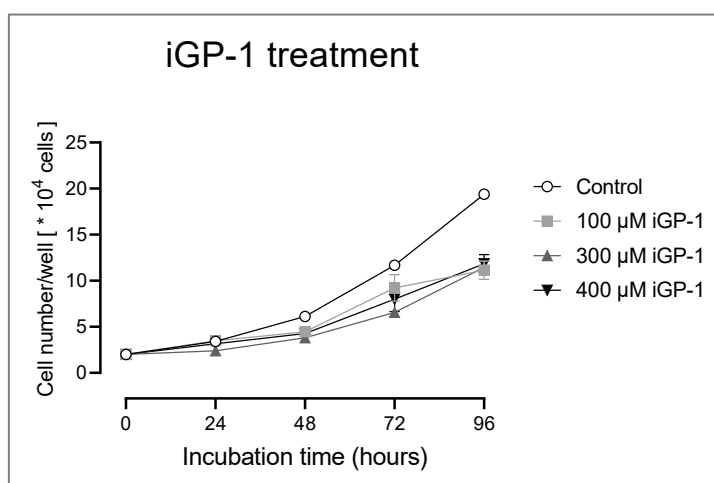


Figure 13. Inhibition of PC-3 cell proliferation by iGP-1.

Cell number at $t_0 = 2 \cdot 10^4$ cells/well. Control cells were mock-treated with 0.25% (v/v) DMSO which corresponds to the DMSO amount necessary to dissolve 400 μM iGP-1. Results are shown as mean values \pm Standard Error of the Mean (SEM). Number of technical replicates ≥ 3 .

5.1.2 Impact of iGP-1 on glycolytic and glutaminolytic metabolic conversion rates of PC-3 cells

300 μM iGP-1, which induced about 45% inhibition of cell proliferation, was chosen as inhibitory concentration to supplement to PC-3 cells in order to investigate the impact of iGP-1 on the metabolic conversion rates. Glycolytic and glutaminolytic conversion rates in cell culture supernatants were characterized by a clear dependency upon cell density in both control as well as iGP-1 inhibited cells (Figure 14). Accordingly, cell density dependencies were taken under consideration in the statistical analysis when conversion rates were compared between control and iGP-1 treated cells (Figure 15).

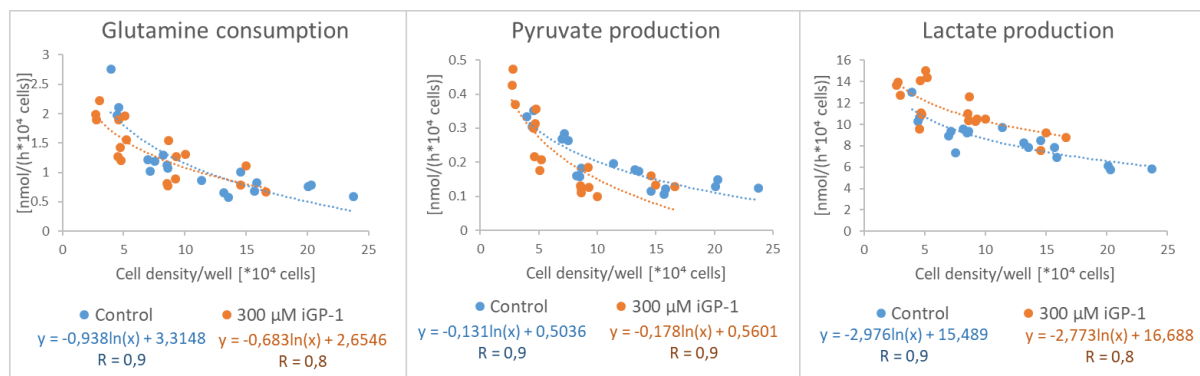


Figure 14. Cell density dependencies of the metabolic turnover rates in mock-treated control and iGP-1 inhibited PC-3 cells using the example of glutamine, pyruvate and lactate.

After passing, the cells were cultivated for 4 days. Every 24 hours, the cultivation supernatant from individual cultivation dishes was preserved for the analysis of the metabolites. In parallel the cell number of the well in question was counted. DMSO 0.2% (v/v) and iGP-1 were added to the cultivation medium directly when passing out.

iGP-1 treated cells were characterized by a significant increase in glucose consumption and lactate production as well as by a significant decrease in glutamate production when compared to controls. On the contrary, iGP-1 did not modify the turnover rates of pyruvate, glutamine, alanine and serine (Figure 15).

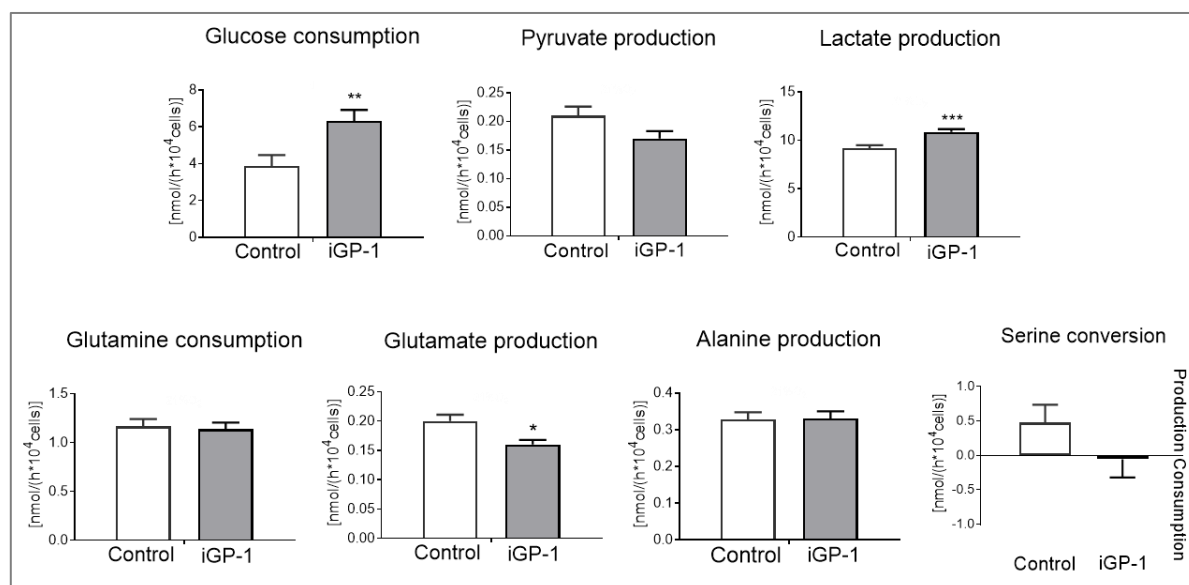


Figure 15. Metabolic conversion rates measured in the cultivation supernatants of mock-treated control and iGP-1-treated PC-3 cells. iGP-1 concentration = 300 μM , DMSO concentration = 0.2% (v/v).

Due to cell density dependencies (compare Figure 14) for the statistical comparison, the turnover rates of the control and iGP-1 treated cells were adjusted to a global mean cell density. In case of exponential cell density dependencies, the metabolic fluxes were logarithmically transformed. The bar graphs show $\bar{x} \pm \text{SEM}$ (Standard Error of the Mean). Back transformed conversion rates: pyruvate, glutamine and glutamate. * $p \leq 0,05$ ** $p \leq 0,01$ and *** $p \leq 0,001$ versus control. $n = 18$.

5.1.3 Impact of RH02211 on cell proliferation and metabolism of PC-3 cells

5.1.3.1 Impact of RH02211 on cell proliferation of PC-3 cells depending upon oxygen pressure and pyruvate concentration in the medium

Since very high iGP-1 concentrations were needed to inhibit 45% of PC-3 cell proliferation (Figure 13), the additional substance RH02211, published as inhibitor of mG3PDH by Sing in 2014, was selected for further studies.

In contrast to iGP-1, RH02211 dosages between 1 μ M and 20 μ M induced a dose dependent complete inhibition of PC-3 cell proliferation. The impact of RH02211 on cell proliferation was investigated at 21% O₂ as well as at 1.5% O₂ since mG3PDH is channeling electrons into the mitochondrial respiratory chain.

The IC₅₀ and IC₉₀ values indicate that oxygen concentrations did not significantly modify the impact of RH02211 on PC-3 cell proliferation (Table 4). Therefore, all following experiments with RH02211 were performed only in the presence of 21% O₂.

Table 4. IC₅₀ and IC₉₀ values of RH02211 in PC-3 cells depending upon oxygen pressure and pyruvate concentrations in the medium. UL= Upper Limits, LL= Lower Limits, n = number of samples.

	IC ₅₀ (μ M)						IC ₉₀ (μ M)						
	21% O ₂			1.5% O ₂			21% O ₂			1.5% O ₂			
	IC ₅₀ value	UL	LL	IC ₅₀ value	UL	LL	IC ₉₀ value	UL	LL	IC ₉₀ value	UL	LL	
RH02211													
+ 0.015 mM Pyruvate	6.1 (n=63)	7.5	4.9	7.9 (n=76)	8.9	7	17.7 (n=63)	24.3	12.1	32.4 (n=76)	37.1	28.0	
RH02211													
+ 2 mM Pyruvate	9.4 (n=48)	10.5	8.3	9.3 (n=54)	10.4	8.1	20.6 (n=48)	23.2	18.0	26.5 (n=54)	30.5	22.6	

Whereas the oxygen pressure did not modify the inhibitory capacity of RH02211 on PC-3 proliferation, the pyruvate concentration in the medium had a significant influence on it.

A significant increase ($p = 0.02$) of the IC₅₀ value of RH02211 was found when PC-3 cells were cultivated in the presence of 2 mM pyruvate in comparison to cultivation in the presence of 0.015 mM pyruvate.

Investigation of the impact of pyruvate on untreated proliferating PC-3 cells revealed a 17% increase of cell proliferation in pyruvate supplemented cells when compared to cells cultured at low pyruvate concentrations. The impact of 0.015 mM and 2 mM pyruvate on PC-3 cell proliferation was tested at both 21% O₂ and 1.5% O₂ (Figure 16). Pyruvate supplementation (2 mM) within the cultivation medium induced an increase of cell proliferation after 96 hours of cultivation independently upon the oxygen supply.

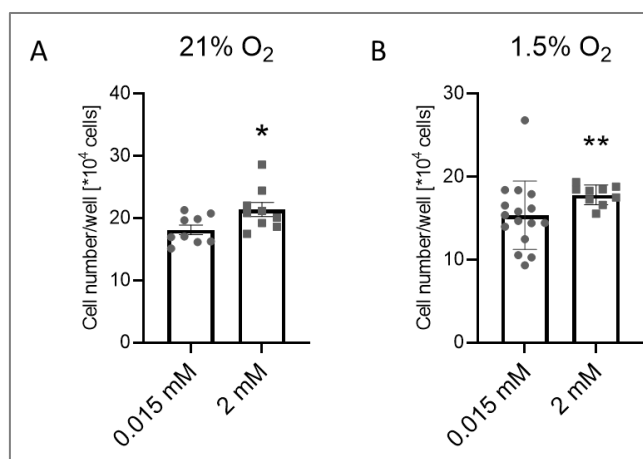


Figure 16. Impact of 0.015 mM and 2 mM pyruvate on PC-3 cell proliferation at 21% O₂ (A) and 1.5% O₂ (B). Data are shown as $\bar{x} \pm \text{SEM}$ (Standard Error of the Mean). * $p \leq 0,05$ and ** $p \leq 0,01$. $n \geq 9$.

The impact of pyruvate supplementation within the culture medium was also investigated on the iGP-1-induced inhibition of PC-3 cell proliferation in the presence of 21% O₂. After an incubation time of 96 hours both 300 μM and 400 μM iGP-1 induced an about 20% inhibition of cell proliferation which was independent upon the inhibitor dosage and lower than the 45% of growth inhibitory observed for iGP-1 in pyruvate starved medium (Figure 17).

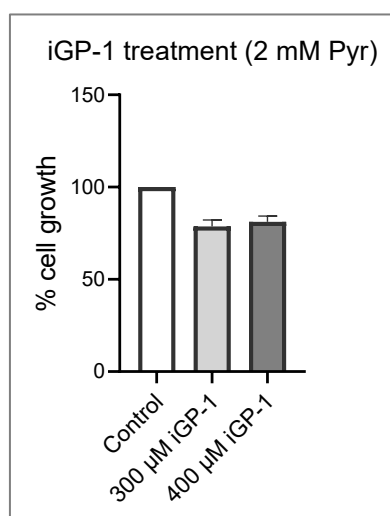


Figure 17. Inhibition of PC-3 cell proliferation by iGP-1 in the presence of 2 mM pyruvate. Cell number at $t_0 = 2 \cdot 10^4$ cells/well. Control cells were mock-treated with 0.25% (v/v) DMSO which corresponds to the DMSO amount necessary to dissolve 400 μM iGP-1. Results are shown as means \pm SEM, $n = 6$.

5.1.3.2 Reversibility of RH02211-induced inhibition of PC-3 cell proliferation

The inhibitory effect of RH02211 on pyruvate-starved PC-3 cell proliferation was completely reversible when RH02211 was supplemented in a concentration of 7 μM (IC₅₀), while PC-3 cells treated with 16 μM (IC₉₅) reached about half of the cell density of the corresponding mock-treated cells (Figure 18).

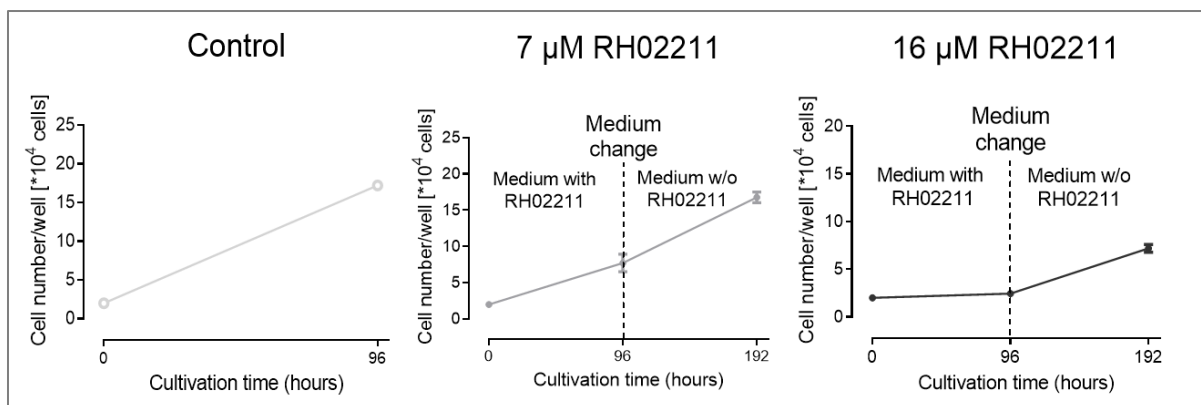


Figure 18. Reversibility of RH02211 induced inhibition of cell proliferation.

After 96 hours of cell cultivation in the presence of RH02211, the medium was replaced with medium without inhibitor. After another 96 hours, the cells were counted. RH02211 concentrations tested: 7 μ M which corresponds to the IC_{50} value and 16 μ M which corresponds to the IC_{90} value of RH02211. Control cells were mock-treated with 0.008 % (v/v) DMSO which corresponds to the DMSO concentration applied when RH02211 was supplemented in a concentration of 16 μ M. Data are presented as mean values \pm SEM. number of samples = 3.

5.1.3.3 Dose dependent impact of RH02211 on the glycolytic and glutaminolytic conversion rates in pyruvate starved PC-3 cells

When PC-3 cells were cultivated in pyruvate starved medium, RH02211 induced a dose dependent increase in glucose consumption, lactate production, glutamine consumption, glutamate and alanine production (Figure 19). Similar to the iGP-1 induced increase of the glycolytic conversion rates, the increase in glucose consumption and lactate production points to an increase of glycolysis in RH02211 treated cells. The decrease in glutamate production together with the simultaneous increase in glutamine consumption indicates that less glutamine was infiltrated into the citric acid cycle in pyruvate starved RH02211 treated cells while iGP-1 treatment mainly induced the channeling of glutamine into the citric acid cycle.

Pyruvate and serine conversion rates were not impaired in RH02211 treated PC-3 cells similarly to PC-3 cells treated with iGP-1.

In contrast to iGP-1, RH02211 induced an increase in alanine production in PC-3 treated cells (Figure 19).

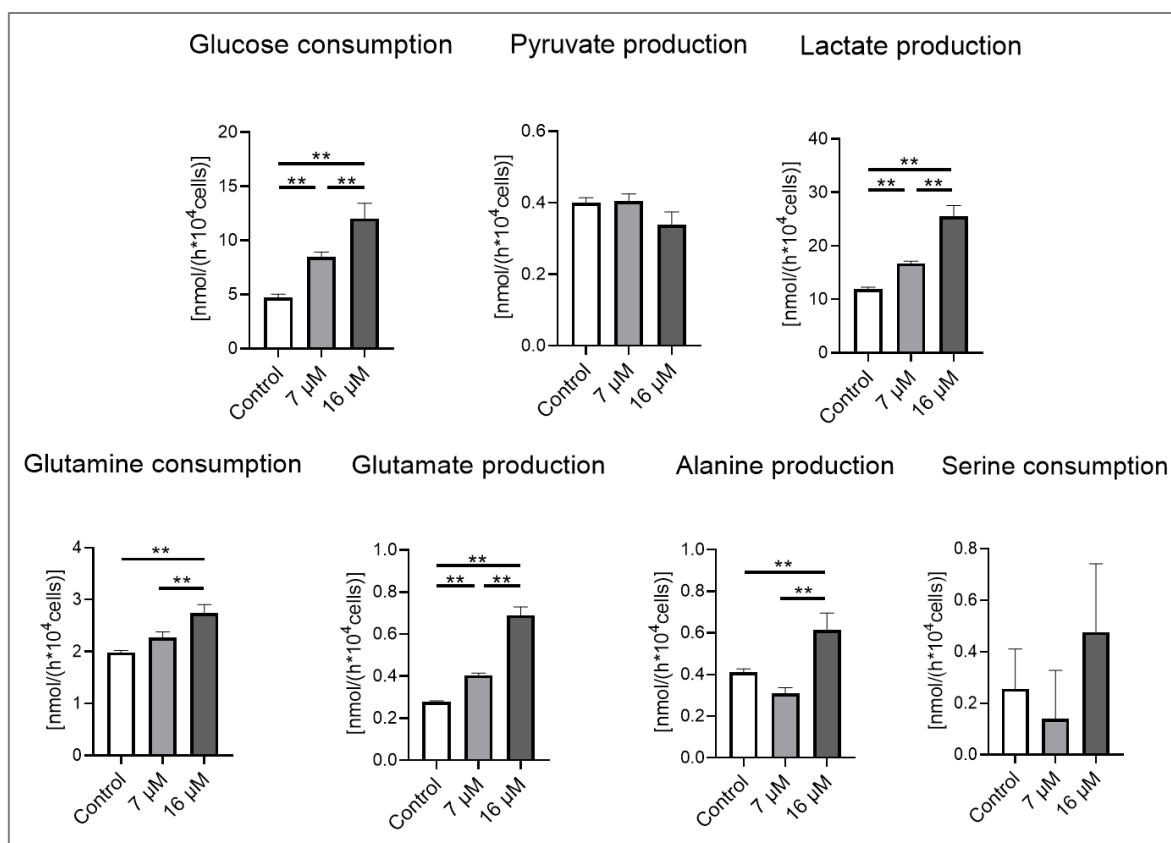


Figure 19. Dose dependent impact of RH02211 on the glycolytic and glutaminolytic conversion rates in pyruvate starved PC-3 cells cultivated at 21% O₂.

7 μM corresponds to the IC₅₀ value, 16 μM corresponds to the IC₉₀ value for inhibiting cell proliferation by RH02211 in pyruvate starved medium. Control cells were mock treated with 0.008% (v/v) DMSO which corresponds to the DMSO concentration supplemented together with 16 μM RH02211. Due to cell density dependencies for the statistical comparison, the turnover rates of the control and RH02211 treated cells were adjusted to a global mean cell density. In case of exponential cell density dependencies, the metabolic fluxes were logarithmically transformed. The bar graphs show $\bar{x} \pm \text{SEM}$ (Standard Error of the Mean). All conversion rates were back transformed except serine. ** $p \leq 0,01$. Number of values per group: $n \geq 17$ (control), $n = 18$ (7 μM RH02211), $n \geq 16$ (16 μM RH02211).

5.1.3.4 Impact of pyruvate on the glycolytic and glutaminolytic conversion rates of PC-3 cells

In order to investigate the impact of extracellular pyruvate on the metabolism of PC-3 untreated cells, 2 mM pyruvate was supplemented into the cultivation medium. PC-3 control cells induced a shift from production of pyruvate to consumption of extracellular pyruvate when cultivated in pyruvate supplemented medium indicating a severe impact of extracellular pyruvate on the metabolism of the cells (Figure 20). The decrease of glucose, lactate, glutamine and glutamate conversion rates indicates that both glycolytic and glutaminolytic fluxes were significantly downregulated in pyruvate supplemented PC-3 cells. Furthermore, extracellular pyruvate induced an increase of serine consumption while alanine production did not change.

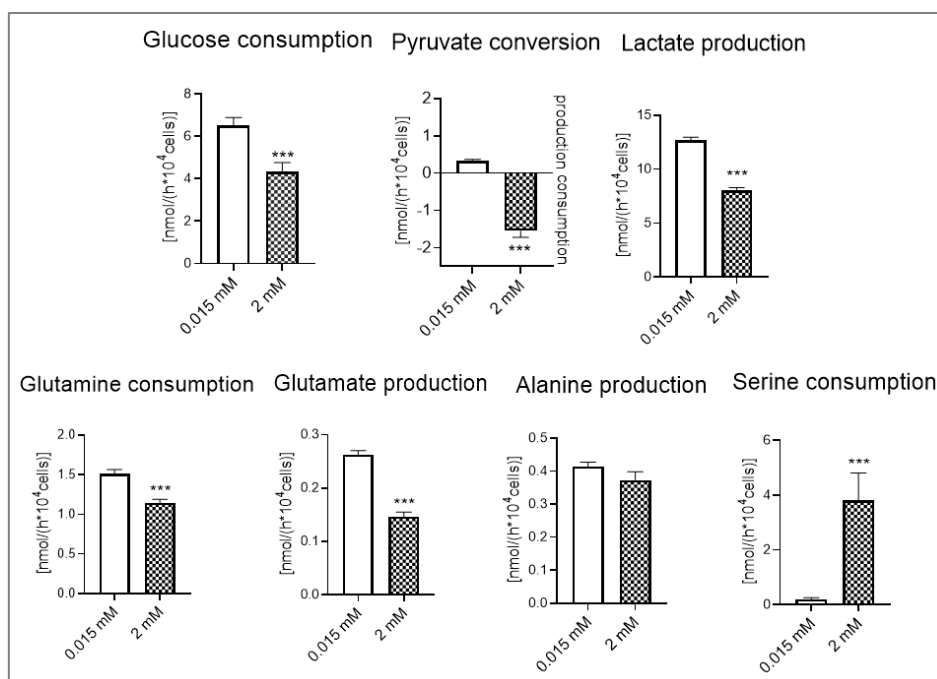


Figure 20. Metabolic flux rates of PC-3 cells depending upon the pyruvate concentration in the medium.

Due to cell density dependencies for the statistical comparison, the turnover rates of the control and RH02211 treated cells were adjusted to a global mean cell density. In case of exponential cell density dependencies, the metabolic fluxes were logarithmically transformed. The bar graphs show $\bar{x} \pm$ SEM (Standard Error of the Mean). Back transformed conversion rate: glutamine. *** $p \leq 0,001$ versus control pyruvate-supplemented cells. Number of values per group: $n = 18$ (0.015 mM Pyruvate), $n \geq 17$ (2 mM Pyruvate).

5.1.3.5 Impact of RH02211 on the glycolytic and glutaminolytic conversion rates depending upon the pyruvate concentration in the medium

The higher IC_{50} concentration of RH02211 required to inhibit PC-3 cell proliferation when cells were grown in pyruvate supplemented medium in comparison to the pyruvate starved ones (Table 4), led us to investigate the impact of the inhibitor RH02211 on the metabolism of pyruvate supplemented cells. The unchanged glucose consumption and lactate production rates indicate that RH02211 did not increase glycolysis in pyruvate supplemented cells in contrast to the pyruvate starved ones (Figure 21). The increase of glutamate production together with the unchanged glutamine conversion rates point to an impairment of glutaminolysis by RH02211 independently upon pyruvate concentration within the cultivation medium. Interestingly RH02211 did not affect the pyruvate conversion rates (consumption in pyruvate supplemented cells and production in pyruvate starved cells).

In pyruvate supplemented RH02211 treated cells the extracellular pyruvate was not used for serine degradation as suggested by the decrease in serine consumption rates (Figure 21).

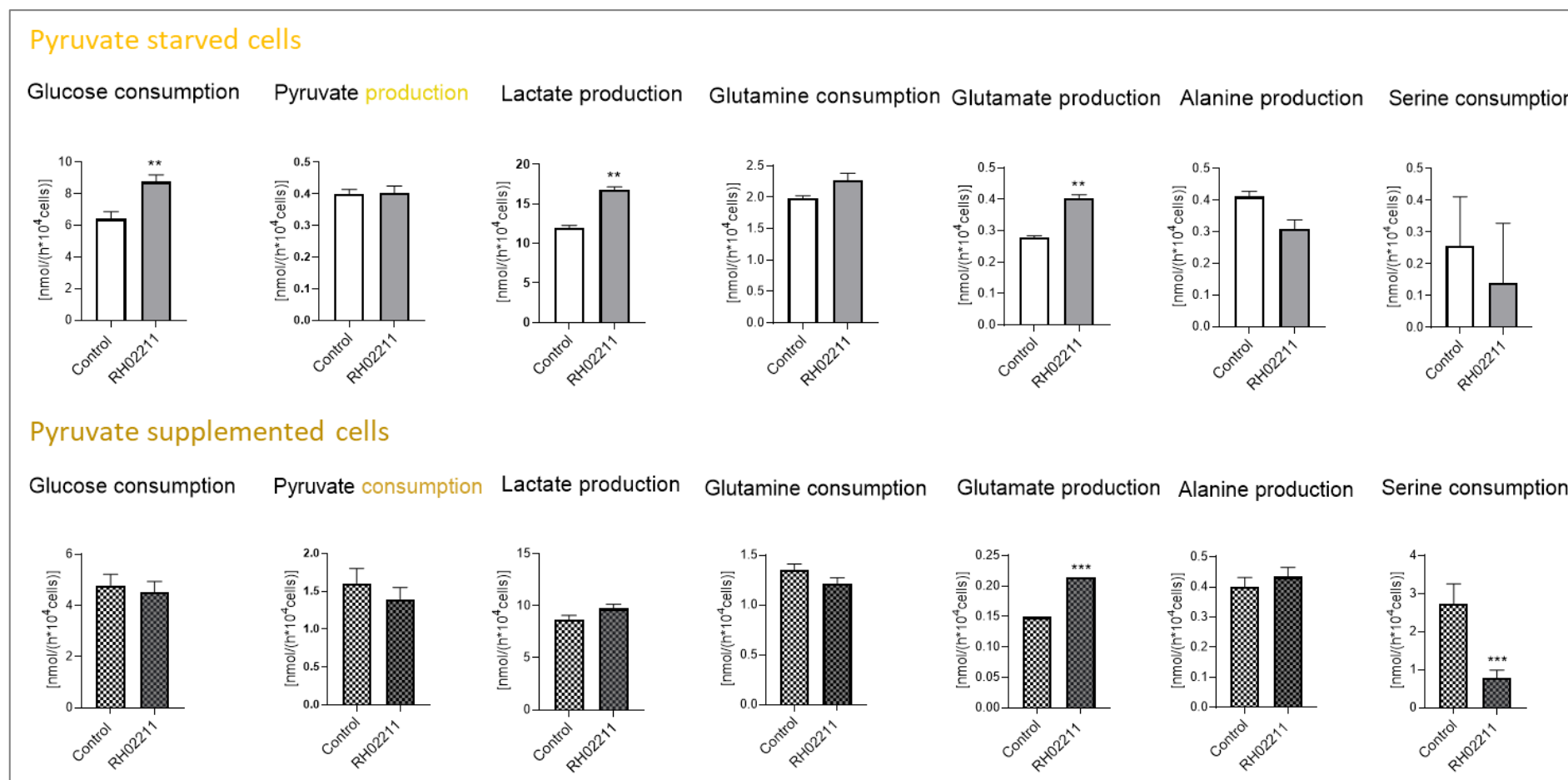


Figure 21. Impact of 7 μM RH02211 on the glycolytic and glutaminolytic conversion rates in PC-3 cells depending upon the presence or absence of pyruvate in the medium. 7 μM corresponds to the IC_{50} value for inhibiting cell proliferation by RH02211 in pyruvate starved medium. Control cells were mock treated with 0.0035% (v/v) DMSO which corresponds to the DMSO concentration supplemented together with 7 μM RH02211. Pyruvate concentration in pyruvate supplemented cells = 2 mM; in pyruvate starved cells = 0.015 mM. Due to cell density dependencies for the statistical comparison, the turnover rates of the control and RH02211 treated cells were adjusted to a global mean cell density. In case of exponential cell density dependencies, the metabolic fluxes were logarithmically transformed. The bar graphs show $\bar{x} \pm \text{SEM}$ (Standard Error of the Mean). Back transformed conversion rates: pyruvate, lactate, glutamine, glutamate and serine in pyruvate starved cells; pyruvate, glutamine and serine in pyruvate supplemented cells. ** $p \leq 0,01$ and *** $p \leq 0,001$ versus control cells. Number of values per group ≥ 17 .

5.1.3.6 Impact of pyruvate and RH02211 on LDH, MDH and GOT isoenzymes as well as the glycolytic enzyme complex

Free flow isoelectric focusing was used to investigate the impact of extracellular pyruvate and RH02211 on the isoenzyme equipment of lactate dehydrogenase (LDH), glutamate oxaloacetate transaminase (GOT) and malate dehydrogenase (MDH) as well as the glycolytic enzyme complex in PC-3 cells cultivated at 21% O₂.

mG3PDH is part of the glycerol 3-P shuttle which transports hydrogen from the cytosol into the mitochondria thereby recycling cytosolic NAD⁺ for an active GAPDH reaction.

Two other mechanisms of cytosolic NAD⁺ regeneration are lactate dehydrogenase as well as the malate aspartate shuttle (Figure 4).

The different LDH isoenzymes are characterized by different isoenzymes. In pyruvate starved PC-3 cells the IEP were: homotetramer H4: 5.6; homotetramer M4: 9.0; hybrids H1M3, H2M2, H3M1: 6.6). In pyruvate starved PC-3 cells the distribution of the isoenzymes (H4 : Hybrids : M4) was 22% : 44% : 34%.

Neither pyruvate supplementation nor 16 μM RH02211 significantly influenced the LDH isoenzyme equipment in PC-3 cells (Table 5).

Table 5. Impact of extracellular pyruvate and RH02211 (16 μM) on the isoenzyme equipment of lactate dehydrogenase (LDH), malate dehydrogenase (MDH) and glutamate oxaloacetate transaminase (GOT) as measured by free flow isoelectric focusing. Control cells were mock treated with 0.008% (v/v) DMSO which corresponds to the DMSO concentration supplemented together with 16 μM RH02211. Cyto = cytosolic isoenzyme, mito = mitochondrial isoenzyme, prec = precursor of the mitochondrial isoenzyme. AUC = area under the curve.

	AUC (%)								
	LDH			GOT		MDH			
	<i>H-type</i> IEP: 5.6	<i>Hybrid</i> IEP: 6.6	<i>M-type</i> IEP: 9.0	<i>Cyto</i> IEP: 5.9	<i>Mito</i> IEP: 9.6	<i>Cyto</i> IEP: 5.4	<i>Prec</i> IEP: 7.9	<i>Mito</i> IEP: 9.6	
Control (0.015 mM pyruvate)	22	49	29	21	79	50	38	12	
	22	43	35	29	71	39	43	18	
	21	41	38	17	83	40	35	25	
$\bar{x} \pm \text{SEM}$	22 ± 0.3	44 ± 2.4	34 ± 2.6	22 ± 3.5	78 ± 3.5	43 ± 3.5	39 ± 2.3	18 ± 3.7	
Control (2 mM pyruvate)	18	42	40	17	83	49	37	15	
	17	46	37	39	61	37	44	19	
RH02211 (0.015 mM pyruvate)	14	42	43	23	77	100	-	-	
	18	44	38	25	75	36	49	15	
	23	43	34	28	72	50	38	12	
$\bar{x} \pm \text{SEM}$	18 ± 2.6	43 ± 0.6	38 ± 2.6	25 ± 1.4	75 ± 1.4	62 ± 19.4	44 ± 4.5	14 ± 1.25	
RH02211 (2 mM pyruvate)	16	41	43	26	74	35	43	22	

Similar to the LDH isoenzymes, no significant change in the isoenzyme distribution by pyruvate supplementation or RH02211 treatment was detectable for MDH and GOT enzymes of the malate aspartate shuttle (Table 5).

Glucose is efficiently converted to pyruvate when glycolytic enzymes are associated within a complex termed glycolytic enzyme complex (Zwerschke et al. 1999; Mazurek et al. 1996; Mazurek et al. 1999; Mazurek et al. 2001). Enzymes associated within the glycolytic enzyme complex focus at a common isoelectric point (IEP) which is different from the IEP of the purified proteins. A migration of enzymes in or out of the glycolytic enzyme complex is reflected by a shift in the IEP of the individual enzymes.

In pyruvate starved PC-3 cells the glycolytic enzyme complex was formed by GAPDH, tetrameric PK, PGK as well as the hybrid forms of LDH which all together focus at an IEP of 6.7 (Figure 22). PGM focused outside the complex at a more acidic IEP. Neither pyruvate supplementation nor RH02211 treatment modified the composition of the glycolytic enzyme complex (data not shown). Table 6 shows the mean IEP values of control PC-3 cells cultivated in pyruvate starved medium.

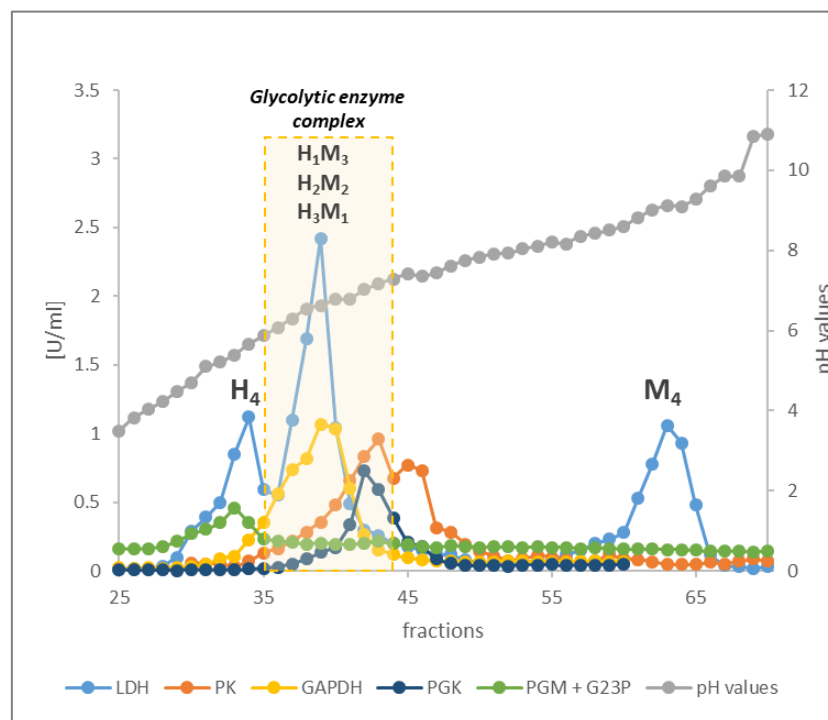


Figure 22. Glycolytic enzyme complex of pyruvate starved PC-3 cells treated with 0.008% DMSO.

Cell extract of 30×10^6 cells was applied onto the column. The figure shows the exemplary result of one of three isoelectric focusing experiments of pyruvate starved control PC-3 cells. RH02211 ($16 \mu\text{M}$) was supplemented 24 hours after passaging. Cells were extracted 48 hours later. The mean cell density at the time point of RH02211 supplementation was 2×10^6 cells. The mean cell density of RH02211-inhibited cells was 4×10^6 while the mock treated control cells reached a mean cell density of 7.5×10^6 . GAPDH: glyceraldehyde 3-phosphate dehydrogenase, LDH: lactate dehydrogenase, PGM: phosphoglycerate mutase; PGK: phosphoglycerate kinase; PK: pyruvate kinase.

Table 6. Isoelectric points (IEP) of glycolytic enzymes in pyruvate starved cells as determined by free flow isoelectric focusing. PC-3 cells were mock-treated with 0.008% DMSO. Neither pyruvate supplementation nor RH02211 had an impact on the IEPs of the glycolytic enzymes. The data present mean values of three independent experiments \pm SD. GAPDH: glyceraldehyde 3-phosphate dehydrogenase, LDH: lactate dehydrogenase, PGM: phosphoglycerate mutase; PGK: phosphoglycerate kinase; PK: pyruvate kinase.

Enzymes	IEP ($\bar{x} \pm SD$)
GAPDH	6.5 \pm 0.2
LDH H ₄	5.5 \pm 0.2
LDH hybrid	6.5 \pm 0.2
LDH M ₄	9.0 \pm 0.1
PGK	6.9 \pm 0.4
PGM	5.2 \pm 0.3
PK tetramer	7.0 \pm 0.3
PK dimer	7.5 \pm 0.1

5.1.3.7 Impact of RH02211 on the tetramer : dimer ratio of M2-PK in PC-3 cells

Pyruvate kinase isoenzyme type M2 consists in a highly active tetrameric form and a nearly inactive dimeric form in proliferating cells. In pyruvate starved control PC-3 cells the separation of the tetrameric and dimeric form of M2-PK by gel permeation revealed a tetramer : dimer ratio of 1 : 1.6. 16 μ M RH02211 had no impact on the tetramer : dimer ratio of M2-PK when PC-3 cells were cultivated in pyruvate starved medium (Figure 23).

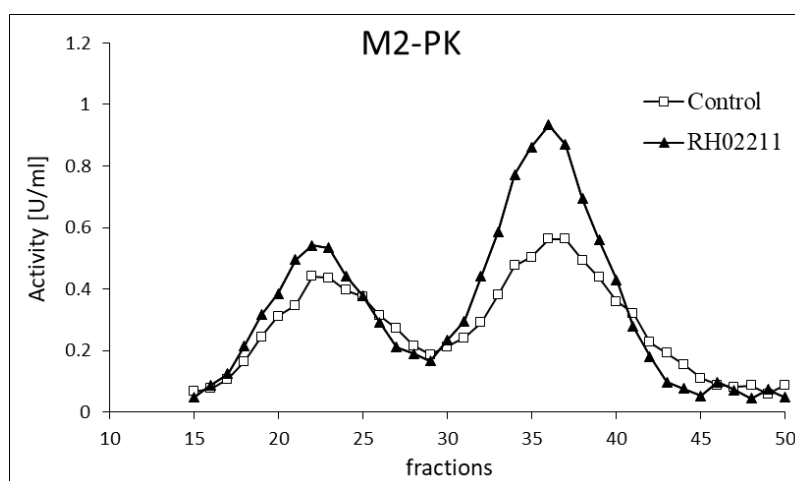


Figure 23. Impact of RH02211 on the tetramer : dimer ratio of M2PK. Result of a gel permeation experiment. RH02211 (16 μ M) was supplemented 24 hours after passaging. Cells were extracted 48 hours later. The mean cell density at the time point of RH02211 supplementation was 2×10^6 . The mean cell density of RH02211-inhibited cells was 4.5×10^6 while the mock treated control cells reached a mean cell density of 9.5×10^6 . Tetramer : dimer ratio calculated as area under the curve (AUC): pyruvate starved control PC-3 cells: 38% : 62%; pyruvate starved PC-3 cells cultivated in the presence of 16 μ M RH02211: 36% : 64%. Cell extract of 30×10^6 cells was applied onto the column. Control cells were mock-treated with 0.008% DMSO.

5.1.3.8 Impact of RH02211 on O₂ consumption in pyruvate starved and pyruvate supplemented PC-3 cells

The oxygen consumption rates were determined after 96 hours of PC-3 cell cultivation in pyruvate starved (0.015 mM) or pyruvate supplemented (2 mM) medium in the presence of 16 μ M RH02211 or 0.008% DMSO (control). Further, 16 μ M RH02211 and 0.008% DMSO were also acutely titrated inside the O2k chambers containing the corresponding treated and mock-treated cells at the beginning of each measurement (titration step: ROUTINE + inhibitor).

In pyruvate starved cells RH02211 induced a significant increase of O₂ consumption in ROUTINE respiration (independently upon the acute titration of the inhibitor inside the O2k chamber), measured in living cells in the absence of fuel substrates in the respiration medium (Figure 24 A - B). In contrast, in pyruvate supplemented cells, the O₂ consumption in ROUTINE respiration was not impaired by 96 hours treatment with RH02211 (neither in the absence of pyruvate nor after acute titration of pyruvate) (Figure 25). However, the acute titration of RH02211 in pyruvate supplemented living cells increased O₂ consumption (ROUTINE + RH02211). RH02211 induced an increase of O₂ consumption in permeabilized cells when glycerophosphate was used as fuel substrate in both pyruvate starved and pyruvate supplemented cells (Figure 24 A – Figure 25).

When succinate was used as fuel substrate of the mitochondrial respiratory system, a decrease of O₂ consumption was induced by RH02211 in pyruvate starved permeabilized cells (Figure 24 B).

5.1.3.9 Impact of RH02211 on H₂O₂ production in pyruvate starved and pyruvate supplemented PC-3 cells

In order to determine the H₂O₂ production rates, PC-3 cells were cultivated as described in the previous chapter 5.1.3.8.

RH02211 induced an increase of H₂O₂ production when either glycerophosphate or succinate were used as fuel substrates in both pyruvate starved as well as pyruvate supplemented cells (Figure 26-27). Since the measurements were performed in permeabilized cells to which RH02211 was acutely titrated during ROUTINE, it was not possible to discriminate if the increase of H₂O₂ production was induced by the 96 hours-treatment or by the acute titration of the inhibitor. However, the acute titration of RH02211 to the control cells induced an increase of H₂O₂ production in pyruvate supplemented cells when glycerophosphate was used as fuel substrate as well as in pyruvate starved cells when succinate was used as fuel substrate.

Therefore, independent upon the pyruvate concentration within the cultivation medium, expositions to the mG3PDH inhibitor RH02211 increased H₂O₂ production in PC-3 treated cells. A control background experiment without cells confirmed that the increase in H₂O₂ production was not due to a reaction of the RH02211 with other chemicals used in the experiments (data not shown).

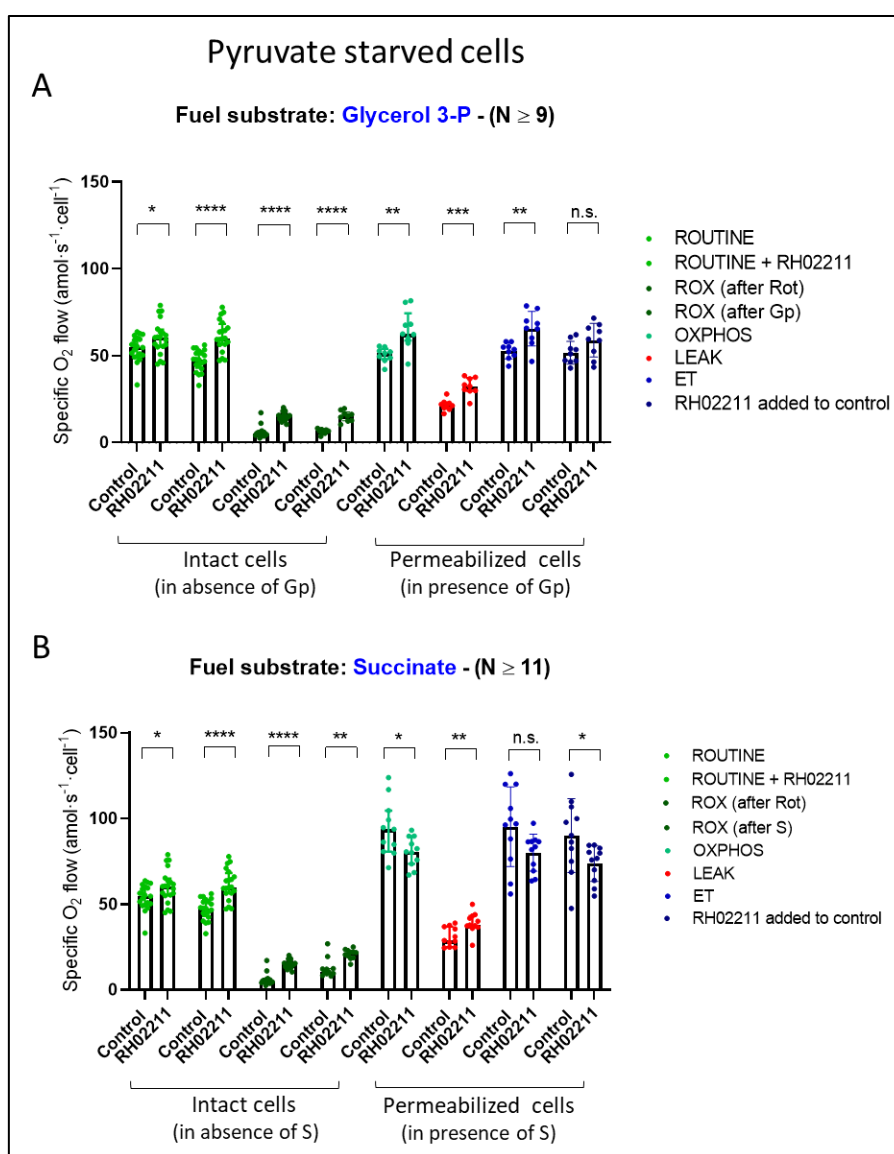


Figure 24. Impact of 16 μM RH02211 on O₂ consumption in pyruvate starved PC-3 cells cultivated at 21% O₂. Cells were cultivated for 96 hours in the presence of 16 μM RH02211 as well as with the corresponding vehicle concentration (0.008% DMSO). Thereafter, PC-3 cells were trypsinized, counted and re-suspended in PBS. $0.7 \cdot 10^6$ cells/ml were added into in the O2k chambers containing 2 ml of MiR05-Kit. 16 μM RH02211 and 0.008% DMSO were also acutely titrated inside the O2k chambers to the 96 hours-RH02211 treated and -mock-treated control cells respectively (step: ROUTINE + RH02211). A) 10 mM glycerophosphate and B) 10 mM succinate were titrated into the O2k chambers as fuel substrates of the mitochondrial respiratory system. Results are shown as median values with interquartile range. N= number of biological repeats.

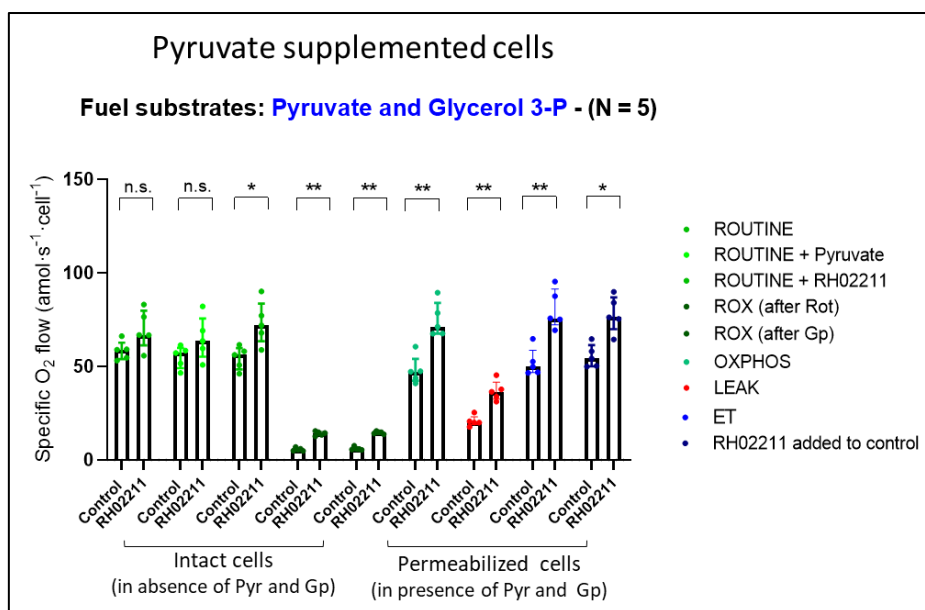


Figure 25. Impact of 16 μM RH02211 on O₂ consumption in pyruvate supplemented PC-3 cells cultivated at 21% O₂. Controls were mock-treated with 0.008% DMSO for 96 hours; the same vehicle concentration was also acutely titrated inside the O₂k chambers at the beginning of each measurement (step: ROUTINE + RH02211). 2 mM pyruvate and 10 mM glycerophosphate were titrated into the O₂k chambers as fuel substrates of the mitochondrial respiratory system. Results are shown as median values with interquartile range. N= number of biological repeats.

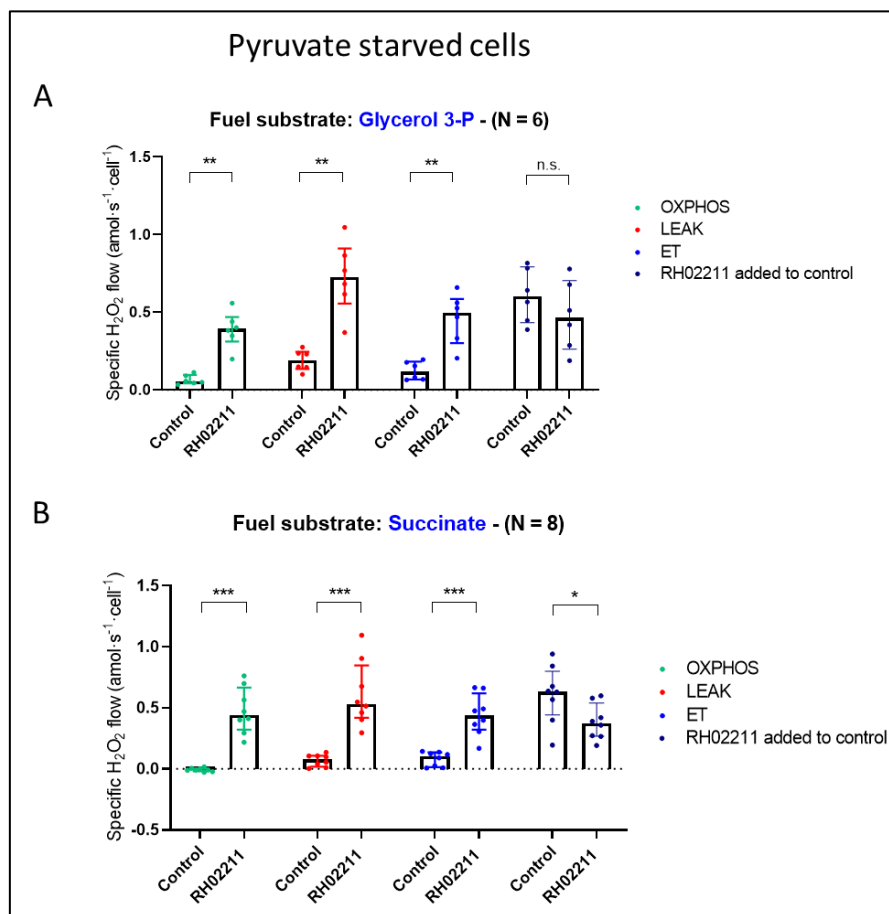


Figure 26. Impact of 16 μM RH02211 on H₂O₂ production in pyruvate-starved PC-3 cells cultivated at 21% O₂. Controls were mock-treated with 0.008% DMSO; the same vehicle concentration was also acutely titrated inside the O₂k chambers at the beginning of each measurement (in ROUTINE). A) 10 mM glycerophosphate and B) 10 mM succinate were titrated into the O₂k chambers as fuel substrates of the mitochondrial respiratory system. Results are shown as median values with interquartile range. N= number of biological repeats.

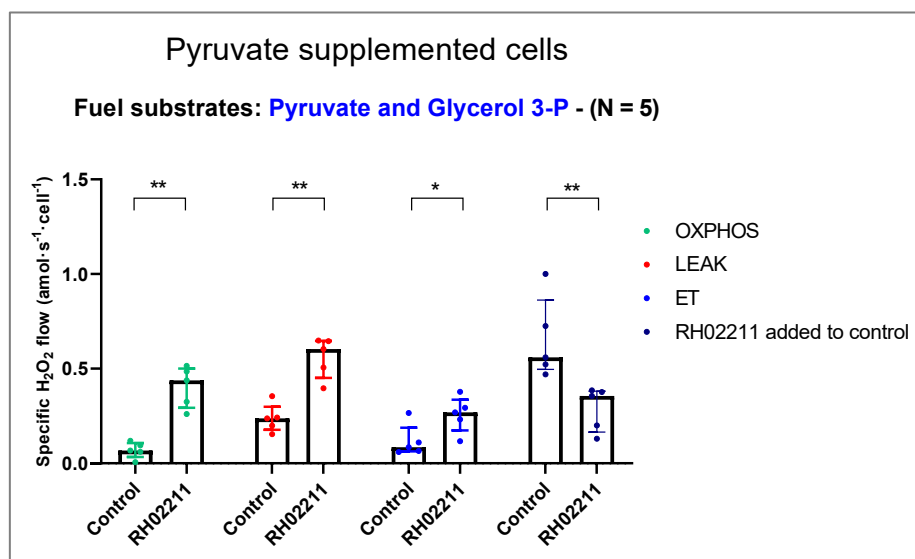


Figure 27. Impact of 16 μM RH02211 on H_2O_2 production in pyruvate supplemented PC-3 cells cultivated at 21% O_2 . Controls were mock-treated with 0.008% DMSO for 96 hours; the same vehicle concentration was also acutely titrated inside the O2k chambers at the beginning of each measurement (in ROUTINE). 2 mM pyruvate and 10 mM glycerophosphate were titrated into the O2k chambers as fuel substrates of the mitochondrial respiratory system. Results are shown as median values with interquartile range. N= number of biological repeats.

5.1.3.10 Impact of RH02211 on intracellular metabolites

The levels of the intracellular glycolytic, glutaminolytic and glycerol 3-P shuttle metabolites were determined after 24 hours of PC-3 cells cultivation in pyruvate starved (0.015 mM) or pyruvate supplemented (2 mM) medium in the presence of 7 μM RH02211 or 0.0035% DMSO (control). In pyruvate starved cells RH02211 induced a significant increase of all measured glycolytic intermediates (Table 7) suggesting an activation of glycolysis. In contrast, RH02211 did not affect the levels of nearly all glycolytic intermediates (except glyceraldehyde 3-P) when PC-3 cells were cultivated in pyruvate supplemented medium.

Intracellular glutamine levels decreased in RH02211-treated cells at both high and low pyruvate concentrations while glutamate levels decreased in the presence of 0.015 mM pyruvate but not in pyruvate supplemented RH02211-treated cells.

The decrease of glycerol 3-P and NAD^+ together with the increase of DHAP in pyruvate starved RH02211-treated cells suggested an impairment of the glycerol 3-P shuttle by RH02211. In contrast, RH02211 did not affect glycerol 3-P, NAD^+ and NADH levels as well as decreased DHAP in pyruvate supplemented cells (Table 7).

Table 7. Impact of 7 μ M RH02211 on intracellular metabolic intermediates in pyruvate starved and pyruvate supplemented PC-3 cells cultivated at 21% O₂. Controls were mock-treated with 0.0035% DMSO. DHAP: dihydroxyacetone phosphate; PEP: phosphoenolpyruvate; 2/3 PG: 2-phosphoglycerate plus 3-phosphoglycerate. Unit of measurement: ion intensity. The data were normalized to cell number and total ion count. The data are shown as median and the significance levels was set to $p < 0.05$. n=5.

<i>Glycolytic metabolites</i>						
	0.015 mM Pyruvate			2 mM Pyruvate		
	<i>Control</i>	<i>RH02211</i>	<i>p value</i>	<i>Control</i>	<i>RH02211</i>	<i>p value</i>
Glucose	73726980	87639033	0.0122	109119546	90087520	0.0947
Glucose 6-P	39162895	46035988	0.0367	59651228	53680469	0.4034
Fructose 6-P	36167324	42572394	0.0216	41026689	42877082	0.6761
Fructose 1,6-BP	99808585	148988964	0.0122	103053010	103409157	0.6761
Glyceraldehyde 3-P	13596741367	15892846827	0.0122	13248056400	15745857147	0.0122
2/3 PG	98703185	122898883	0.0122	162161825	149070553	0.6761
PEP	1904738951	1768764783	0.0122	2024499800	1871384723	0.0601
Pyruvate	12603599	17151887	0.0367	72594295	56009576	0.2101
Lactate	761401138	1059241685	0.0122	1153781981	1072440839	0.2963
<i>Glutaminolytic metabolites</i>						
	0.015 mM Pyruvate			2 mM Pyruvate		
	<i>Control</i>	<i>RH02211</i>	<i>p value</i>	<i>Control</i>	<i>RH02211</i>	<i>p value</i>
Glutamine	4033062913	3858104422	0.0122	4353863503	4009867336	0.0122
Glutamate	4950405249	4477572758	0.0122	4351311375	4341975752	0.6761
<i>Glycerol 3-P shuttle metabolites</i>						
	0.015 mM Pyruvate			2 mM Pyruvate		
	<i>Control</i>	<i>RH02211</i>	<i>p value</i>	<i>Control</i>	<i>RH02211</i>	<i>p value</i>
DHAP	114218463	133686100	0.0216	103137810	95355562	0.0216
Glycerol 3-P	26442442	24330265	0.0122	6962052	7921776	0.1437
NAD⁺	642340177	614099307	0.0122	663000434	649635740	0.0947
NADH	4669301	5428532	0.2101	1489935	3409926	0.4034

5.2 Targeting mitochondrial CIII in PC-3 prostate cancer cells

5.2.1. Impact of mitochondrial complex III inhibitors on PC-3 cell proliferation in presence of 21% and 1.5% oxygen supply

Three commercially available inhibitors with different target points on complex III (CIII) were selected: Antimycin A (AA) which inhibits the electron flow at the Q_i site of CIII, Myxothiazol (Myx) which inhibits the electron flow at the Q_0 site of CIII (Xia et al. 1997) as well as S3QEL-2 which inhibits ROS production at the Q_0 site of CIII but according to Orr et al. does not affect oxidative phosphorylation (OXPHOS)(Orr et al. 2015).

PC-3 cell proliferation was inhibited by all three complex III inhibitors after 96 hours of treatment. AA and Myx did not reveal differences in their inhibitory effects on cell proliferation when cultivated in the presence of 21% O_2 , as reflected by nearly identical IC_{50} and IC_{95} values (Table 8). In contrast, cultivation at 1.5% O_2 induced an 18-fold increase of the IC_{50} value of AA in comparison to 21% O_2 which reflects a significant weakening of the growth inhibitory effect of AA under hypoxic conditions.

The inhibitory effect of Myx on cell proliferation was not affected from oxygen supply.

When the two Q_0 -site inhibitors of CIII (Myx and S3QEL-2) were compared the inhibitory effect of S3QEL-2 on the cell proliferation rate of PC-3 cells was noticeable weaker than that of Myx as reflected by the higher IC_{50} values of S3QEL-2 than those of Myx at both 21% and 1.5% O_2 .

As also found for Myx hypoxia had no significant impact on the inhibition of cell proliferation by S3QEL-2 (Table 8 A).

Table 8. IC_{50} (A) and IC_{95} (B) values of Antimycin A, Myxothiazol and S3QEL-2 at 21% and 1.5% O_2 .

UL= Upper Limits, LL= Lower Limits, n= number of samples. IC_{50} = statistically calculated inhibitor concentration which induced a 50% inhibition of cell proliferation. IC_{95} = statistically calculated inhibitor concentration which induced a 95% inhibition of cell proliferation.

A	IC_{50} (nM)					
	21% O_2			1.5% O_2		
	IC_{50} value	UL	LL	IC_{50} value	UL	LL
Antimycin A	2.3 (n=80)	2.8	1.9	42 (n=49)	111	16
Myxothiazol	2.6 (n=50)	3.1	2.2	2.3 (n=32)	2.6	2
S3QEL-2	9200 (n=77)	11500	6900	13500 (n=64)	18800	8200

B	IC_{95} (nM)					
	21% O_2			1.5% O_2		
	IC_{95} value	UL	LL	IC_{95} value	UL	LL
Antimycin A	10 (n=80)	17	6	2238 (n=49)	19691	254
Myxothiazol	11 (n=50)	17.5	7	6.6 (n=32)	9.1	4.7

In the case of S3QEL-2 the amount of DMSO required for the solubilization of higher concentrations of the inhibitor had itself an inhibitory effect on PC-3 cell proliferation.

Accordingly, in the subsequent experiments only the IC_{50} concentrations of S3QEL-2 were used in order to investigate the impact of S3QEL-2 on the metabolism of PC-3 cells.

The growth inhibitory effect of AA and Myx on PC-3 cells was reversible even at the IC_{95} concentrations. Cell proliferation started again after replacement of the AA or Myx containing medium with inhibitor free medium (Figure 28 and 29).

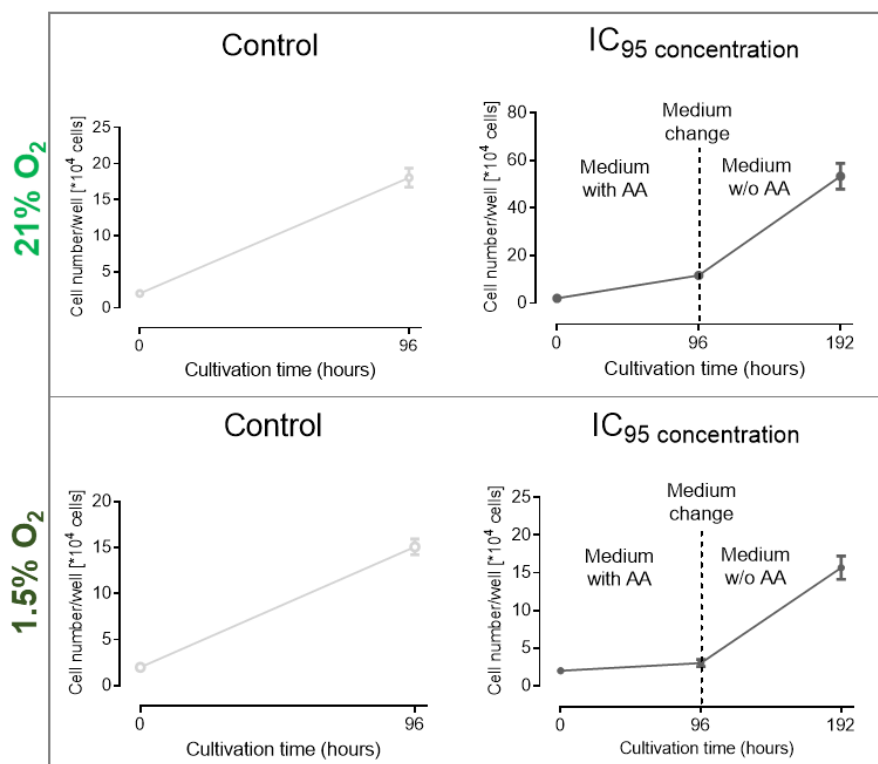


Figure 28. Reversibility of AA induced inhibition of PC-3 cell proliferation.

Cells were cultivated as described in Materials and Methods. After 96 hours of cell cultivation in the presence of AA, the medium was replaced with medium without inhibitor. After another 96 hours, the cells were counted. Concentrations tested: IC_{95} . Control cells were mock-treated with the corresponding vehicle concentration. Data are presented as mean values \pm SEM. Number of samples = 3.

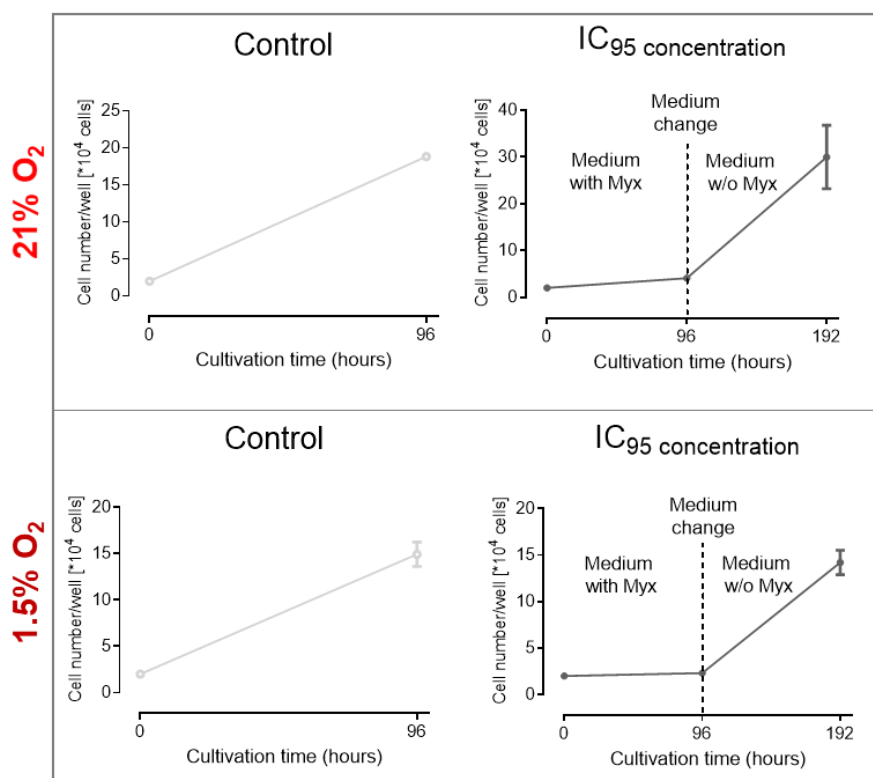


Figure 29. Reversibility of Myx induced inhibition of PC-3 cell proliferation.

Cells were cultivated as described in Materials and Methods. After 96 hours of cell cultivation in the presence of Myx, the medium was replaced with medium without inhibitor. After another 96 hours, the cells were counted. Concentrations tested: IC₉₅. Control cells were mock-treated with the corresponding vehicle concentration. Data are presented as mean values \pm SEM. Number of samples = 3.

5.2.2. Impact of mitochondrial complex III inhibitors on glycolytic and glutaminolytic flux rates in PC-3 cells cultivated in presence of 21% and 1.5% O₂

After 96 hours of treatment the CIII inhibitors AA and Myx induced a significant increase of lactate production in PC-3 cells independent upon the point of attack (site Q_i of CIII by AA or site Q_o of CIII by Myx) or the oxygen supply (Figures 30 - 31). An increase of lactate production was also induced by S3QEL-2 when PC-3 cells were cultivated at 21% O₂ but not at 1.5% O₂ (Figure 32). The lactate released by the cells may be due to the degradation of glucose as well as the breakdown of glutamine and serine.

In presence of 1.5% O₂ AA did not significantly modify the glucose consumption rates, in contrast a significant increase in glucose consumption was induced by AA at 21% O₂ as well as by Myx and S3QEL-2 under both oxygen conditions.

Myx induced a decrease in glutamine uptake at 21% O₂ while glutamine uptake was not affected by either Myx at 1.5% O₂ or AA and S3QEL-2 at both oxygen supply. However, less glutamine was incorporated into the citric acid cycle via glutamate as indicated by the increased glutamate production rates in AA- and Myx-treated cells under both conditions as well as in S3QEL-2-treated cells under hypoxic conditions (Figures 30-32). S3QEL-2 did not change glutamate production rates at 1.5% O₂.

Pyruvate was released from PC-3 cells since they were cultivated without pyruvate supplementation in the cultivation medium. Intracellularly pyruvate may derive from the degradation of glucose, serine and glutamine. If not converted to acetyl-CoA intracellular pyruvate can be released from the cells directly or after conversion to lactate or alanine.

AA increased alanine production at both 21% and 1.5% O₂ while pyruvate conversion rates did not change. At both oxygen supply Myx induced a decrease of pyruvate release. Alanine production rates increased at hypoxia but not at 21% O₂. Decreased pyruvate production rates were also induced by S3QEL-2 at 1.5% O₂ but not at 21% O₂ while alanine production increased at 21% O₂ but not at hypoxia in S3QEL-2-treated cells.

Both AA and S3QEL-2 did not modify serine consumption rates while Myx increased serine consumption at both oxygen supply (Figures 30-32).

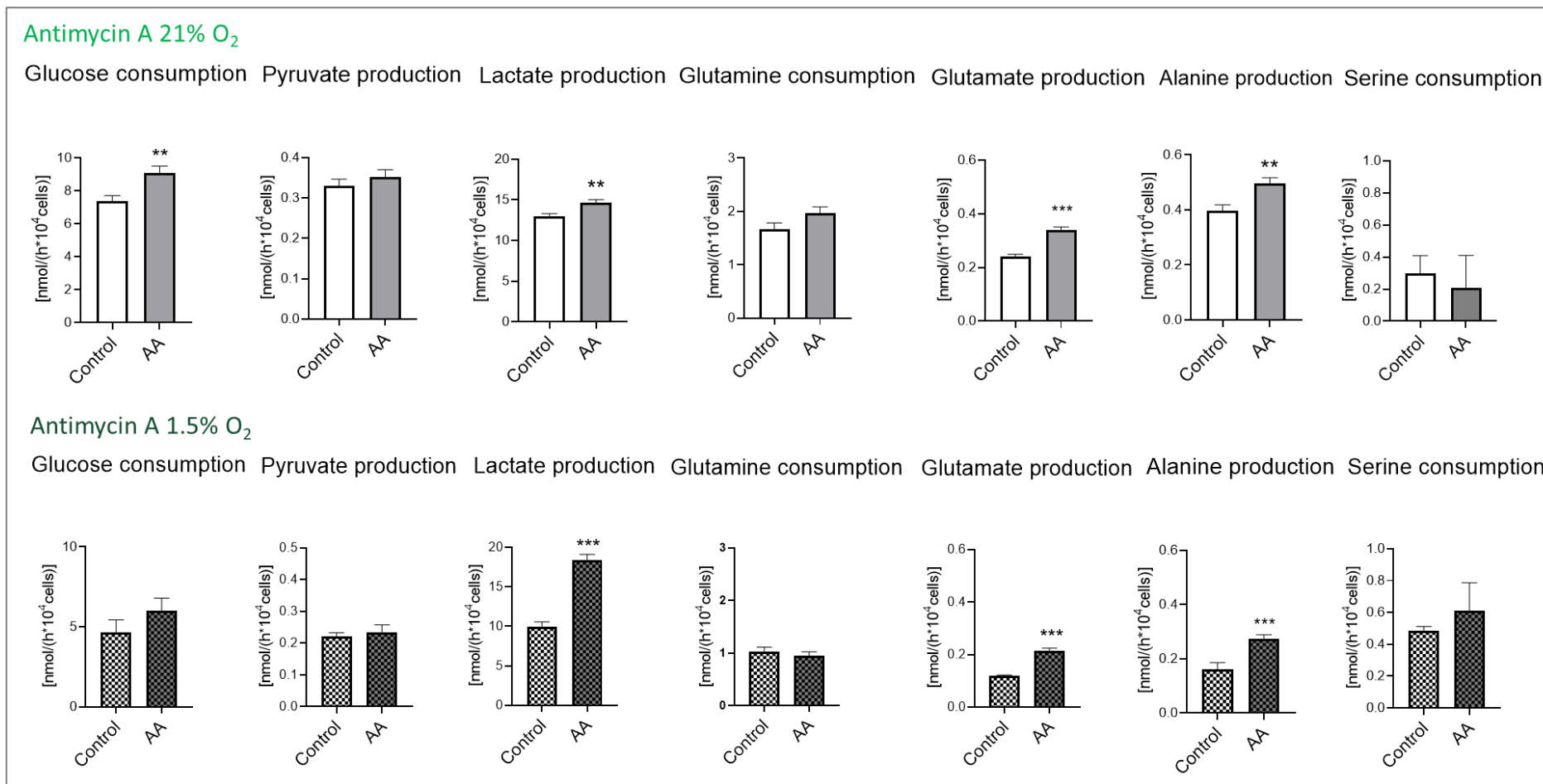


Figure 30. Impact of Antimycin A on the glycolytic and glutaminolytic conversion rates in PC-3 cells cultivated at 21% and 1.5% O₂.

The supplemented AA concentrations corresponded to the IC₅₀ concentrations for inhibiting cell proliferation: 2.5 nM AA in presence of 21% O₂ and 42 nM in presence of 1.5% O₂. Controls were mock-treated with 0.00001% Ethanol when cultivated in presence of 21% O₂ and 0.08% Ethanol when cultivated in presence of 1.5% O₂. Due to cell density dependencies of the metabolite conversion rates for the statistical comparison the turnover rates of the control and AA treated cells were adjusted to a global mean cell density. In case of exponential cell density dependencies, the metabolic fluxes were logarithmically transformed. The bar graphs show $\bar{x} \pm \text{SEM}$ (Standard Error of the Mean). Backtransformed conversion rates: pyruvate and glutamate at both 21% O₂ and 1.5% O₂. ** $p \leq 0,01$ and *** $p \leq 0,001$. Number of values per group: $n = 18$ at 21% O₂, $n \geq 17$ at 1.5% O₂.

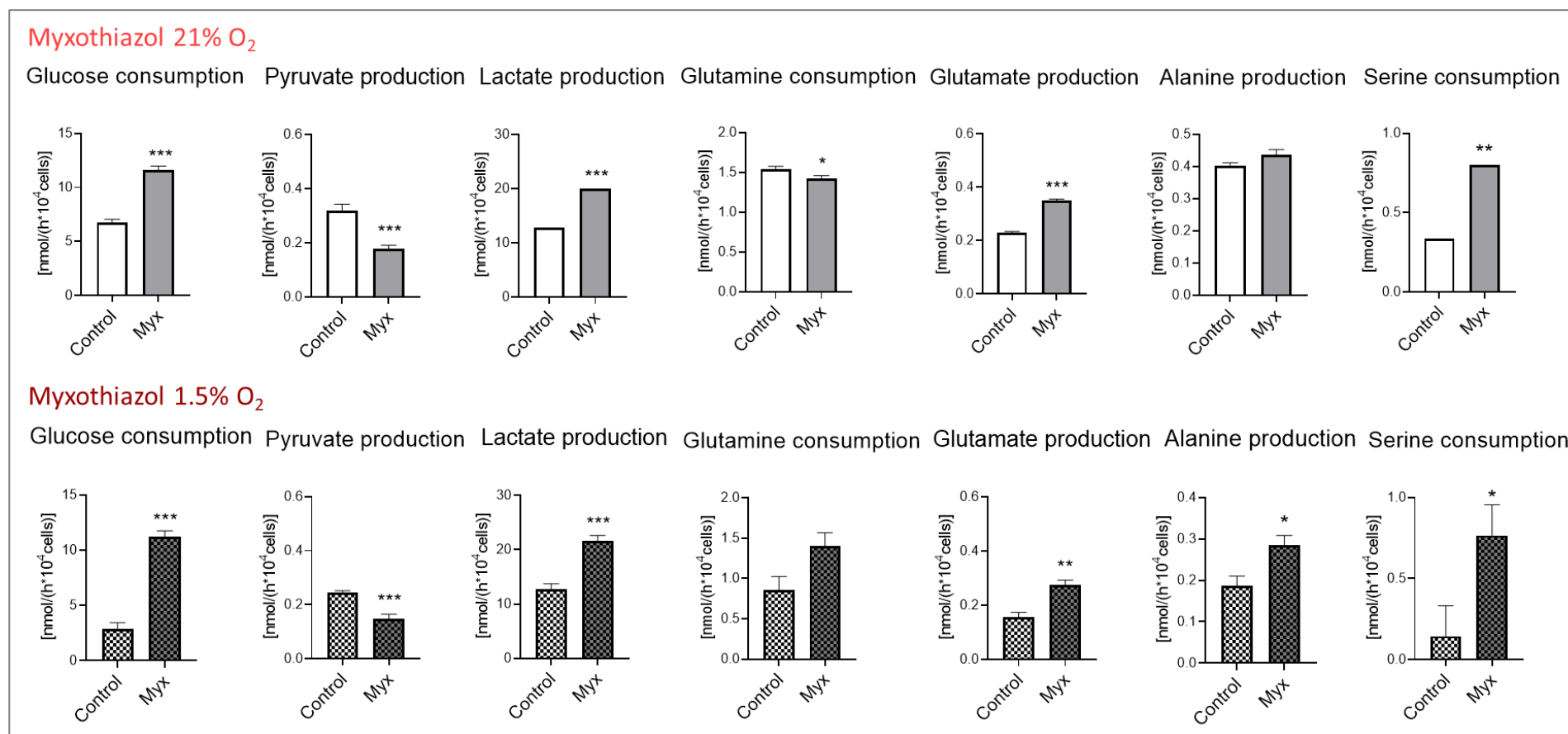


Figure 31. Impact of Myxothiazol on the glycolytic and glutaminolytic conversion rates in PC-3 cells cultivated at 21% and 1.5% O₂. Supplemented Myx concentrations corresponded to IC₅₀ concentrations for inhibiting cell proliferation: 2.5 nM Myx in presence of 21% O₂ and 1.5% O₂. Controls were mock-treated with 0.000025% DMSO when cultivated in presence of 21% O₂ and 1.5% O₂. Control and Myx treated cells were adjusted to a global mean cell density. In case of exponential cell density dependencies, the metabolic fluxes were logarithmically transformed. The bar graphs show $\bar{x} \pm \text{SEM}$ (Standard Error of the Mean). Backtransformed conversion rates: glucose, pyruvate and glutamine at 21% O₂. * p ≤ 0,05, ** p ≤ 0,01 and *** p ≤ 0,001. Number of values per group: n ≥ 15.

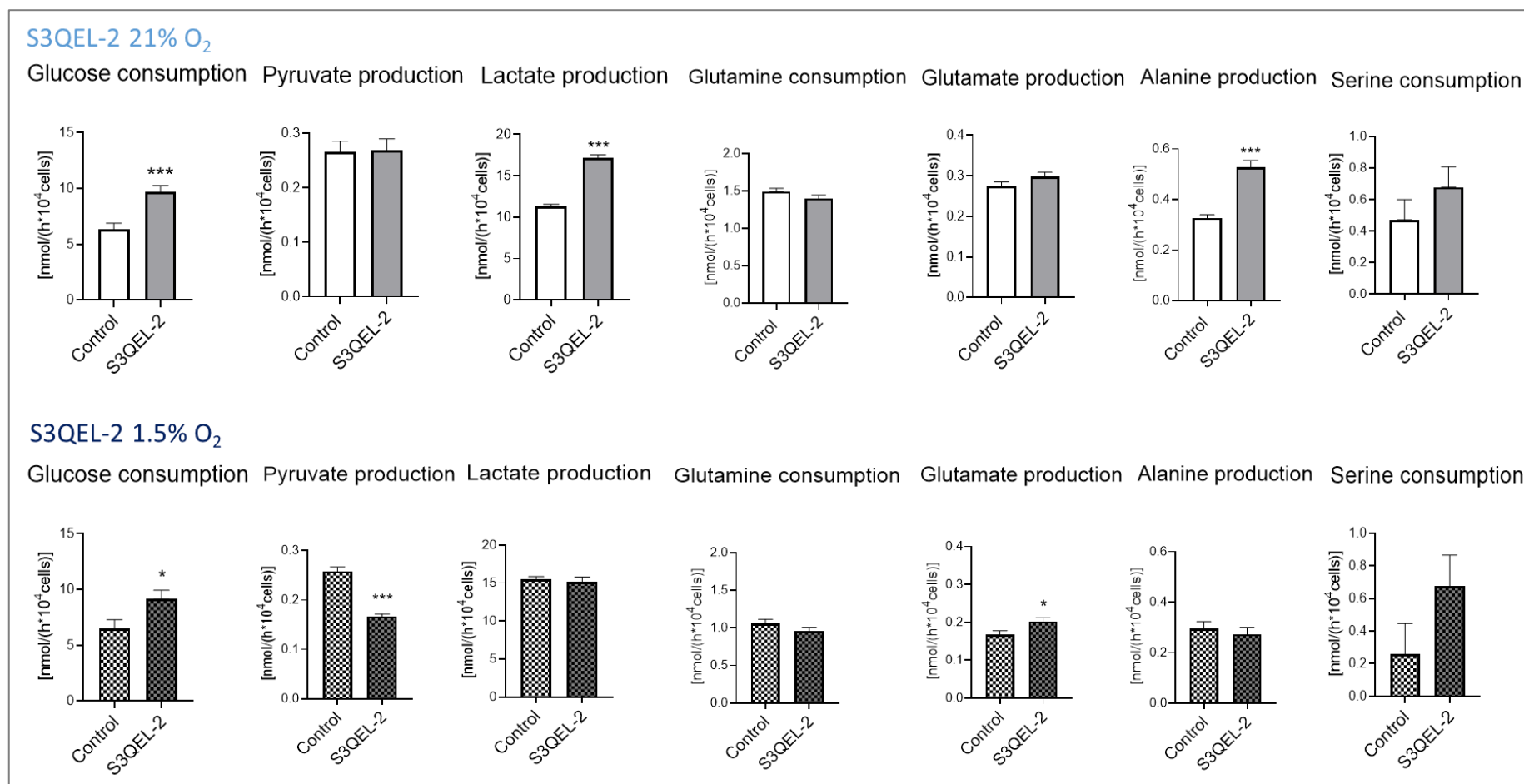


Figure 32. Impact of S3QEL-2 on the glycolytic and glutaminolytic conversion rates in PC-3 cells cultivated at 21% and 1.5% O₂.

The supplemented S3QEL-2 concentrations corresponded to the IC₅₀ concentrations for inhibiting cell proliferation: 9 μM S3QEL-2 in presence of 21% O₂ and 13.5 μM in presence of 1.5% O₂. Controls were mock-treated with 0.06% DMSO when cultivated in presence of 21% O₂ and 0.09% DMSO when cultivated in presence of 1.5% O₂. Due to cell density dependencies of the metabolite conversion rates for the statistical comparison the turnover rates of the control and S3QEL-2 treated cells were adjusted to a global mean cell density. In case of exponential cell density dependencies, the metabolic fluxes were logarithmically transformed. The bar graphs show $\bar{x} \pm \text{SEM}$ (Standard Error of the Mean). Backtransformed conversion rates: pyruvate, glutamine and glutamate at 21% O₂; pyruvate and glutamine at 1.5% O₂. * $p \leq 0,05$ and *** $p \leq 0,001$. Number of values per group: $n = 18$.

5.2.3. Impact of hypoxia on LDH, MDH and GOT isoenzymes as well as the glycolytic enzyme complex

Free flow isoelectric focusing was used to investigate the impact of hypoxia on the glycolytic enzyme complex as well as on the composition of LDH, MDH and GOT isoenzyme equipment.

Glucose is efficiently converted to pyruvate when glycolytic enzymes are associated within a complex termed glycolytic enzyme complex.

In PC-3 cells cultivated at 21% O₂ the glycolytic enzyme complex consisted of GAPDH, tetrameric M2-PK as well as the hybrid forms of LDH which all together focus at an IEP around 6.7.

In PC-3 control cells hypoxia induced a dimerization of M2-PK which was associated with a migration of the enzyme out of the complex (Figure 33). In addition, lactate dehydrogenase V_{max} activity slightly but not significantly ($p = 0.055$) increased in hypoxic conditions (Table 9). The V_{max} activities of M2-PK, Aldolase, GAPDH, PGK and PGM did not change when PC-3 cells were cultivated at 1.5% O₂ in comparison to those of PC-3 cells cultivated at 21% O₂ (Table 9).

Table 10 shows that in PC-3 cells hypoxia induced a significant shift to the M-type isoenzyme of LDH (LDHA isoenzyme) as well as to the mitochondrial isoenzyme of GOT while MDH isoenzyme profile was not modified by hypoxia.

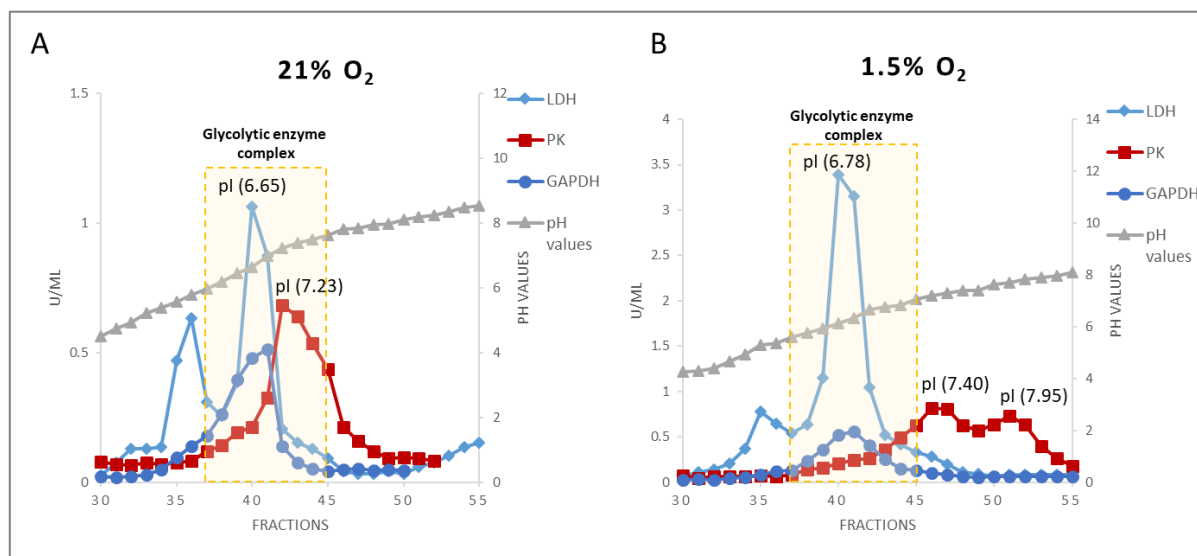


Figure 33. Comparison of the glycolytic enzyme complex of PC-3 cells at 21% O₂ (A) and 1.5% O₂ (B). Cell extract of 30*10⁶ cells was applied onto the column. The figure shows the exemplary result of one of a total of three isoelectric focusings. GAPDH: glyceraldehyde 3-phosphate dehydrogenase, LDH: lactate dehydrogenase, PK: pyruvate kinase.

Table 9. Impact of 1.5% O₂ on the Vmax activities of the glycolytic enzymes.

GAPDH: glyceraldehyde 3-phosphate dehydrogenase, LDH: lactate dehydrogenase, M2-PK: pyruvate kinase M2; PGM: phosphoglycerate mutase; PGK: phosphoglycerate kinase. Results are shown as mean values \pm SEM, n = 3.

Vmax (U/*10 ⁶ cells) $\bar{x} \pm$ SEM		
	21% O ₂	1.5% O ₂
LDH	1.26 \pm 0.30	2.33 \pm 0.27
M2-PK	0.72 \pm 0.34	0.18 \pm 0.04
Aldolase	0.05 \pm 0.02	0.07 \pm 0.01
GAPDH	0.53 \pm 0.12	0.67 \pm 0.02
PGK	0.34 \pm 0.09	0.65 \pm 0.02
PGM	0.14 \pm 0.04	0.18 \pm 0.004

Table 10. Impact of 1.5% O₂ on the isoenzyme equipment of lactate dehydrogenase (LDH), malate dehydrogenase (MDH) and glutamate oxaloacetate transaminase (GOT) measured by isoelectric focusing.

AUC: area under the curve, cyto= cytosolic isoenzyme, mito= mitochondrial isoenzyme, prec= precursor of the mitochondrial isoenzyme. * p< 0.05 and ** p \leq 0.01. Results are shown as mean values \pm SEM, n = 3.

AUC (%), $\bar{x} \pm$ SEM								
	LDH			GOT		MDHox		
	<i>H-type</i>	<i>Hybrid</i>	<i>M-type</i>	<i>cyto</i>	<i>mito</i>	<i>cyto</i>	<i>prec</i>	<i>mito</i>
21% O ₂	18 \pm 0.6	37 \pm 3.2	45 \pm 2.6 (**)	31 \pm 3.6 (*)	69 \pm 3.6 (*)	62 \pm 12.4	23 \pm 4.7	14 \pm 8
1.5% O ₂	7 \pm 0.3	27 \pm 1	66 \pm 1.3 (**)	17 \pm 2.2 (*)	83 \pm 2.2 (*)	57 \pm 21.9	6 \pm 4.6	48 \pm 25.3

5.2.4. Impact of complex III inhibitors on LDH, MDH and GOT isoenzymes as well as the glycolytic enzyme complex

Glycolytic and glutaminolytic conversion rates measured in the cultivation supernatants indicated that glucose becomes the main energetic source for PC-3 cell proliferation when CIII was inhibited by either Myx or S3QEL-2 at high and low oxygen supply as well as by AA at 21% O₂. The subsequent experiments were performed only at high oxygen supply. When all glycolytic enzymes are associated within the glycolytic enzyme complex glucose is very efficiently converted to pyruvate and lactate.

Myx, AA and S3QEL-2 did not have an impact on the composition of the glycolytic enzyme complex (data not shown) as well as on the composition of the lactate dehydrogenase, glutamate oxaloacetate transaminase and malate dehydrogenase isoenzyme equipment (Tables 11-13). Accordingly, the increase of glycolysis in AA, Myx and S3QEL-2 treated PC-3 cells could not be linked to changes in the glycolytic enzyme complex.

Table 11. Impact of Antimycin A on the isoenzyme equipment of lactate dehydrogenase (LDH), malate dehydrogenase (MDH) and glutamate oxaloacetate transaminase (GOT) as measured by free flow isoelectric focusing. The supplemented AA concentration corresponded to the IC₉₅ concentration for inhibiting cell proliferation: 10 nM. Control was mock-treated with 0.00001% Ethanol. AUC: area under the curve, IEP: isoelectric point, cyto= cytosolic isoenzyme, mito= mitochondrial isoenzyme, prec= precursor of the mitochondrial isoenzyme. n = 1.

	AUC (%)								
	LDH			GOT		MDHox			
	<i>H-type</i> IEP: 5.4	<i>Hybrid</i> IEP: 6.7	<i>M-type</i> IEP: 8.9	<i>Cyto</i> IEP: 5.7	<i>Mito</i> IEP: 9.7	<i>Cyto</i> IEP: 5.4	<i>Prec</i> IEP: 7.8	<i>Mito</i> IEP: 9.7	
Control	20	54	26	34	66	48	33	19	
Antimycin A	22	41	37	22	78	44	38	18	

Table 12. Impact of Myxothiazol on the isoenzyme equipment of lactate dehydrogenase (LDH), malate dehydrogenase (MDH) and glutamate oxaloacetate transaminase (GOT) as measured by free flow isoelectric focusing. The supplemented Myx concentration corresponded to the IC₉₅ concentration for inhibiting cell proliferation: 10 nM. Control was mock-treated with 0.00005% DMSO. AUC: area under the curve, IEP: isoelectric point, cyto= cytosolic isoenzyme, mito= mitochondrial isoenzyme, prec= precursor of the mitochondrial isoenzyme. n = 1.

	AUC (%)								
	LDH			GOT		MDHox			
	<i>H-type</i> IEP: 5.3	<i>Hybrid</i> IEP: 6.4	<i>M-type</i> IEP: 9	<i>Cyto</i> IEP: 5.7	<i>Mito</i> IEP: 9.7	<i>Cyto</i> IEP: 5.3	<i>Prec</i> IEP: 7.5	<i>Mito</i> IEP: 9.8	
Control	23	37	39	27	73	58	29	13	
Myxothiazol	21	41	38	34	66	46	38	16	

Table 13. Impact of S3QEL-2 on the isoenzyme equipment of lactate dehydrogenase (LDH), malate dehydrogenase (MDH) and glutamate oxaloacetate transaminase (GOT) as measured by free flow isoelectric focusing. The supplemented S3QEL-2 concentration corresponded to the IC₅₀ concentration for inhibiting cell proliferation: 9 μM. Control was mock-treated with 0.06% DMSO. AUC: area under the curve, IEP: isoelectric point, cyto= cytosolic isoenzyme, mito= mitochondrial isoenzyme, prec= precursor of the mitochondrial isoenzyme. n = 1.

	AUC (%)								
	LDH			GOT		MDHox			
	<i>H-type</i> IEP: 5.4	<i>Hybrid</i> IEP: 6.4	<i>M-type</i> IEP: 8.9	<i>Cyto</i> IEP: 5.6	<i>Mito</i> IEP: 9.7	<i>Cyto</i> IEP: 5.4	<i>Prec</i> IEP: 7.9	<i>Mito</i> IEP: 9.6	
Control	19	43	38	18	82	31	37	32	
S3QEL-2	20	42	38	22	78	28	33	39	

5.2.5. Impact of CIII inhibitors on H₂O₂ production in PC-3 cells cultivated at 21% O₂

Measurement of H₂O₂ production rates were performed using the O2k-FluoRespirometer from Oroboros Instruments GmbH, Innsbruck, Austria.

PC-3 cells were cultivated for 96 hours in presence of 2.5 nM AA, 2.5 nM Myx or 12 μM S3QEL-2 (= IC₅₀ values of inhibitors in cell proliferation assays). The corresponding inhibitor concentration was titrated acutely inside the O2k chambers at the beginning of each measurement (during ROUTINE). Under the described cultivation and measurement conditions, none of the three complex III inhibitors significantly changed H₂O₂ production rates (Figure 34).

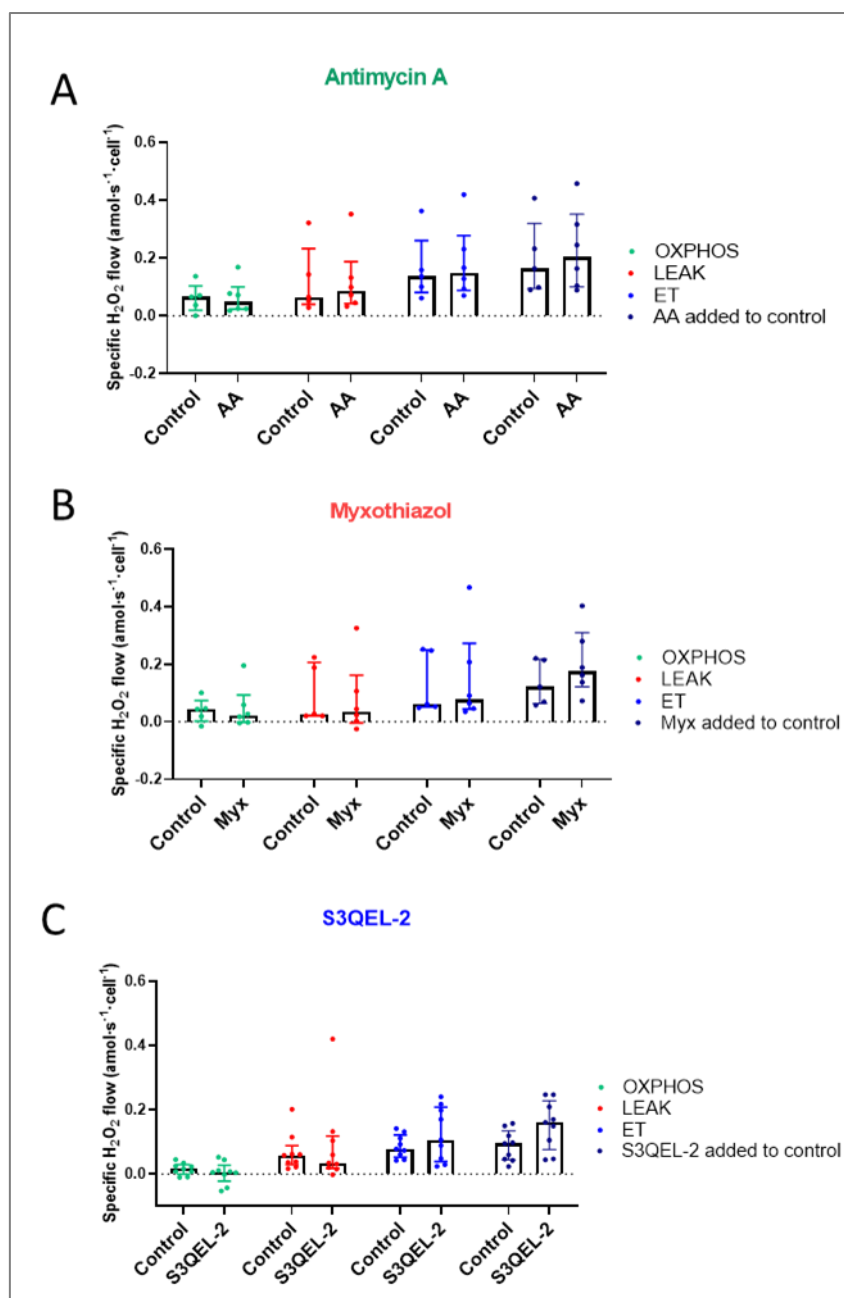


Figure 34. Impact of CIII inhibitors on H₂O₂ production in PC-3 cells cultivated on presence of 21% O₂. IC₅₀ concentrations were tested. 10 mM Succinate was titrated into the O2k chambers as fuel substrate of the mitochondrial respiratory system. Control cells were mock-treated for 96 hours with the vehicle concentration corresponding to the amount used to dissolve the respective inhibitors (0.000012% and 0.08% DMSO respectively for Myx and S3QEL-2 treatment, 0.00001% Ethanol for AA treatment); the corresponding vehicle concentrations were also acutely titrated inside the O2k chambers at the beginning of each measurement (in ROUTINE). At the last step tested (columns at the right), the control cells received A) 10 nM AA, B) 10 nM Myx, C) 30 μM S3QEL-2 respectively; treated cells also received a further titration of the inhibitors, completing 10 nM AA, 10 nM Myx and 30 μM S3QEL-2 respectively. Results are shown as median values with interquartile range. Number of biological repeats ≥ 5.

5.2.6. Impact of CIII inhibitors on O₂ consumption in PC-3 cells cultivated at 21% O₂

PC-3 cells were cultivated for 96 hours in presence of 2.5 nM AA, 2.5 nM Myx or 12 μM S3QEL-2 (= IC₅₀ values of inhibitors in cell proliferation assays). Measurement of oxygen consumption rates with the O2k-FluoRespirometer from Oroboros Instruments GmbH, Innsbruck, Austria revealed a severe inhibition of oxygen consumption by the acute titration of AA and Myx in both intact (ROUTINE + inhibitor) and permeabilized (OXPPOS) PC-3 cells when succinate was used

as fuel substrate (Figure 35). S3QEL-2 induced a slight significant decrease in oxygen consumption in permeabilized (OXPHOS) PC-3 cells with succinate as substrate but not in intact cells (ROUTINE and ROUTINE + inhibitor) (Figures 35 - 36). The impact of S3QEL-2 on oxygen consumption was more evident in the O₂k traces of the experiments (Figure 37). A clear decrease of oxygen consumption was induced by the acute titration of S3QEL-2 into both control and treated PC-3 cells if compared to the oxygen levels of the previous ET respiratory state (Figures 36-37).

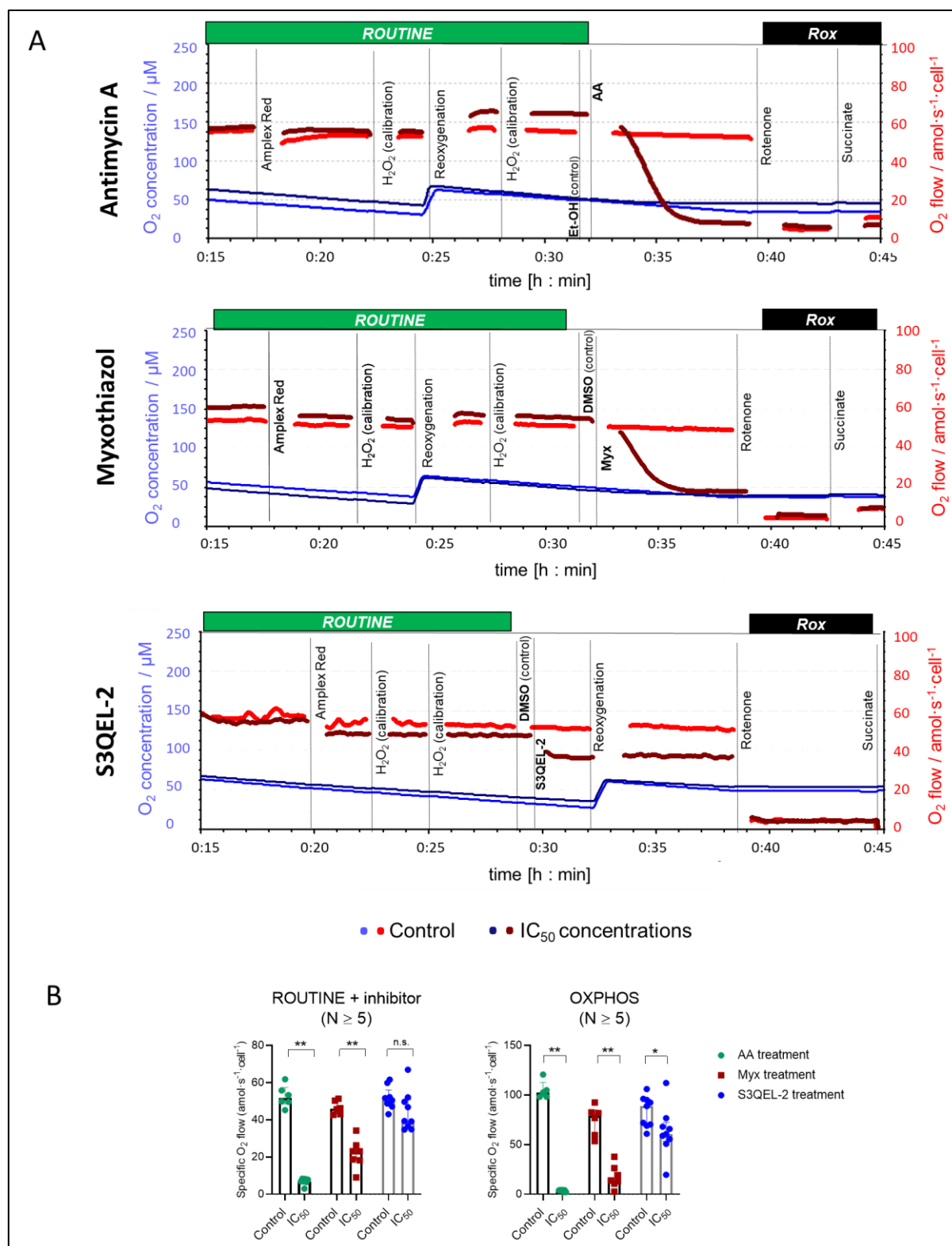


Figure 35. Comparison of the impact of AA, Myx and S3QEL-2 IC₅₀ concentrations on ROUTINE and OXPPOS respiration. Control cells were mock-treated for 96 hours with the vehicle concentration corresponding to the amount used to dissolve the respective inhibitors (0.000012% and 0.08% DMSO respectively for Myx and S3QEL-2 treatment, 0.00001% Ethanol for AA treatment); the corresponding vehicle concentrations were also acutely titrated inside the O2k chambers at the beginning of each measurement (in ROUTINE). A) Representative traces of the O₂ flow per cell measurements with control (red) and treated (purple) PC-3 cells. The inhibitors AA, Myx and S3QEL-2 were titrated to the corresponding treated cells as well as the corresponding vehicles were titrated to control cells while measuring ROUTINE respiration. The O₂ concentration inside the chambers is also represented (light and dark blue respectively in control and treated PC-3 cells). B) ROUTINE + inhibitor and OXPPOS respiration bars show median values with interquartile range. N: number of biological repeats.

6 Discussion

6.1 Metabolism dependency upon cell density

Proliferating cells, including cancer cells, in order to proliferate require a high energy supply as well as large amounts of precursors (i.e. nucleic acids, amino acids, phospholipids) for synthesis of cell building blocks (Eigenbrodt and Glossmann 1980; DeBerardinis et al. 2008). Both energetic and synthetic needs are mainly fulfilled by two metabolic pathways, glycolysis and glutaminolysis (Mazurek et al. 2005). In cell culture, cells do not have constant proliferation rates because it is necessary to regularly make subcultures in order to keep them alive. After initially seeding, cells are in a lag phase during which cells do not divide themselves or only few cell divisions take place. Thereafter, cell growth proceeds to a log phase, where cells are characterized by high proliferation rates, and finally to a stationary and death phase where the proliferation rate decreases and cells start to die. Cells have different metabolic demands depending upon the growth phase which in turn is associated with a specific cell density. Therefore, while performing cell culture experiments it is necessary to take care about the cell density in which the cells are cultivated because it can affect both proliferation and metabolism. Dependencies of glycolytic and glutaminolytic flux rates as well as of enzyme activities on cell density were described in different cell lines (Mazurek et al. 1997; Mazurek et al. 1999; Mazurek et al. 2001). In MCF-7 and MDA-MB-453 breast cancer cell lines 6-phosphofructo-1-kinase, glyceraldehyde 3-phosphate dehydrogenase and enolase activities strongly increased with cell densities, whereas the glycolytic flux rate decreased at high cell densities in MDA-MB-453 cells or remained unchanged in MCF-7 cells. Only the decreased hexokinase activity correlated with the reduced glycolytic flux rate at high cell density (Mazurek et al. 1997). Also the activities of the glutaminolytic enzymes glutamate dehydrogenase and malate dehydrogenase revealed a strong dependency upon cell density in both MCF-7 and MDA-MB-453 cell lines. Glutamate dehydrogenase activity increased with cell density in both cell lines while malate dehydrogenase activity increased in MCF-7 cells and decreased in MDA-MB-453 cells when cell densities increased (Mazurek et al. 1997). Lactate production as well as glucose and glutamine consumption strongly decreased with increasing cell density in tumorigenic rat liver oval OC/CDE cells, MCF-7 breast cancer cells as well as in non-transformed high glycolytic NIH3T3 mouse embryonic fibroblast cells (Mazurek et al. 1999; Mazurek et al. 1997; Mazurek et al. 2001). The decreased glycolytic and glutaminolytic turnover rates in high density cells in comparison to the low ones indicate that plated cells, when nearly confluent, decrease their energetic and metabolic demand due to the lower proliferation rates which are characteristic of the stationary growth phase. In contrast, after the initial latent phase, low density cells are usually characterized by a high rate of

cell division and require a large amount of energy and cell building blocks coming from the complete breakdown of glucose and glutamine to lactate. In isolated rat hepatocytes changes in metabolic activities as function of cell density have been shown. Fatty acid, cholesterol and protein synthesis as well as pyruvate, lactate, citrate and acetyl-CoA production rates decreased as the cell density increased (Jurin and McCune 1985). Accordingly, in control PC-3 cells lactate, pyruvate and glutamine conversion rates measured in cell culture supernatants decreased with increasing cell density (Figure 14). Dependencies of the glycolytic and glutaminolytic conversion rates upon cell density were found also when PC-3 cell proliferation was 50% inhibited, in comparison to control cells, after 96 hours treatment either with the mG3PDH inhibitors iGP-1 (Figure 14) and RH02211 or the CIII inhibitors AA, Myx and S3QEL-2 (data not shown). Therefore, cell density dependencies were taken under consideration in the statistical analysis when conversion rates were compared between control and treated cells.

The relationship between specific oxygen consumption as well as H_2O_2 production and cell density described in literature is controversial. In different mammalian cell lines the specific oxygen consumption rate was not affected by cell density when cell densities between 1 and 20 million cells/ml were tested (Jorjani and Ozturk 1999). In contrast, in lymphocyte cultures a reduction to 1/10 in specific oxygen consumption rate was found when cell density increased from 0.001 to 10 million cells/ml (Sand et al. 1977). In hybridoma cells, when cell density increased from 0.6 to 10 million cells/ml, the cell specific oxygen consumption was reduced to a quarter (Wohlpert et al. 1990). Oxygen consumption rates together with lactate production levels were found high in low density fibroblasts while those rates and levels strongly decreased once fibroblasts reached confluence (Bereiter-Hahn et al. 1998). Further, the H_2O_2 production rates increased with cell density in human melanoma and neuroblastoma cell lines (Szatrowski and Nathan 1991). Exposition to simulated sunlight irradiation did not modify the H_2O_2 production rates in low density HaCaT skin cells, in contrast a significant decrease in H_2O_2 production was observed in high density HaCaT cells (Zanchetta et al. 2010).

In order to measure both oxygen consumption and H_2O_2 production, PC-3 cells were trypsinized since the O2k-FluoRespirometer (Oroboros Instruments, Innsbruck, Austria) requires non adherent cells for the measurements. PC-3 cells were trypsinized once they had reached a mid-high density in the cell culture dishes (after 96 hours from cell seeding). Thereafter, the measurements were performed with a cell density of 0.7 million cells/ml. Additional cell densities were not investigated.

6.2 Impact of hypoxia on the glycolytic enzyme complex as well as the LDH, MDH and GOT isoenzymes

It has been known for a long time that under oxygen starving conditions glycolysis is the main energetic pathway in normal cells (called “Pasteur effect”), whereas in aerobic conditions energy is mainly produced by OXPHOS within the mitochondria since glucose carbons are mainly channelled into the TCA cycle (Krebs 1972; Vadlakonda et al. 2013). However, proliferating cells as well as cancer cells often show high glycolytic activity even in the presence of oxygen (Warburg 1956).

Due to the rapid proliferation of cancer cells, solid tumors quickly run out of nutrients and oxygen supply from the normal vasculature and therefore become hypoxic (Carmeliet et al. 1998). The oxygen level in hypoxic tumor tissues tends to have median oxygen levels $< 2\%$ (range from 0.2% to $4.2\% O_2$) while normal tissues are ordinarily maintained at $3 - 7\%$ oxygen (McKeown 2014). In normal human lung tissue the oxygen concentration is 5.6% while in non-small cell lung cancer is between $1.9 - 2.2\%$ (Ziółkowska-Suchanek 2021). Therefore, in order to perform the experiments under more physio-pathological conditions we performed the experiments at $1.5\% O_2$ (hypoxia/pathological hypoxia) as well as at $21\% O_2$ (hyperoxia).

It is well known that a decrease in oxygen levels leads to stabilization of HIF-1 α and activation of the transcriptional complex HIF-1 which upregulates the transcription of various cancer-related genes involved in cell survival, angiogenesis and metabolism (Semenza 2003; Semenza 2010a). Further, HIF-1 plays an important role in the glycolytic switch activating the transcription of genes encoding the glycolytic enzymes LDHA, PGK, HK and M2-PK (Semenza 2010b; Luo et al. 2011). M2-PK isoenzyme is characteristic of cancer cells and in contrast to the other PK isoenzymes it can also occur in a dimeric form in addition to the tetramer (Eigenbrodt et al. 1992; Zwerschke et al. 1999). The ratio between the highly active tetrameric and the nearly inactive dimeric form of the M2-PK is regulated by different post-translational modifications (Prakasam et al. 2018). Several studies suggested that hypoxia induces an increase of the reactive oxygen species concentration causing an oxidation of M2-PK at cysteine 358 which leads to the dissociation of the enzyme to the less active dimeric form (Anastasiou et al. 2011; Iqbal et al. 2013). For example, in HepG2 and BeL7402 human hepatocellular carcinoma cells as well as in H1299 human cell lung and PC-3 prostate cancer cells insulin-induced ROS led to a dimerization of M2-PK and to a decrease of its activity. M2-PK activity reduction increased the glycolytic intermediate pool diverting glucose flux towards macromolecular synthesis (Li et al. 2014b; Iqbal et al. 2013).

Anastasiou et al. measured an acute increase of the intracellular ROS concentrations followed by a decrease in M2-PK activity in A549 human cancer cells cultured at $1\% O_2$ for 3 hours as well as

after 15 minutes treatment with 1 mM H₂O₂ (Anastasiou et al. 2011). Accordingly, our results show that long term cultivation (7 days) of PC-3 cells under hypoxic conditions (1.5% O₂) induced a dimerization of M2-PK (Figure 33 B). The literature shows that the tetrameric form of M2-PK could be associated together with other glycolytic enzymes forming a so called “glycolytic enzyme complex” (Mazurek et al. 1996; Mazurek et al. 1999; Zwerschke et al. 1999; Mazurek et al. 2005). The glycolytic enzyme complex can be isolated by free flow isoelectric focusing. Enzymes associated within the glycolytic enzyme complex focus at a common isoelectric point (IEP) which is different from the IEP of the purified proteins (Mazurek et al. 2005). For example, in human breast cancer MCF-7 cells the glycolytic enzymes GAPDH, PGK, enolase and M2-PK focused together at a pH of about 7.0 (Mazurek et al. 1996). In addition, it has been shown that RNA is involved in the formation of this complex between glycolytic enzymes (Simon et al. 1989; Nagy and Rigby 1995). In MCF-7 cells the association of the glycolytic enzymes was altered after RNase treatment, indicating that besides the enzymes also RNA is involved in the glycolytic enzyme complex (Mazurek et al. 1996). A migration of enzymes in or out of the glycolytic enzyme complex is reflected by a shift in the IEP of the individual enzymes. The dimeric form of M2-PK focuses outside the complex at a more alkaline pI value. When all glycolytic enzymes are associated within the glycolytic complex glucose is very efficiently converted to pyruvate and lactate (Mazurek et al. 2005).

In PC-3 cells cultivated at 21% O₂ the glycolytic enzyme complex consisted of GAPDH, tetrameric M2-PK as well as the hybrid forms of LDH which all together focus at an IEP around 6.7 (Figure 33 A). PGM focused outside of the glycolytic enzyme complex together with the H-type of LDH while part of NDPK was associated within the complex (data not shown). Cultivation of PC-3 cells at 1.5% O₂ induced a migration of M2-PK and LDH out of the glycolytic enzyme complex to a more alkaline pH value which corresponds with a dimerization of M2-PK and a shift of LDH towards the M-type (Figure 33 B, Tables 9 and 10).

The homotetramer M-type has a high affinity for pyruvate and predominates in tissues with high glycolytic activity (Markert et al. 1975; Sumida et al. 1995). Increased LDHA (M4 type) expression supported glycolysis in cancer cells (Cai et al. 2019). The overexpression of the M-type of LDH is characteristic for cells cultivated under hypoxic conditions favouring the reduction of pyruvate to lactate thereby recycling NAD⁺ for the glycolytic GAPDH reaction (Semenza et al. 1996; Eales et al. 2016; Feng et al. 2018). The V_{max} activities of M2-PK, Aldolase, GAPDH, PGK and PGM did not change when PC-3 cells were cultivated at 1.5% O₂ in comparison to those of PC-3 cells cultivated at 21% O₂ (Table 9).

Besides LDH the malate aspartate shuttle plays an important role for the recycling of cytosolic NAD⁺. The malate aspartate shuttle consists of the enzymes MDH and GOT (Mary C. McKenna

et al. 2006). Both MDH and GOT exist as cytosolic (cMDH, cGOT) and mitochondrial (mMDH, mGOT) isoenzymes (Figure 4). In addition to the cytosolic and mitochondrial isoform of MDH, another form of MDH occurs. In MCF-7 breast cancer cells, this third form of MDH was identified as the cytosolic precursor of the mitochondrial isoenzyme (Mazurek et al. 1996). The literature shows that increased cytosolic MDH activities supported glycolysis in actively proliferating cells and cancer cells (Hanse et al. 2017; Zhang et al. 2019). Cultivation of PC-3 cells under hypoxic conditions induced a shift to the mitochondrial GOT isoenzyme while the composition of MDH isoenzyme equipment was not modified by hypoxia. Accordingly, the GOT isoenzyme pattern was shifted in favor of the mitochondrial GOT isoenzyme in Guinea pigs incubated for 24 – 72 hours at hypoxia (Schmidt et al. 1977). The malate aspartate shuttle can transport hydrogen in both directions: from cytosol into the mitochondria or from the mitochondria into the cytosol. Measurements of MDH activities in malate to oxaloacetate and oxaloacetate to malate direction revealed that the cytosolic isoenzyme has a higher capacity for the malate to oxaloacetate direction which means that the malate aspartate shuttle should favor the flow of hydrogen from the mitochondria to the cytosol. However, as far as investigated the hydrogen flow in tumor cells works from the cytosol to the mitochondria. The explanation for this is that the mitochondrial form of MDH binds to the mitochondrial form of GOT. As a consequence the availability of mitochondrial glutamate favors the flow of hydrogen from cytosol to mitochondria by trapping oxaloacetate as aspartate (Mazurek et al. 1996). In PC-3 cells the mitochondrial form of malate dehydrogenase does also cofocus with the mitochondrial isoenzyme of glutamate oxaloacetate transaminase. In VHL-deficient human renal carcinoma with constitutive normoxic activation of HIF-1 alpha the stabilization of HIF-1 alpha reduced the expression of both the cytosolic and mitochondrial GOT (Meléndez-Rodríguez et al. 2019).

6.3 Impact of pyruvate on cell metabolism

Pyruvate is a key metabolic intermediate in several cellular pathways. Pyruvate can derive from glucose via glycolysis as well as can derive from lactate taken up from outside the cells or synthesized intracellularly from amino acids. In differentiated cells, in aerobic conditions pyruvate is mainly channeled into the TCA cycle via pyruvate dehydrogenase supporting energy production or serves as a precursor of numerous amino acids and metabolic intermediates (Mathioudakis et al. 2011). When oxygen is not available in sufficient quantity to the cell, instead of entering the TCA cycle, pyruvate is reduced to lactate in order to regenerate NAD^+ for the GAPDH reaction and thus maintaining high glycolytic rates necessary for energy production. The reduction of pyruvate to lactate occurs also in highly proliferating cells such as cancer cells when oxygen is present (Warburg effect/aerobic glycolysis) (Warburg 1956). Through carboxylation to oxaloacetate by

pyruvate carboxylase pyruvate is also a starting point for gluconeogenesis. Furthermore, pyruvate is a reaction partner in the glutamate pyruvate transaminase reaction regulating the ratio between pyruvate, aspartate, alpha ketoglutarate and alanine. Several studies have shown that cell proliferation strongly depends upon the pyruvate concentration in the cell cultivation medium. Exogenous pyruvate is transported inside the cell through the cytoplasmic membrane by H⁺-monocarboxylated cotransporters (MCT) (Garcia et al. 1994; Halestrap and Price 1999). Diers et al. demonstrated that breast cancer cells (MCF-7, MB231 and T-47D) proliferate more rapidly when cultivated for 72 hours in pyruvate-only (1 mM) media in comparison to the counterparts cultivated in glucose-only (5.56 mM) media. Growth of cells on pyruvate-only media was comparable to that of cells grown in complete media containing both glucose and pyruvate (Diers et al. 2012). Further, inhibition of the MCT using increasing concentrations (50-500 μ M) of α -cyano-4-hydroxycinnamic acid (CHC) for 4 hours decreased cellular pyruvate uptake and cell growth without blocking lactate excretion in MCF-7 cells. Accordingly, inhibition of pyruvate uptake but not lactate release by 1.5 mM CHC impaired the growth of breast cancer-derived metastases in different mouse models (Elia et al. 2019). Diers et al. suggested that in several cell types glycolysis alone is not sufficient to support rapid proliferation and therefore the supplementation of energy substrates that can be metabolized through the TCA cycle, such as pyruvate, allows a more rapid cell proliferation when compared to glucose (Diers et al. 2012). Due to its importance in cell proliferation and metabolism, pyruvate is supplemented in a lot of commercially available cultivation media.

PC-3 cell proliferation increased when cells were cultivated at both 1.5% and 21% O₂ in pyruvate supplemented medium for 96 hours in comparison to those cells cultivated in pyruvate starved conditions (Figure 16). Accordingly, exogenous pyruvate was required to maintain the survival and proliferation of cancer (143B206, 143B, HeLa and Hep3B) and non-cancer cells (H9c2, rat cardiomyocytes) in hypoxic conditions (2% O₂) as well as of cells with defective electron transport chain by acting as an oxygen surrogate to accept electrons, through its reduction to lactate, and thus maintaining NAD⁺ homeostasis as well as ATP levels necessary to sustain the high glycolytic rates (Yin et al. 2016). Being reduced to lactate via LDH, extracellular pyruvate recycles cytosolic NAD⁺ for the GAPDH reaction maintaining high glycolytic rates in proliferating cells, such as cancer cells.

In contrast, an inhibitory effect of exogenous pyruvate on cancer cell growth was attributed to its function to repress histone gene expression, leading to less compact chromatin, deregulated gene expression and cell cycle arrest (Ma et al. 2019). Accordingly, Zhang et al. found that in human cholangiocarcinoma cells the oncogene c-myc decreases intracellular pyruvate levels by increasing LDHA and M2-PK expression which consequently decreases the histone deacetylase inhibition

and protects cancer cells from apoptosis (Zhang et al. 2019). Therefore, the impact of pyruvate on cell proliferation is still controversial since pyruvate increased but also decreased cancer cell proliferation as described in literature.

Another mechanism for NAD^+ recycling is the glycerol 3-P shuttle via the cytosolic and mitochondrial G3PDH reactions. Since supplementation of extracellular pyruvate to the cultivation medium may be an escape mechanism in the experiments with mG3PDH inhibitors, we conducted our experiments with two different pyruvate concentrations within the cell cultivation medium. In pyruvate starved PC-3 cells pyruvate was not supplemented to the cultivation medium, however we determined a pyruvate concentration of 0.015 mM within the medium, which originated from the supplemented FBS. In the experiments with pyruvate supplementation (pyruvate supplemented cells) the final pyruvate concentration in the medium was 2 mM. The pyruvate concentration in the blood is around 0.1 mM, therefore low pyruvate concentrations in the cultivation medium better simulate the physiological conditions (Sullivan and Stern 1983).

Measurements of metabolic conversion rates within the cultivation supernatants of PC-3 cells revealed a severe impact of extracellular pyruvate on the metabolism of the control cells which shifted from pyruvate production to pyruvate consumption in pyruvate supplemented medium (Figures 20 and 38). In pyruvate supplemented PC-3 cells the reduction of the lactate production rates suggests that extracellular pyruvate was not reduced to lactate via the LDH reaction but channeled into other metabolic pathways, such as the citric acid cycle (Figure 38).

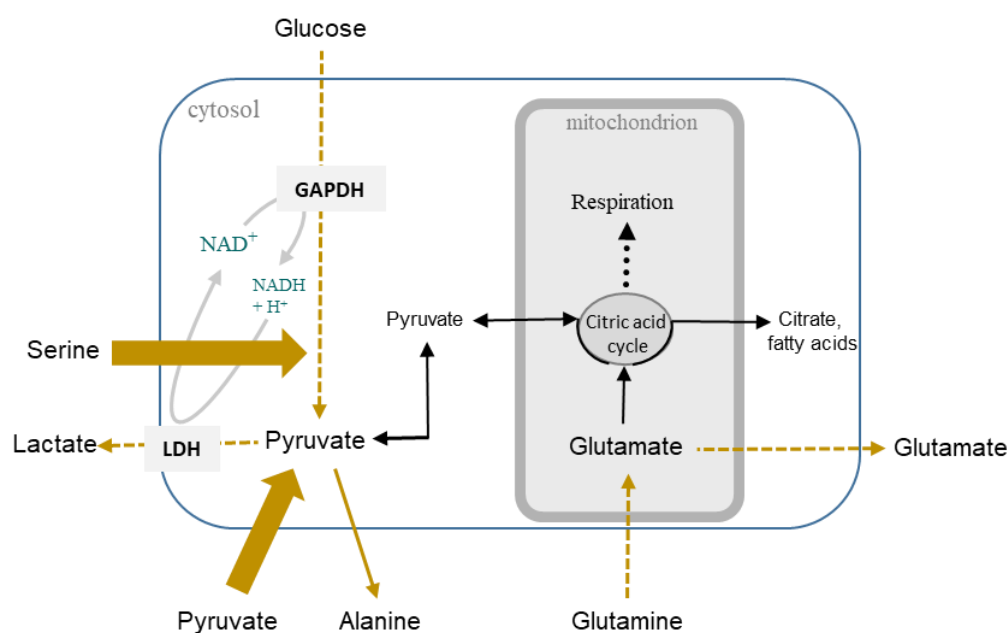


Figure 38. Impact of 2 mM pyruvate on the glycolytic and glutaminolytic conversion rates in PC-3 cells. Wide arrow: increased flux rate (pyruvate supplemented vs pyruvate starved), thin arrow: unchanged flux rate (pyruvate supplemented vs pyruvate starved), dotted arrow: decreased flux rate (pyruvate supplemented vs pyruvate starved).

However, no changes in the LDH isoenzyme equipment were measured in pyruvate supplemented cells (Table 5). The complete oxidation of pyruvate within the citric acid cycles could explain the parallel reduction of glucose and glutamine consumption in pyruvate supplemented cells in comparison to the pyruvate starved ones. Accordingly, several studies suggested that exogenous pyruvate was channelled into the TCA cycle driving the mitochondrial respiration and leading to more rapid cell proliferation rates (Takakusagi et al. 2014; Diers et al. 2012). Indeed, *in vitro* and *in vivo* studies showed that increasing exogenous pyruvate concentrations (0.2 – 2 mM) affected mitochondrial respiration in a dose-dependent manner. Basal oxygen consumption rates increased in murine squamous cell carcinoma SCCVII and human colon cancer HT29 cell lines when cultured in media that contained 0.2 – 2 mM pyruvate in comparison to the corresponding cell lines cultivated in absence of pyruvate (Takakusagi et al. 2014; Diers et al. 2012).

In pyruvate supplemented PC-3 cells (Figure 20 and 38), the glycolytic enzymes GAPDH, PK, LDH (hybrid isoforms) as well as part of PGK and NDPK remained associated within the glycolytic enzyme complex although glucose and lactate conversion rates decreased (data not shown). In addition, measurements of metabolite conversion rates within the cultivation medium revealed that serine consumption rates increased in pyruvate supplemented PC-3 cells. When serine is degraded, its amino group is transferred to pyruvate with production of alanine and hydroxypyruvate via serine-pyruvate transaminase. However, the alanine production rates did not change in pyruvate supplemented PC-3 cells (Figure 38).

When embryonic stem cells (ESCs) were exposed to oxidative stress, GAPDH and LDHA mRNA levels increased when cultivated in presence of exogenous pyruvate (2.5 mM) for 72 hours suggesting that pyruvate was mainly converted to lactate allowing the NAD^+ - recycle (Ramos-Ibeas et al. 2017). Several studies describe a protective effect of extracellular pyruvate in oxidative stress models (Long and Halliwell 2009; Kládna et al. 2015; Babich et al. 2009). The mechanism by which pyruvate decreases oxidative stress was described by Nath et al., who demonstrated that pyruvate can react with H_2O_2 by an oxidative decarboxylation reaction producing acetate, CO_2 and H_2O (Nath et al. 1994). A dose-dependent antioxidant effect of exogenous pyruvate (concentrations tested: 2.5 - 25 mM) was demonstrated in fibroblasts and ESCs exposed to increasing concentrations of H_2O_2 for 72 hours (Ramos-Ibeas et al. 2017). Wang et al. (2007) described a cytoprotective effect of exogenous pyruvate against the H_2O_2 -induced cell death in human neuroblastoma SK-N-SH cells. Exogenous pyruvate (from 0.1 to 4 mM) dose-dependently decreased ROS production and increased cell survival of SK-N-SH cells exposed to 150 μM for 18 hours in comparison to those cells exposed to the same concentration of H_2O_2 and cultivated in absence of pyruvate (Wang et al. 2007). Treatments of rat cerebellar granular cell cultures with 10 mM exogenous pyruvate for 1 hour upregulated the expression of the antioxidant enzyme

glutathione peroxidase, which remove H_2O_2 by oxidizing glutathione (GSH) (Fernandez-Gomez et al. 2006). Therefore, pyruvate thanks to its antioxidant and free radical scavenger activity was suggested as anti-inflammatory and neuroprotective metabolite (Abusalamah et al. 2020; Kladna et al. 2015; Xia et al. 2016; Wang et al. 2007).

In our studies, we did not measure the H_2O_2 production as well as the oxygen consumption rates in PC-3 control cells depending upon pyruvate concentration.

6.4 Impact of mG3PDH targeting on PC-3 prostate cancer cell proliferation and metabolism

The aim of this study was to investigate whether targeting of mG3PDH has potential for cancer therapy in cancer cells with high mG3PDH activity. In order to carry out the study PC-3 prostate cancer cells were selected as cell line characterized by high mG3PDH activity (Chowdhury et al. 2005). Two commercially available substances (iGP-1 and RH02211) which have been published as mG3PDH inhibitors were investigated (Orr et al. 2014; Singh 2014).

iGP-1 was established as mG3PDH inhibitor of rat skeletal mitochondria by Orr et al. in 2014.

In frozen-thawed skeletal muscle mitochondria the inhibition of the mG3PDH oxidoreductase activity by iGP-1 was measured as the rate of reduction of 50 μ M 2,6-dichlorophenolindophenol (DCPIP) by 26.7 mM glycerol phosphate in the presence of iGP-1 (concentrations tested from 0.25 to 80 μ M) and of the mitochondrial inhibitors rotenone (4 μ M), myxothiazol (2 μ M), antimycin A (2.5 μ M) and potassium cyanide (1 mM) (Orr et al. 2014). The RH02211-induced inhibition of the mG3PDH activity was measured by incubating mG3PDH enzyme purified from PC-3 cell cDNA with RH02211 ($EC_{50} \pm SEM : 27.96 \pm 13.9 \mu$ M) in presence of 30 mM glycerol-3-P. The mG3PDH activity was assayed by the reduction of resazurin, an artificial electron acceptor (Singh 2014).

The impact of the mG3PDH inhibitors on cell proliferation and metabolism of PC-3 cells was studied after long time incubation periods (96 hours) of the cells with the corresponding inhibitor in order to have protocols close to clinical settings with long treatment protocols (Cockrell and Axelrod 2019). Our results show that 100 - 400 μ M iGP-1 induced an about 45% inhibition of PC-3 cell proliferation which was independent upon the inhibitor dosage after 96 hours of treatment (Figure 13). Accordingly, a growth blockade of chromosomal instability (CIN) tumors by 1 mM iGP-1 in *Drosophila* as well as 72 hours treatment of medulloblastoma cells with 100 μ M iGP-1 resulted in significant inhibition of tumor growth (Hussain et al. 2017; Di Magno et al. 2020).

In comparison to iGP-1, a dose-dependent complete inhibition of PC-3 cell proliferation was induced by RH02211. Since cultivation of PC-3 cells in hypoxic conditions did not significantly

modify the IC_{50} value of RH02211 (Table 4), all subsequent experiments with RH02211 were performed in the presence of 21% O_2 only.

mG3PDH is part of the glycerol 3-P shuttle which is involved in transporting hydrogen from cytosol into the mitochondria thereby recycling NAD^+ for the cytosolic GAPDH reaction. Another mechanism to recycle NAD^+ is the transfer of hydrogen to pyruvate with production of lactate catalysed by lactate dehydrogenase. Therefore, we investigated whether extracellular pyruvate is an escape mechanism for mG3PDH targeting. The impact of the mG3PDH inhibitor RH02211 on PC-3 cell proliferation was investigated at low and high pyruvate concentration within the cultivation medium (0.015 mM and 2 mM pyruvate respectively).

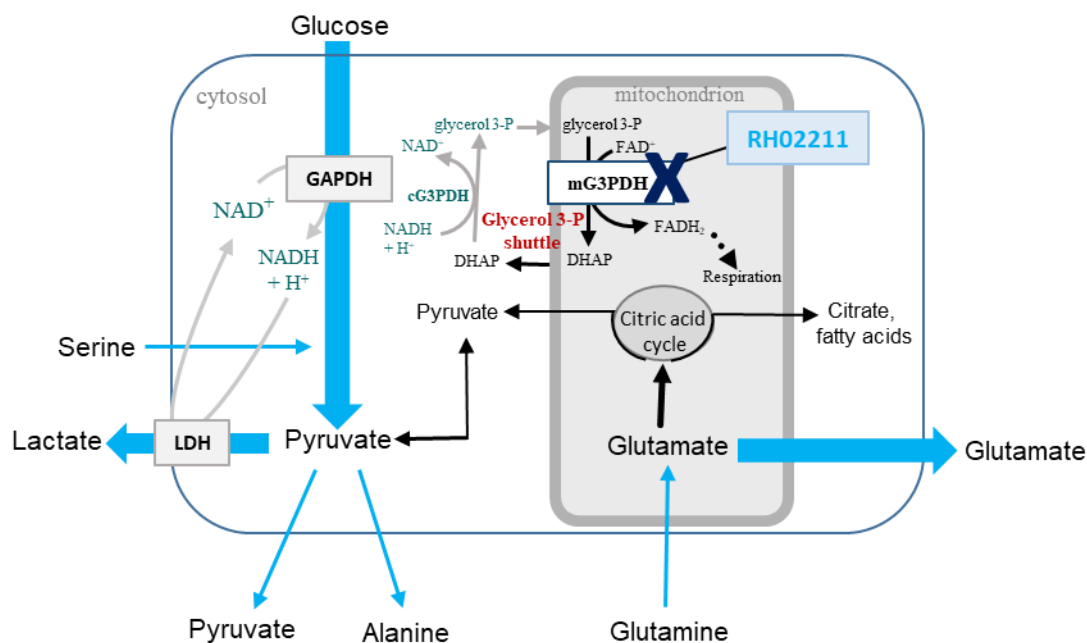
The IC_{50} value of RH02211 was 1/50 of the IC_{50} value of iGP-1 in PC-3 cells cultivated in the presence of 21% O_2 and 0.015 mM pyruvate in the medium (pyruvate starved cultivation conditions) (Table 4). In pyruvate supplemented cultivation conditions the IC_{50} value of RH02211 was 1.5-fold higher than the IC_{50} value of the same inhibitor calculated in the presence of 0.015 mM pyruvate (Table 4) which reflects a weakening effect of extracellular pyruvate on the RH02211 induced inhibition of cell proliferation. Also the iGP-1-induced inhibition of PC-3 cell proliferation was weaker in pyruvate supplemented cultivation conditions (20% inhibition) than in pyruvate starved ones (45% inhibition) (Figures 13 and 17). These results point to an escape mechanism of extracellular pyruvate during RH02211 and iGP-1 induced inhibition of cell proliferation.

Since the iGP-1 dosages required to inhibit PC-3 cell proliferation were extremely higher than the RH02211 ones, the impact of iGP-1 on PC-3 metabolism was not tested in the presence of exogenous pyruvate. Due to the influence of the pyruvate concentrations in the medium on the RH02211-induced inhibition of PC-3 cell proliferation, accordingly all subsequent experiments were performed at both low and high pyruvate concentrations. Several studies showed that cancer cells proliferate more rapidly when cultivated in pyruvate supplemented medium (Elia et al. 2019; Ma et al. 2019; Zhang et al. 2019; Diers et al. 2012). In addition to being reduced to lactate, exogenous pyruvate could be metabolized through the TCA cycle providing energy and metabolic intermediates for a more rapid cancer cell proliferation (Diers et al. 2012).

The impact of 7 μ M RH02211 (named IC_{50} concentration) on the metabolic conversion rates was investigated in both pyruvate starved and pyruvate supplemented PC-3 cells (Figures 39 and 40). In addition to 7 μ M, in pyruvate starved PC-3 cells the impact of 16 μ M RH02211 (named IC_{90} concentration) on the metabolic conversion rates was also tested (Figure 39). Measurements of the metabolic conversion rates in the cultivation supernatants revealed a RH02211-induced dose dependent increase of glucose consumption and lactate production in pyruvate starved cells pointing to an increase of glycolysis (Figure 39). In pyruvate starved cells the RH02211-induced upregulation of glycolysis was also confirmed by the increased intracellular glycolytic intermediates

levels (glucose, glucose 6-P, fructose 6-P, fructose 1,6-bisphosphate, glyceraldehyde 3-P, DHAP, 2+3 phosphoglycerate, PEP, pyruvate and lactate) measured by mass spectrometry (Table 7).

7 μM RH02211



16 μM RH02211

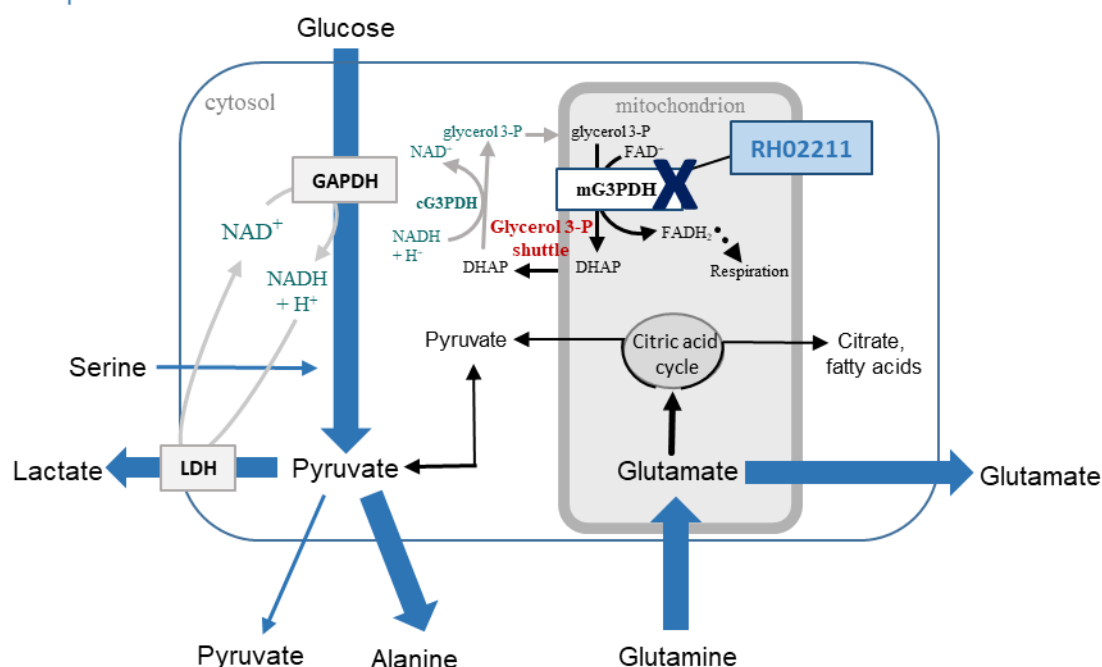


Figure 39. Metabolic schemes of the impact of RH02211 on the glycolytic and glutaminolytic conversion rates in pyruvate starved PC-3 cells.

Pyruvate concentrations = 0.015 mM. Wide arrow: increased flux rate (vs control), thin arrow: unchanged flux rate (vs control), dotted arrow: decreased flux rate (vs control).

In contrast, in pyruvate supplemented cells RH02211 did not affect glucose and lactate conversion rates (Figure 40) as well as the levels of the intracellular glycolytic intermediates (Table 7). Accordingly, in pyruvate supplemented PC-3 cells the unchanged LDH isoenzyme equipment (Table 5) together with the unchanged lactate production rate suggest that the conversion of extracellular pyruvate to lactate via LDH was not the mode of action for the weakening effect of extracellular pyruvate on the RH02211 induced inhibition of cell proliferation.

A possible explanation is that extracellular pyruvate was mainly channeled into TCA cycle supporting energy production and increasing PC-3 cancer cell proliferation when mG3PDH was inhibited by RH02211.

The increased glycolytic conversion rates in pyruvate starved RH02211 treated PC-3 cells which were also observed in pyruvate starved iGP-1 treated PC-3 cells suggest that the capacity of LDH and or the malate aspartate shuttle was sufficient to recycle cytosolic NAD^+ when mG3PDH was targeted (Figures 39 and 41). The LDH isoenzyme equipment as well as the isoenzyme equipment of GOT and MDH were not changed by RH02211 (Table 5). In the same way, the composition of the glycolytic enzyme complex was not impaired by RH02211 independent upon the pyruvate concentration in the medium (data not shown).

A common effect induced by RH02211, independently upon the pyruvate concentration within the medium, was an increase of glutamate production in parallel to unchanged glutamine conversion rates which points to an impairment of glutamine infiltration into the citric acid cycle (Figure 40). The measurements of intracellular glutamine and glutamate concentrations (decreased glutamine and glutamate levels in pyruvate starved cells; decreased glutamine and unchanged glutamate concentrations in pyruvate supplemented cells) do also confirm that RH02211 impaired glutamine metabolism (Table 7). In contrast, the decrease in glutamate release induced by iGP-1 together with the unchanged glutamine consumption rates indicate that glutamine was mainly channeled into the citric acid cycle in iGP-1 treated cells (Figure 41). These results indicate that RH02211 and iGP-1 had a different impact on the glutamine metabolism of PC-3 cells.

Interestingly, RH02211 did not affect pyruvate conversion rates (consumption in pyruvate supplemented PC-3 cells and production in pyruvate starved PC-3 cells). The decrease in serine consumption in pyruvate supplemented RH02211 treated PC-3 cells suggests that the extracellular pyruvate was not used for serine degradation (Figure 40). At the time of writing, no studies regarding the impact of iGP-1 and RH02211 on metabolic conversion rates have been described.

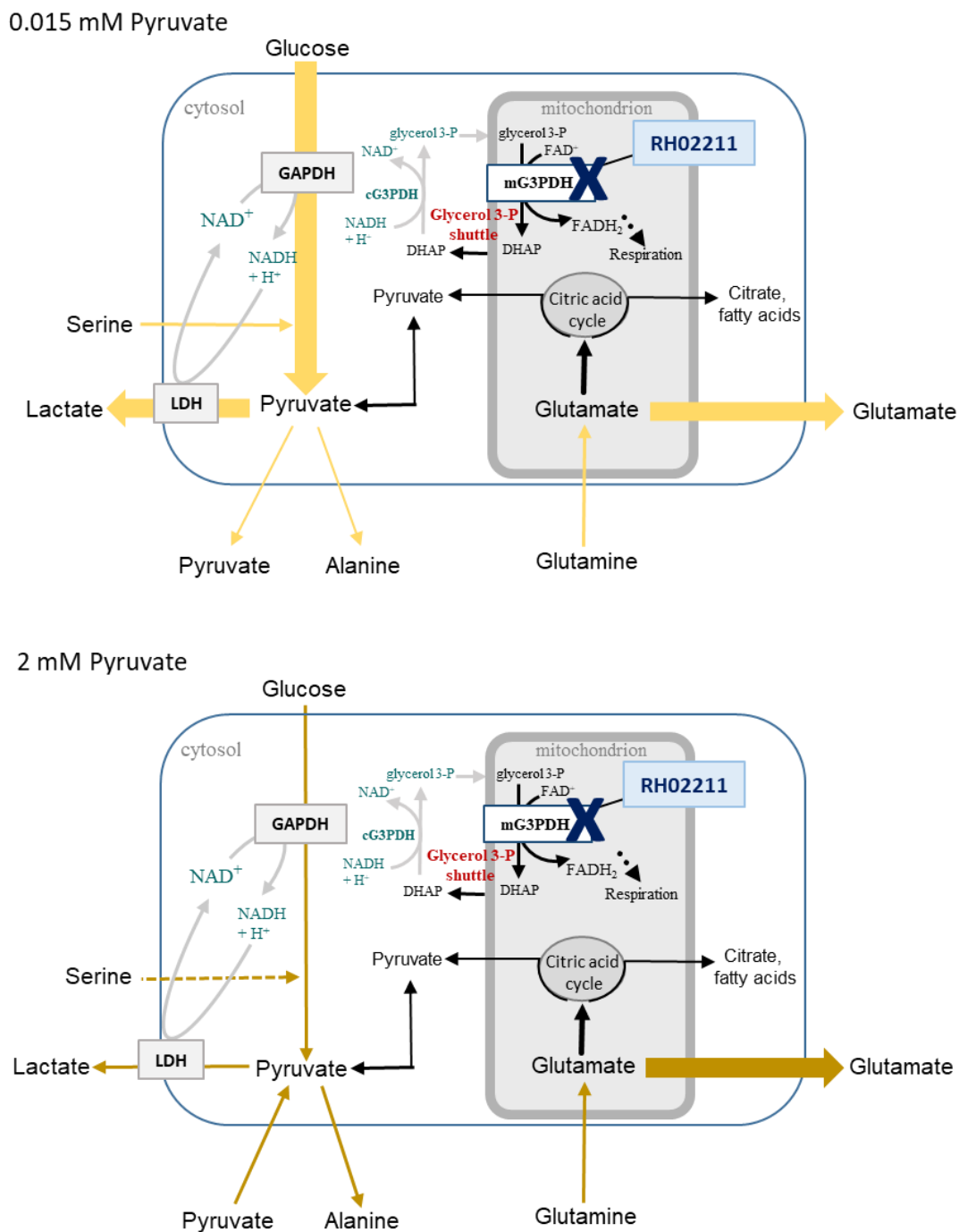


Figure 40. Impact of 7 μ M RH02211 on the glycolytic and glutaminolytic conversion rates in PC-3 cells depending upon the pyruvate concentration in the medium. Wide arrow: increased flux rate (vs control), thin arrow: unchanged flux rate (vs control), dotted arrow: decreased flux rate (vs control).

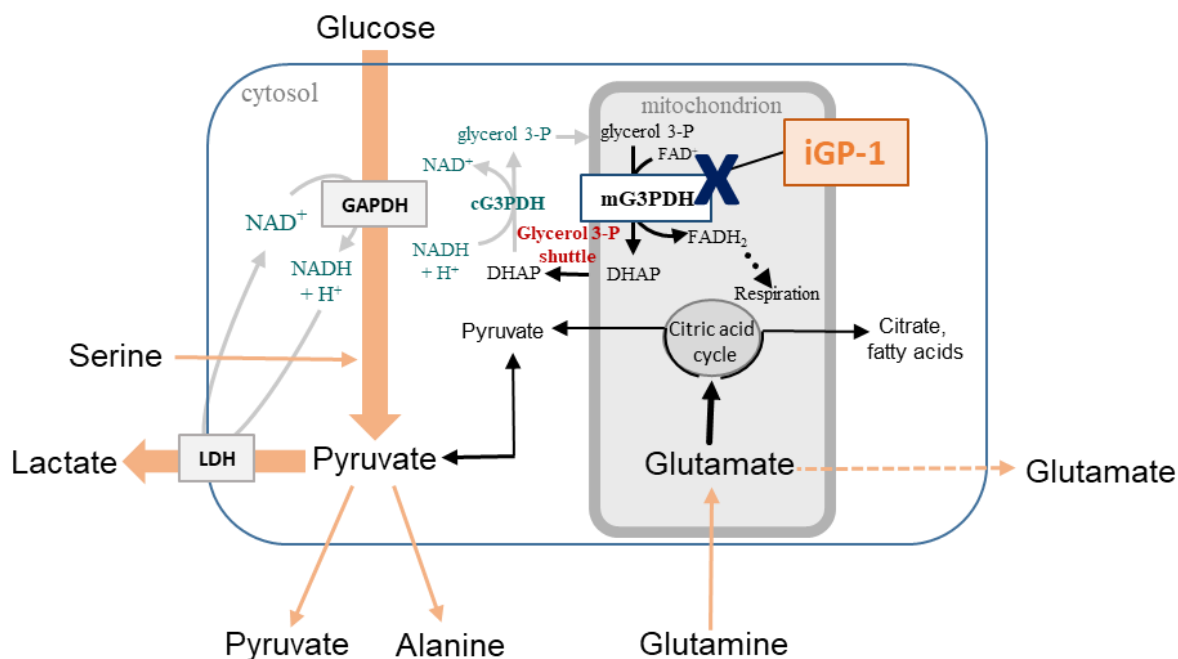


Figure 41. Impact of 300 μM iGP-1 on the glycolytic and glutaminolytic conversion rates in PC-3 cells. Wide arrow: increased flux rate (vs control), thin arrow: unchanged flux rate (vs control), dotted arrow: decreased flux rate (vs control).

Chowdhury et al. suggested that mG3PDH is an important site of electron leakage leading to ROS production in PC-3 prostate cancer cells (Chowdhury et al. 2005). mG3PDH produces superoxide toward each side of the mitochondrial inner membrane, suggesting that the Q-binding pocket of mG3PDH is the major site of superoxide generation (Orr et al. 2012; Mráček et al. 2013). In literature it is described that short term (15 minutes) application of 1-30 μM RH02211 induced a drop in H_2O_2 production in PC-3 cells (Singh 2014). In the corresponding experiments PC-3 cells were cultivated in presence of 1 mM pyruvate in the medium which might be an explanation for the described reduction of H_2O_2 production. Indeed, several studies describe an antioxidant effect of extracellular pyruvate in different oxidative stress models (Long and Halliwell 2009; Kladna et al. 2015; Babich et al. 2009; Ramos-Ibeas et al. 2017). In PC-3 cells an increase of H_2O_2 production was measured independently upon the pyruvate concentration in the medium after long term application (96 hours) combined with the acute titration of RH02211 (Figure 26-27). Besides the application length/treatment protocol of RH02211 another difference between Singh's experiments and ours lies in the H_2O_2 measurement method. Singh measured extracellular H_2O_2 using the HRP/Amplex Red assay in absence of exogenous superoxide dismutase by the EnVision 2102 multilabel reader, whilst we used the HRP/Amplex Red assay at saturating exogenous SOD levels in combination with the O2k-FluoRespirometer (Oroboros Instruments, Innsbruck, Austria). The HRP/Amplex Red assay detects hydrogen peroxide (H_2O_2) that is formed by spontaneous dismutation of superoxide through endogenous SOD. The addition of exogenous SOD at saturating levels ensures that all reactive oxygen species that may have been produced by

the cells are converted to H₂O₂. Further, by using the O2k-FluoRespirometer total cellular H₂O₂ production rates were measured since the measurements were performed after permeabilization of the PC-3 cells plasma membrane with digitonin. In addition, as described in the material and methods section, in order to measure H₂O₂ production rates by the Oroboros Fluorespirometer PC-3 cells treated for 96 hours with RH02211 or vehicle had to be trypsinized. The trypsinized cells were added into the O2k chambers together with RH02211. Due to this protocol it cannot be excluded that the H₂O₂ measured was acutely produced once the cells were added inside the O2k chambers.

It has been shown that increased levels of reactive oxygen species lead to stabilization of HIF-1 α and activation of the transcriptional complex HIF-1 which upregulates the transcription of various cancer-related genes involved in cell survival, angiogenesis and metabolism (Chandel et al. 2000; Semenza 2010a; Semenza 2003). Further, HIF-1 plays an important role in the glycolytic switch activating the transcription of genes encoding the glycolytic enzymes LDHA, PGK, HK and M2-PK (Semenza 2010b; Luo et al. 2011). In our experiments the RH02211-induced increase of ROS correlated with an upregulation of glycolysis. An enzyme that is directly regulated by ROS is the pyruvate kinase isoenzyme type M2 found in tumor cells. M2-PK is characteristic of cancer cells and in contrast to the other PK isoenzymes it can occur in a tetrameric as well as dimeric form (Eigenbrodt et al. 1992; Zwerschke et al. 1999). In pyruvate starved control PC-3 cells the separation of the tetrameric and dimeric form of M2-PK by gel permeation revealed a tetramer : dimer ratio of 1 : 1.6 (Figure 23). In comparison the tetramer : dimer ratio of M2-PK was 1 : 6 in MCF-7 and MDA-MB 453 breast cancer cells when cultivated in presence of 5 mM glucose (Mazurek et al. 1997). The ratio between the highly active tetrameric and the nearly inactive dimeric form of the M2-PK is regulated by different post-translational modifications, such as oxidation by ROS (Prakasam et al. 2018). Although H₂O₂ production increased in RH02211-treated PC-3 cells, the tetramer : dimer ratio of M2-PK determined by gel permeation was 1 : 1.8 indicating that it was not impaired by RH02211 (Figure 23). In contrast, the literature shows that short term expositions to high reactive oxygen concentrations led to an oxidation of M2-PK and to the dissociation of the enzyme to the less inactive dimeric form (Anastasiou et al. 2011; Iqbal et al. 2013). 15 minutes treatment with 1 mM H₂O₂ induced an increase of the intracellular ROS concentrations followed by a decrease in M2-PK activity in A549 human cancer cells (Anastasiou et al. 2011). A possible explanation for the not impaired M2-PK tetramer dimer ratio could be linked to our experiment design (long term incubation time) in comparison to the published studies. It has been proposed that the shift to the dimeric M2-PK leads to accumulation of glycolytic glucose 6-P, which can be channelled into the pentose phosphate pathway generating the NADPH required by the enzyme glutathione reductase to reduce oxidized glutathione for new ROS detoxification (Anastasiou et al.

2011). Owing to the reversible nature of cysteine oxidation (Mitchell et al. 2018), it could be that after 96 hours of RH02211 treatment PC-3 cells were able to produce sufficient reduced glutathione which, even if not enough to decrease ROS levels, was able to reduce the M2-PK oxidised cysteines restoring the tetramer dimer ratio of the enzyme. Accordingly, the enzymatic activity of M2-PK increased by 4-fold when protein solutions of 0.0025 mg/ml M2-PK obtained from purified transformed *E.coli* BL21 cells were incubated for 3 hours with reducing agents (either 100 μ M GSH or 100 μ M DTT) (Mitchell et al. 2018). Mass spectrometry experiments revealed that RH02211 upregulated the pentose phosphate pathway (increased levels of NADPH, gluconate, 6-phosphogluconate, ribose + ribulose 5-P) and increased the glutathione levels (both oxidized and reduced) for antioxidant defence (very new data, not shown).

In pyruvate starved and pyruvate supplemented PC-3 cells the RH02211-induced increase of H₂O₂ production was associated with an increase of O₂ consumption rates (OXPHOS) when cells were permeabilized and glycerophosphate was used as fuel substrate (Figures 24-25). On the contrary, in pyruvate starved permeabilized cells a decrease of O₂ consumption was induced by RH02211 when succinate was used as fuel substrate suggesting that RH02211 treatment impaired unexpectedly succinate oxidation but not the glycerophosphate ones (Figure 24). In living PC-3 cells 96 hours treatment with RH02211 increased O₂ consumption in pyruvate starved cells but not in the pyruvate supplemented ones (ROUTINE). However, the acute titration of RH02211 increased O₂ consumption independently upon the presence or absence of pyruvate in the cultivation medium (ROUTINE + RH02211) (Figures 24-25). No impact of RH02211 on oxygen consumption is described in literature at yet. Acute titrations of 25 and 80 μ M iGP-1 significantly decreased glycerol phosphate-dependent respiration in isolated skeletal muscle mitochondria using a Seahorse XF24 Analyzer (Orr et al. 2014).

Both glycerophosphate and succinate are fuel substrates of the mitochondrial electron transfer pathway by transferring reducing equivalents to the CoQ pool. On the inner surface of the inner mitochondrial membrane succinate is oxidized to fumarate at the level of complex II by succinate dehydrogenase supporting the electron flux via flavin adenine dinucleotide (FADH₂) to the CoQ. A reduced flavin prosthetic group (FADH₂) is also generated by the oxidation of glycerophosphate to dihydroxyacetone phosphate by mG3PDH on the outer face of the inner mitochondrial membrane. The reduced flavoprotein donates its reducing equivalents to the electron transfer-pathway at the level of CoQ (Gnaiger 2020).

A possible explanation for the higher glycerophosphate-linked respiration in permeabilized PC-3 cells compared to the succinate-linked ones could be that long-term incubation with RH02211 may change the response to glycerophosphate, probably with a higher mG3PDH activity or expression. Measurements of intracellular metabolite concentrations revealed a decrease of glycerol 3-P,

increase of DHAP as well as a decrease of NAD^+ levels in pyruvate starved RH02211-treated PC-3 cells which reflects that RH02211 indeed targets the glycerol 3-P shuttle (Figure 42). The decrease in glycerol 3-P, increase in DHAP as well as the increase in O_2 consumption and H_2O_2 production points to an activation of mG3PDH which is in contrast to the first description of Singh 2014. Singh cultivated PC-3 cells in presence of pyruvate. In our experiments DHAP levels dropped in pyruvate supplemented RH02211-treated cells which points to an inhibition of mG3PDH. While in pyruvate starved RH02211 treated PC-3 cells NAD^+ levels decreased in pyruvate supplemented RH02211 treated PC-3 cells NAD^+ levels were not impaired which may be explained by a recycling of NAD^+ via lactate dehydrogenase (Figure 42). As already assumed by Singh in 2014 besides targeting mG3PDH other modes of actions can not be excluded. Our experiments were performed with PC-3 cells which are characterized by high mG3PDH activity. In future experiments it will be interesting to investigate the impact of RH02211 on tumor cells with low mG3PDH activity.

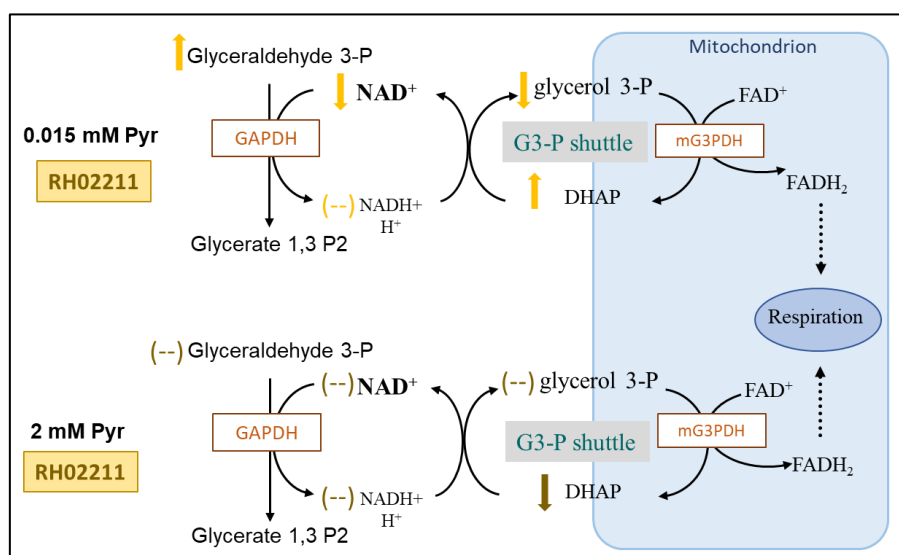


Figure 42. Impact of RH02211 on mG3PDH activity and on the glycerol 3-P shuttle in pyruvate starved and pyruvate supplemented PC-3 cells. Up arrow: increase (vs control), dashed line: no change (vs control), down arrow: decrease (vs control).

Table 14. Summary tables showing the impact of the mG3PDH inhibitors on the metabolic conversion rates of PC-3 cells cultivated in the presence of 0.015 mM pyruvate and 21% O₂. A) Comparison between the impact of iGP-1 and RH02211 (300 μM iGP-1 and 7 μM RH02211 ~ IC₅₀ values); B) Dose-dependent impact of RH02211 (7 μM ~ IC₅₀ value, 16 μM ~ IC₉₀ value).

A

	300 μM iGP-1 (vs DMSO control)	7 μM RH02211 (vs DMSO control)
Glucose consumption	↑	↑
Lactate production	↑	↑
Pyruvate production	=	=
Alanine production	=	=
Serine consumption	=	=
Glutamate production	↓	↑
Glutamine consumption	=	=

B

	RH02211 (vs DMSO control)	
	7 μM	16 μM
Glucose consumption	↑	↑↑
Lactate production	↑	↑↑
Pyruvate production	=	=
Alanine production	=	↑
Serine consumption	=	=
Glutamate production	↑	↑↑
Glutamine consumption	=	↑

Table 15. Summary table showing the impact of extracellular pyruvate (2 mM) on the metabolism of control PC-3 cells as well as on RH02211-inhibited PC-3 cells cultivated at 21% O₂.

	Control	7 μ M RH02211		
	2 mM Pyruvate (vs 0.015 mM Pyr)	0.015 mM Pyruvate (vs DMSO control)	2 mM Pyruvate (vs DMSO control)	
Metabolic conversion rates	Glucose consumption	↓	↑	=
	Lactate production	↓	↑	=
	Pyruvate production/consumption	Shift from production to consumption	production =	consumption =
	Alanine production	=	=	=
	Serine consumption	↑	=	↓
	Glutamate production	↓	↑	↑
	Glutamine consumption	↓	=	=
Enzymes	LDH isoenzymes	=	=	=
	GOT	=	=	=
	MDH	=	=	=
	Tetramer : dimer ratio of M2-PK	=	=	=
Oroboros	O ₂ consumption (Substate: Gp)	Not measured	↑	↑
	O ₂ consumption (Substate: S)	Not measured	↓	Not measured
	H ₂ O ₂ production	Not measured	↑	↑

6.5 Impact of mitochondrial CIII inhibitors on PC-3 prostate cancer cell proliferation and metabolism

The aim of this study was to investigate the impact of mitochondrial complex III targeting on PC-3 cell proliferation and metabolism. In order to carry out the study the impact of three different commercially available substances (Antimycin A, Myxothiazol and S3QEL-2) was investigated on PC-3 cell proliferation and metabolism. Antimycin A (AA) and Myxothiazol (Myx) inhibit CIII by different mode of actions. AA blocks the electron flow from cyt b_H to ubiquinone (Q) overlapping the quinone reduction site Q_i while Myx acts at the proximal niche of Q_o and stops the electron flow from ubiquinol (QH₂) to the iron-sulfur center, and, indirectly, also to cyt b_L (Figure 7) (Xia et al. 1997). Differently from AA and Myx that directly inhibit the mitochondrial respiration by inhibiting the electron flow at the level of CIII, the S3QEL-2 compound was published as suppressor of superoxide/hydrogen peroxide production from site III_{Q_o} without inhibiting the OXPHOS (Figure 7) (Orr et al. 2015; Fang et al. 2020).

The oxygen levels in hypoxic tumor tissues are < 2% while normal tissues are ordinarily maintained at 3 - 7% oxygen (McKeown 2014). Therefore, in order to perform the experiments under more

physio-pathological conditions we performed the experiments at 1.5% O₂ (hypoxia/pathological hypoxia) as well as at 21% O₂ (hyperoxia) used in a majority of the published culture studies.

Our results show that all three CIII inhibitors induced a dose dependent inhibition of PC-3 cell proliferation after 96 hours of treatment at both 21% and 1.5% O₂ (Table 8). 2.3 nM AA inhibited 50% of PC-3 cell proliferation at 21% O₂, whereas at 1.5% O₂ PC-3 cell proliferation was inhibited by 42 nM AA. These results suggest that cultivation under hypoxic conditions led to a significant weakening of the growth inhibitory effect of AA as reflected by an 18-fold increase of the IC₅₀ value of AA under hypoxic conditions in comparison to 21% O₂ ($p < 0.001$).

Several studies published from the group of Han et al. have shown the dose-dependent inhibitory effect of AA on the cell proliferation of different cell lines cultivated at 21% O₂. 2-100 μ M AA induced a significant cell growth inhibition of human pulmonary adenocarcinoma A549 cells after 72 hours of treatment with an IC₅₀ of 2 μ M at 24 hours (Han et al. 2008). Further, a 24 hours treatment with AA inhibited the growth of human pulmonary fibroblast (HPF) cells with an IC₅₀ of \sim 150 μ M as well as of human pulmonary adenocarcinoma Calu-6 cells with an IC₅₀ of about 100 μ M (Park and You 2016; Han and Park 2009). These data suggest that HPF cells seemed to be more resistant to AA than the lung cancer cells A549 and Calu-6. The growth inhibitory effect of AA in HPF, A549 and Calu-6 cells was associated with an induction of a G1 phase arrest and apoptosis as well as increasing ROS levels and glutathione (GSH) depletion (Han and Park 2009; Park and You 2016; Han et al. 2008). The antiproliferative and pro-apoptotic effect of AA was associated with loss of the mitochondrial membrane potential in Calu-6 lung cancer cells as well as in CAL 27 and Ca9-22 oral cancer cell lines (Yu et al. 2020; Han and Park 2010). In HeLa cells 2, 10 and 50 μ M AA induced an arrest in the S phase of the cell cycle after 72 hours of treatment. In As4.1 juxta-glomerular cells an arrest in all the cell cycle phases as well as a loss of the mitochondrial membrane potential was observed when treated with 0.05 μ M AA for 48 hours (Han et al. 2008; Park et al. 2007b). The wide range of the AA concentration (2-150 μ M) required to inhibit 50% of cell proliferation after 24 hours treatment in different cancer cell lines is probably linked to the different basal activities of antioxidant enzymes and mitochondria that each cell type possesses (Park and You 2016).

The IC₅₀ values for AA determined by us for the PC-3 cells are significantly lower than the IC₅₀ values published in other studies. An explanation for the lower IC₅₀ values could be found in the cell line and the significantly longer incubation time (96 hours) in comparison to other studies. Accordingly, in Calu-6 cells treated with AA the IC₅₀ decreased from 100 μ M at 24 hours to 50 μ M after 72 hours treatment (Han and Park 2009). In comparison treatment of human glioma cells for 3 hours with 100 μ M AA induced a 93% inhibition of cell proliferation (Jeong et al. 2003).

No studies describing the impact of AA on cell proliferation under hypoxic conditions were found at the time point of writing this thesis.

Jeong et al. (2003) describe AA as a chemical hypoxia inducer due to its ability to reduce oxygen reduction within the mitochondria by inhibiting CIII. The significant higher AA IC_{50} found for AA when PC-3 cells were cultivated in presence of 1.5% O_2 in comparison to 21% O_2 points to an increased resistance of hypoxic PC-3 cells to the AA-induced cell growth inhibitory effect. In human lung carcinoma A549 cells 1-48 hours exposition to 1% O_2 significantly increased the expression of the antiapoptotic molecules Bcl-2 and Bcl-XL (Park et al. 2002). Accordingly, we can speculate an inhibition of apoptosis by hypoxia as possible explanation for the higher AA concentrations necessary to inhibit PC-3 cell proliferation at 1.5% O_2 .

In contrast to AA, no differences in the IC_{50} s values were found when PC-3 cells were treated for 96 hours with Myx at 21% O_2 ($IC_{50} = 2.6$ nM) in comparison to those cultivated at 1.5% O_2 ($IC_{50} = 2.3$ nM) (Table 8 A). Therefore, the inhibitory effect of Myx on cell proliferation was not affected from oxygen supply. In comparison, treatment of human lymphoblastic T-cell line Jurkat cells with 1 μ M Myx for 24 – 48 hours in presence of 21% O_2 reversibly blocked the G1/S phase of the cell cycle (Conradt et al. 1989). In Jurkat lymphocyte cells and isolated rat carotid body type I cells Myx compromised the generation of the protonmotive force as well as dissipated the electrochemical proton gradient leading, consequently, to the mitochondrial membrane potential collapses (Makowska et al. 2000; Wyatt and Buckler 2004).

As discussed above for the cell growth inhibitory effect of AA, a possible explanation for the lower Myx inhibitory concentrations found for PC-3 cells in comparison to those described in literature could be the longer incubation time (96 hours) of PC-3 cells with Myx as well as the different response to Myx-induced ROS production of the different cell lines since Myx, like AA, it is described in literature as a ROS inducer from CIII (Starkov and Fiskum 2001). No studies describing the impact of Myx on cell proliferation under hypoxic conditions were found at the time point of writing this thesis.

The IC_{50} of AA and Myx were not significantly different when PC-3 cells were cultivated in the presence of 21% O_2 (Table 8 A). In contrast the inhibitory effect of AA which inhibits Q_i site of complex III but not of Myx which inhibits site Q_o of complex III was weakened in hypoxia, suggesting that hypoxia has an impact on Q_i site inhibition but not on Q_o site inhibition of CIII. Taken together these results revealed that during 96 hours incubation the antiproliferative effect of Q_i site inhibition was more pronounced at high oxygen supply whereas the antiproliferative effect of Q_o site of CIII inhibition was independent upon oxygen supply.

Likewise Myx, the inhibitory effect of S3QEL-2 on PC-3 cell proliferation was not affected from oxygen supply. Indeed, 9.2 μ M S3QEL-2 inhibited 50% of cell proliferation when cells were

cultivated at 21% O₂ and 13.5 μM S3QEL-2 was the IC₅₀ value at 1.5% O₂ (Table 8 A). Any impact of S3QEL-2 on cell proliferation is published at the time point of writing this thesis.

The IC₅₀ value of S3QEL-2 for inhibition of PC-3 cell proliferation was about 3500 times higher in comparison to Myx. Even if both compounds act at the level of the Q_o site of CIII, the stronger inhibitory effect of Myx is probably linked to its ability to block the electron flux through CIII differently to S3QEL-2.

Data generated using the O2k-FluoRespirometer from Oroboros Instruments, indicate that oxygen consumption driven by succinate (fuel substrate) and rotenone (CI inhibitor) strongly decreased in Myx-treated PC-3 cells but also slightly decreased in S3QEL-2-treated permeabilized cells cultivated at 21% O₂ (Figure 35).

The inhibition of mitochondrial respiration by Myx is well documented in literature. Myx inhibits respiration by preventing an electron being transferred from the ubiquinol to the Rieske iron-sulfur protein (Figure 7) (Turrens 1997). The inhibitory Myx property was demonstrated in skeletal muscle, liver and heart mitochondria (Taylor et al. 1994; Thierbach and Reichenbach 1981; Becker et al. 1981; Young et al. 2002). Dawson et al. demonstrated that acute titration of 10 μM Myx inhibited cellular respiration in rat liver hepatocytes (Dawson et al. 1993). In contrast to our results, Orr et al. (2015) described no impact of S3QEL-2 on mitochondrial respiration independently upon the fuel substrates (succinate, glutamate, glycerophosphate) tested. Acute titration of 16 μM S3QEL-2 did not modify the respiration rates driven by succinate plus rotenone in rat muscle isolated mitochondria. Further, 34 μM S3QEL-2 had no impact on basal and uncoupled respiration driven by pyruvate and glutamine in human embryonic kidney cells (HEK-293) measured for 3 hours using a Seahorse XF24 (Orr et al. 2015). Pyruvate and glutamine feed electrons mainly into mitochondrial CI by being converted into TCA intermediates and stimulating dehydrogenases with reduction of NAD⁺ to NADH. Succinate is oxidized to fumarate at the level of complex II by succinate dehydrogenase supporting the electron flux via FADH₂ to the CoQ (Gnaiger 2020). When succinate is titrated in combination with rotenone the NADH-linked dehydrogenases are inhibited since the electron supply from succinate through complex I failed and therefore CII is the only source of reducing equivalents for the CoQ (Figure 46). A possible explanation for the slight decrease of the respiratory rates found in our experiments with PC-3 cells treated with 12 μM S3QEL-2 could be the longer exposition time (96 hours) to the drug combined with its acute titration during the measurements in comparison to the exposition times (up to 3 hours) investigated by Orr et al. (2015). In AML12 hepatocytes respiration was not affected by 0.5 μM S3QEL1.2. However the exposition time to the inhibitor was not specified in the publication (Fang et al. 2020).

The weaker effect of S3QEL-2 on mitochondrial respiration compared to Myx may be an explanation for the significantly higher IC_{50} values of S3QEL-2 in comparison to Myx for the inhibition of PC-3 cell proliferation.

Likewise Myx, also AA (2.5 nM) strongly inhibited mitochondrial respiration in PC-3 cells (Figure 35). The inhibitory property of AA on cellular respiration is very well described in literature. AA inhibits cellular respiration by blocking the electron flow from cyt b_H to ubiquinone at the level of site III_{Q_i} (Figure 7) (Xia et al. 1997). Cellular oxygen consumption in yeast strains was inhibited by 2 $\mu\text{g}/\text{ml}$ ($= 3.8 \mu\text{M}$) AA (Deffieu et al. 2013). In Deffieu et al. details regarding the incubation time with AA in oxygen consumption measurements were not found. In rat liver mitochondria 0.75 μM AA inhibited about 50% of oxygen consumption when measured in the presence of 5 mM succinate after 1 hour incubation (Janssens et al. 2000). The lower AA-concentration required to inhibit mitochondrial respiration in PC-3 cells could be probably linked to the different treatment protocol (96 hours treatment plus acute titration of the inhibitor during the measurements) in comparison to those described in literature. Due to the well know inhibitory effect on mitochondrial respiration, acute titrations of AA in the μM range (0.5 – 2.5 μM) are commonly used in respirometry at the end of the experiment protocols to completely inhibit the oxygen consumption dependent from mitochondria (Gu et al. 2021; Gnaiger 2020). The Residual oxygen consumption (Rox) remaining after AA-inhibition is due to oxidative side reactions remaining after inhibition of the electron transfer pathway. Mitochondrial respiration is usually corrected for Rox. Accordingly to Gnaiger (2020), 2.5 μM AA was titrated into the O2k chambers at the end of every respirometry experiment performed with PC-3 cells.

The metabolic flux rates indicate that both site Q_i inhibition by AA and site Q_o inhibition of complex III by Myx was associated with an increase in lactate production as well as an increase in glutamate release independent upon the oxygen concentrations (Figures 43-44). An increase in lactate release was also induced by S3QEL-2 at 21% O_2 but not at 1.5% O_2 (Figure 45).

In Myx and S3QEL-2 treated PC-3 cells at both low and high oxygen supply as well as in AA treated cells at 21% O_2 the increase in lactate production correlated with an increase in glucose consumption. Since PC-3 cells were cultivated without pyruvate supplementation, cells released intracellular pyruvate into the cultivation medium. Intracellular pyruvate may derive from the degradation of glucose, serine and glutamine. If not converted to acetyl-CoA intracellular pyruvate can be released from the cells directly or after conversion to lactate or alanine. The unchanged or decreased pyruvate production rates together with the increased release of lactate and alanine suggest that intracellular pyruvate was presumably released as lactate and alanine in PC-3 cells cultivated in the presence of either AA at both 21% O_2 and 1.5% O_2 , Myx at 1.5% O_2 and S3QEL-2 at 21% O_2 (Figures 43-45). When PC-3 cells were treated with Myx at 21% O_2 intracellular

pyruvate was presumably mainly released as lactate since lactate production increased while pyruvate release decreased and alanine release did not change (Figure 44). Due to the inhibition of respiration by AA and Myx we assume that infiltration of pyruvate into the citric acid cycle did not play an important role when PC-3 cells were treated with the two inhibitors.

The increase in glutamate release in S3QEL-2-treated cells cultivated at hypoxia as well as in AA- and Myx-treated cells cultivated at 21% and 1.5% O₂ indicates that less glutamine was infiltrated into the citric acid cycle leading to an impairment of glutaminolysis (Figures 43-45).

In contrast, glutaminolysis seems not to be impaired by S3QEL-2 at 21% O₂ since glutamine consumption and glutamate release were not affected. A possible explanation for the different effect of S3QEL-2 on glutamine metabolism could be that at 21% O₂ glutamine was infiltrated into the TCA cycle. On the contrary, glutamine was mainly released as glutamate when the mitochondrial respiration was inhibited by hypoxia. In perfused rat hippocampal slices hypoxia (25 minutes exposition) induced a pronounced glutamate release (Potter et al. 1991). Further a time-dependent increase of extracellular glutamate in the media of human liver cancer Hep3B cells was induced by 24-48 hours of exposition to 1% O₂, as compared to cells maintained at 20% O₂, indicating that reduced oxygen availability triggers increased glutamate release. The increase of glutamate release was mediated by HIF-dependent expression of the SLC1A1 and SLC1A3 genes encoding glutamate transporters (Hu et al. 2014).

At 21% O₂ the only slight decrease of mitochondrial respiration in S3QEL-2-inhibited cells may allow glutamine infiltration into the TCA cycle. In contrast, when respiration is nearly completely inhibited by AA and Myx glutamine cannot be channelled into the TCA and therefore is released as glutamate.

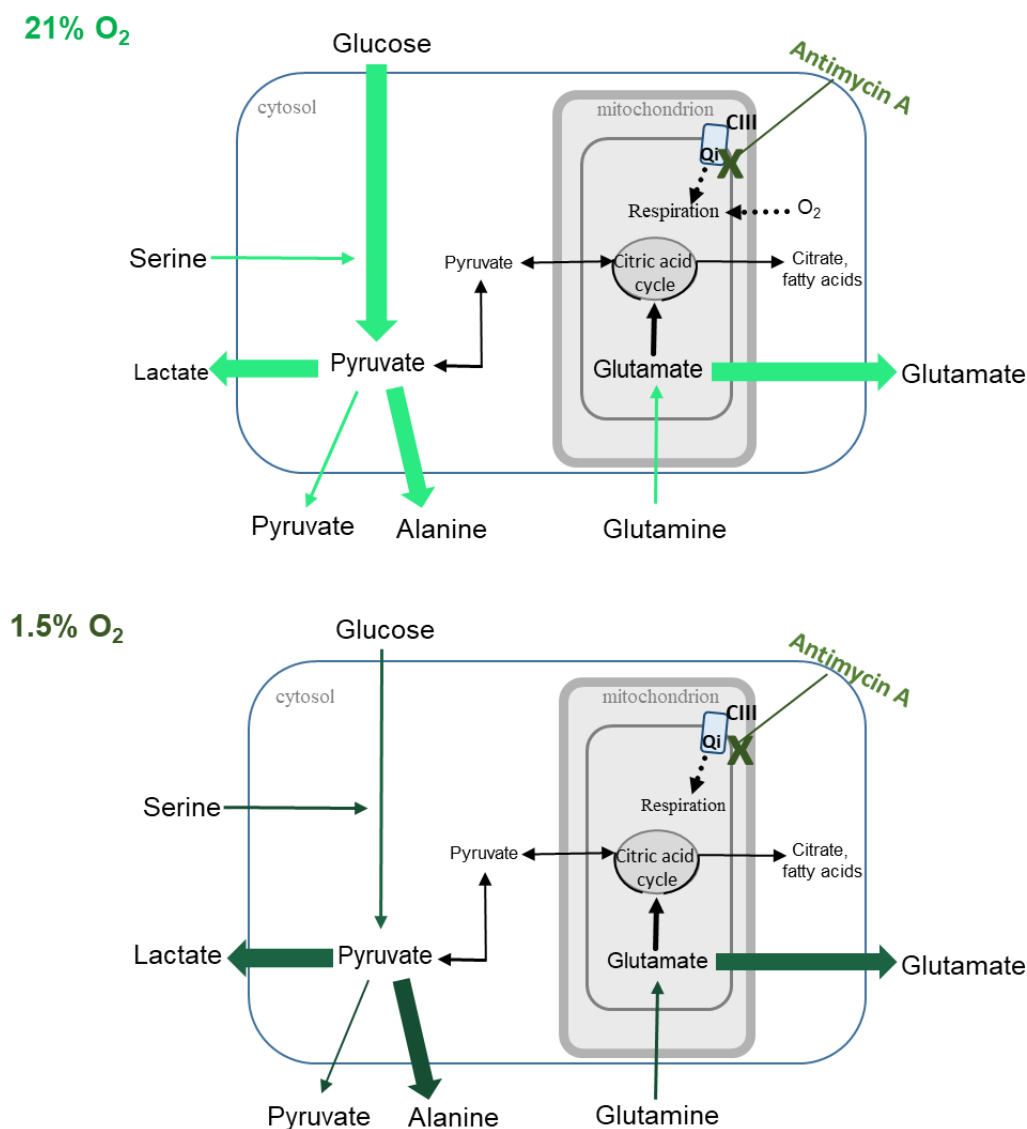


Figure 43. Impact of the IC_{50} concentrations of Antimycin A at both 21% and 1.5% O_2 on the glycolytic and glutaminolytic conversion rates in PC-3 cells.

Wide arrow: increased flux rate (vs control), thin arrow: unchanged flux rate (vs control).

To sum up, when the electron flux through CIII is inhibited by AA, Myx and S3QEL-2 glucose becomes the main energetic source due to the inability or reduced ability to produce energy in the mitochondria. Extensive observations have been made, in the literature, that cells with impaired mitochondrial function utilize glycolysis over oxidative phosphorylation for energy regeneration (Li et al. 2014a). Tiefenthaler et al. (2001) demonstrated that apoptosis-associated loss of mitochondrial ATP production shifts cellular energy production to compensatory glycolysis. In particular, in human acute lymphoblastic leukaemia cell line CCRF-CEM 10 $\mu\text{mol/l}$ AA induced apoptosis and loss of the mitochondrial membrane potential together with increased lactate production rates (Tiefenthaler et al. 2001). In rat reticulocytes an increase of glucose uptake and lactate formation was observed when cellular respiration was blocked for 15 minutes by 10 $\mu\text{g/ml}$ ($= 18.8 \mu\text{M}$) AA (Ghosh and Slovirer 1973). In isolated nerve terminals the supplementation of 1 nM – 1 μM AA or 10 nM – 10 μM Myx to depolarized synaptosome induced a 60 – 90 % inhibition

of complex III as well as an increase of Ca^{2+} independent glutamate release (Kilbride et al. 2011). At the time point of writing this thesis, no data showing the impact of S3QEL-2 on the glycolytic and glutaminolytic conversion rates are published.

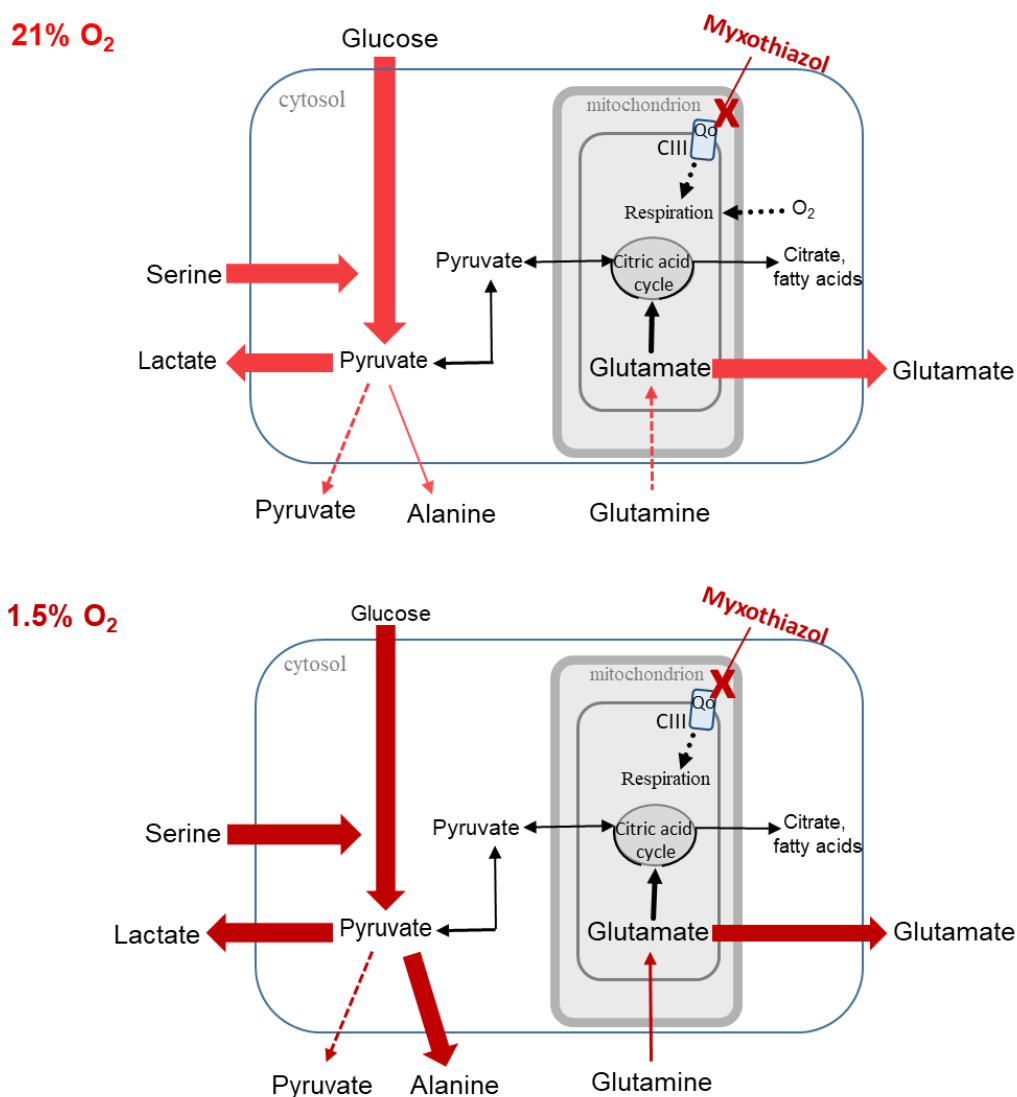


Figure 44. Impact of the IC₅₀ concentrations of Myxothiazol at both 21% and 1.5% O₂ on the glycolytic and glutaminolytic conversion rates in PC-3 cells.

Wide arrow: increased flux rate (vs control), thin arrow: unchanged flux rate (vs control), dotted arrow: decreased flux rate (vs control).

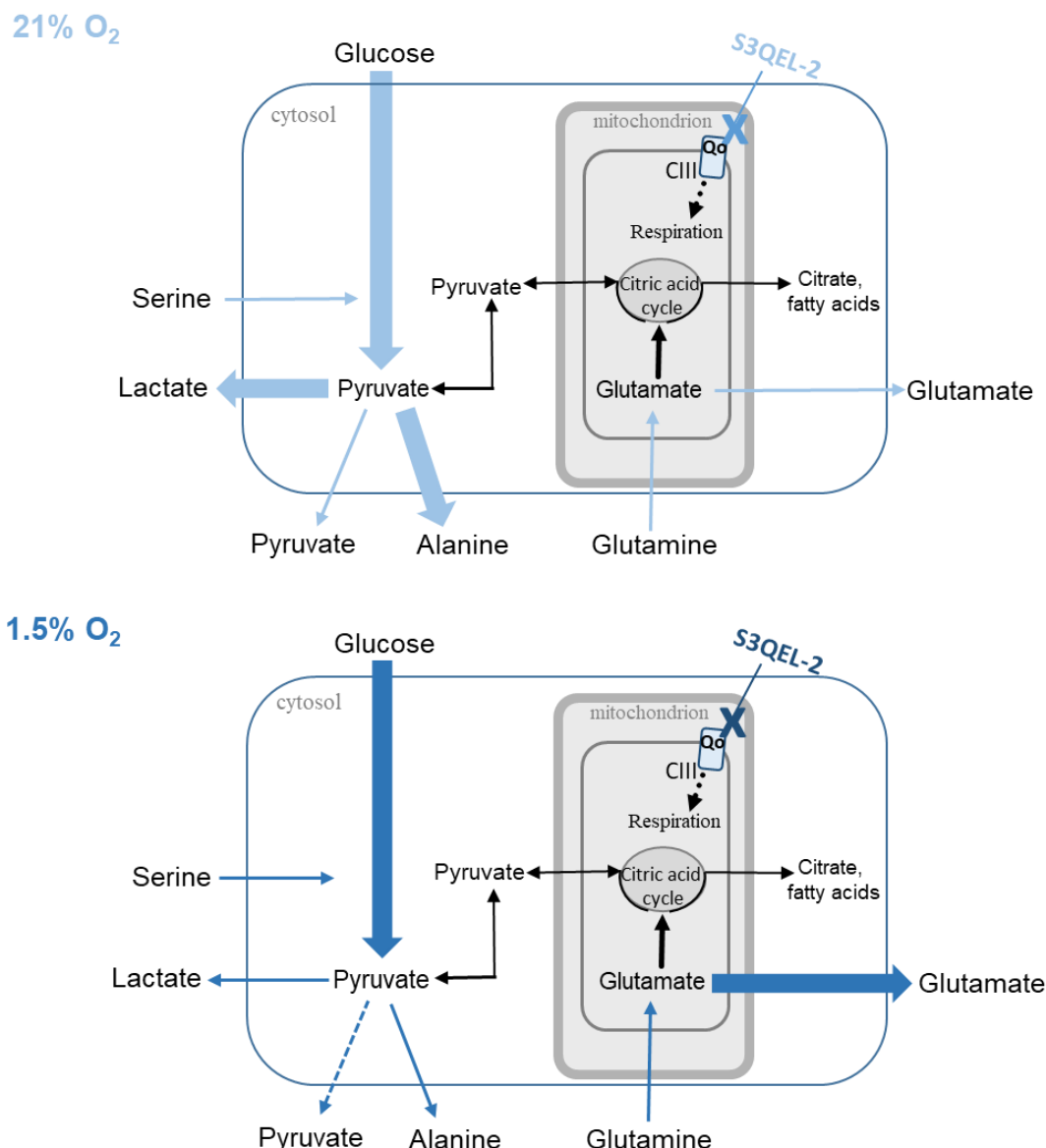


Figure 45. Impact of the IC₅₀ concentrations of S3QEL-2 at both 21% and 1.5% O₂ on the glycolytic and glutaminolytic conversion rates in PC-3 cells.

Wide arrow: increased flux rate (vs control), thin arrow: unchanged flux rate (vs control), dotted arrow: decreased flux rate (vs control).

Mitochondrial CIII has been shown to participate in ROS production in isolated yeast cytochrome *bc*₁ complex and submitochondrial particles from bovine heart mitochondria (Muller et al. 2003; Dröse and Brandt 2008; Jezek and Hlavatá 2005). Increased levels of ROS lead to stabilization of HIF-1 α and activation of the transcriptional complex HIF-1 which upregulates the transcription of various cancer-related genes involved in cell survival, angiogenesis and metabolism (Chandel et al. 2000; Semenza 2010a; Semenza 2003). Further, HIF-1 plays an important role in the glycolytic switch activating the transcription of genes encoding the glycolytic enzymes LDHA, PGK, HK and M2-PK (Semenza 2010b; Luo et al. 2011). Increased ROS causes also GAPDH inactivation which promotes the pentose phosphate pathway (PPP) required for cell building blocks synthesis. For example, in mammalian P388D1 cells, GAPDH was inhibited within minutes of exposure to H₂O₂

(100 μM) mainly via direct inactivation of the enzyme since the active site cysteine of GAPDH is highly sensitive to inhibitory oxidative modifications of ROS (Mullarky and Cantley 2015; Cochrane 1991).

Both AA and Myx were published as ROS inducers because both inhibitors extend the life of Q^- by inhibiting the flow of electrons through CIII at Q_0 . The Q^- can then react with the O_2 dissolved in the inner mitochondrial membrane to form O_2^- (Figure 7A) (Thomas et al. 2001; Jezek and Hlavatá 2005). Differently from AA and Myx, the S3QEL-2 compound was published as suppressor of superoxide/hydrogen peroxide production from site III_{Q_0} without inhibiting the OXPHOS (Orr et al. 2015; Fang et al. 2020).

Several studies describe an increase of H_2O_2 production in different cell lines after long- and short-term incubation with AA and Myx at 21% O_2 . A dose dependent increase of intracellular O_2^- and H_2O_2 levels is described in human lung cancer A549 cells when 2-100 μM AA was applied for 72 hours (Han et al. 2008). Increased levels of intracellular ROS were measured in HeLa cells treated with 50 μM AA for 72 hours (Park et al. 2007a). Interestingly, in renal As4.1 cancer cells Han et al. (2007b) described a dose dependent accumulation of O_2^- in the first 50 minutes of incubation with 0.005 μM – 10 μM AA; after 90 minutes O_2^- generation reached its maximum with 0.5 mM AA and thereafter decreased (Han et al. 2007). In isolated yeast cyt bc_1 complex as well as in submitochondrial particles from bovine heart mitochondria increased H_2O_2 production rates were induced by either 10 μM AA or 10 μM Myx (Muller et al. 2003; Dröse and Brandt 2008).

Li et al. (2014a) described increased mitochondrial ROS levels in human pro-myelocytic leukemia HL-60 cells treated with either AA ($\text{EC}_{50} = 17.7 \mu\text{M}$) or Myx ($\text{EC}_{50} = 3.3 \mu\text{M}$) for 6 hours. Increased levels of H_2O_2 have been reported even when isolated bovine and rat mitochondria were treated with 1 μM Myx and fueled with succinate (Starkov and Fiskum 2001).

Differently from AA and Myx, Orr et al. (2015) has described that S3QEL-2 induced a selective decrease in site III_{Q_0} superoxide/ H_2O_2 production in isolated rat muscle mitochondria by using succinate as substrate. Additionally, 6 hours-treatment with 10-30 μM S3QEL-2 inhibited total cellular ROS in insulin secreting beta INS-1 cells during tunicamycin-induced ER stress (Orr et al. 2015).

During oxidation of a single substrate (succinate, glutamate plus malate, palmitoylcarnitine or glycerol 3-phosphate) superoxide/ H_2O_2 are produced from multiple sides of the mitochondrial respiratory complexes (Quinlan et al. 2013). Quinlan et al. demonstrated in rat skeletal muscle mitochondria that during succinate oxidation most of the superoxide production was from the site of quinone reduction in complex I (site I_{Q}), with small contributions from the flavin site in complex I (site I_{F}) and the quinol oxidation site in complex III (site III_{Q_0}). The rotenone addition led to an

oxidation of NADH as the electron supply from succinate through complex I failed and to an increase in the reduction level of cyt b as all flow was diverted through complex III (Figure 46). Indeed, the primary mechanism of H_2O_2 production during succinate oxidation is a reverse electron transport (RET) into complex I, because the H_2O_2 production with succinate is very sensitive to rotenone, the classic Q-site inhibitor of complex I (Figure 46). RET is strongly stimulated by high mitochondrial membrane potential, which thermodynamically allows electron donation from CII to CI (Quinlan et al. 2013; Murphy 2009).

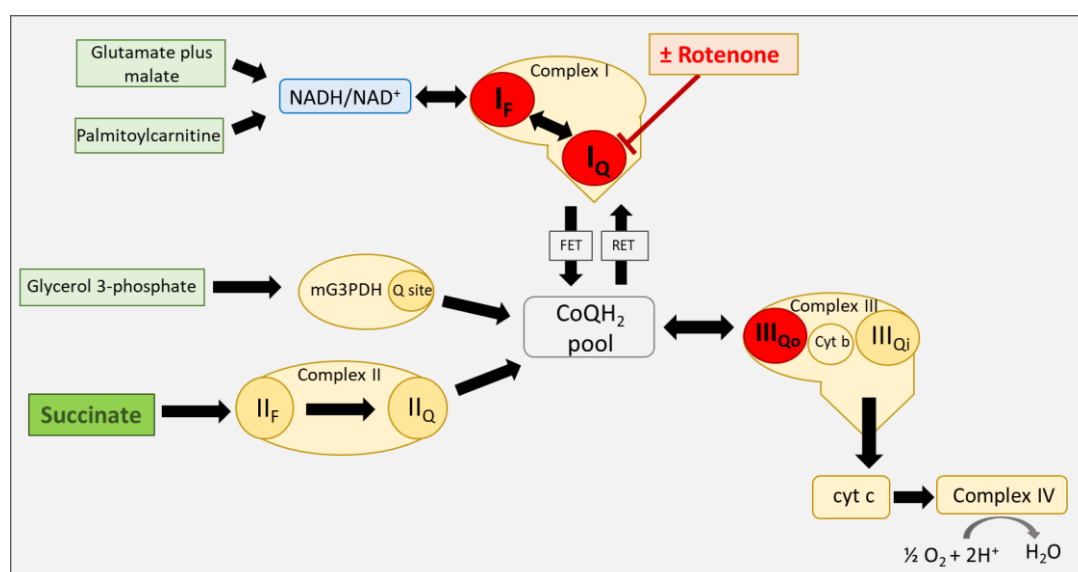


Figure 46. Electron flows through the mitochondrial respiratory complexes and sites of ROS production during oxidation of different substrates. Observed sites of ROS production (red dots) during succinate oxidation are shown. FET: forward electron transfer; RET: reverse electron transfer.

With succinate as single substrate (when superoxide is primarily from I_Q) S3QEL-2 reduced H_2O_2 production rates by an average of 16%. When the I_Q production was eliminated by rotenone, the S3QEL-2 induced reduction of H_2O_2 was 43%. (Orr et al. 2015). Therefore, S3QEL-2 suppressed H_2O_2 production when it was mainly produced by site III_{Qo} . In isolated rat skeletal muscle mitochondria the S3QEL-2 IC_{50} value against site III_{Qo} superoxide/ H_2O_2 production was 1.7 μM (Orr et al. 2015).

S3QELs inhibitors suppressed hydrogen peroxide release in seven different cell lines coming from three different species (human, mouse and rat) and from seven different tissues. 0.1 and 1 μM S3QEL1.2 decreased H_2O_2 release in A-549 (human lung epithelial), N27a (rat dopaminergic neural cells), AML12 (mouse liver) and BJ-1 (human foreskin fibroblasts) cells as well as 1 and $\sim 8 \mu M$ S3QEL1.2 lowered H_2O_2 release in HeLa (human cervix epithelial), U-2OS (human bone epithelial cells) and H9c2 (rat heart myoblasts) cells in a dose independent manner. However the exposition time to the inhibitor was not specified in the publication (Fang et al. 2020).

In contrast to the published studies, 2.5 nM AA, 2.5 nM Myx and 12 μ M S3QEL-2 had no impact on H₂O₂ production rates in PC-3 cells (Figure 34). Besides the unchanged H₂O₂ production rates, also the glycolytic enzymes activities, the lactate dehydrogenase isoenzyme pattern and the composition of the glycolytic enzyme complex were not changed by none of the three inhibitors although the glycolytic conversion rates increased.

The AA and Myx concentration (2.5 nM) tested in our experiments with PC-3 cells were much lower in comparison to those described in literature (range: 0.005 – 17.7 μ M). In contrast, the S3QEL-2 concentration (12 μ M) was in the concentration range which was tested by Orr et al., (0.1 – 30 μ M).

A possible explanation for the different results concerning the H₂O₂ production in AA, Myx and S3QEL-2-treated PC-3 cells compared to the published literature could be due to the different measurement methods. The published extracellular and intracellular H₂O₂ measurements have been performed using Amplex Red reagent and 2',7'-dichlorofluorescein respectively and detected by microplate readers as well as by FACStar flow cytometers (Park et al. 2007a; Dröse and Brandt 2008; Orr et al. 2015; Han et al. 2008). In addition mitochondrial ROS were measured using MitoSox Red reagent and detected by FACSalibus (Li et al. 2014a).

In contrast, in PC-3 cells the H₂O₂ production rates were measured using the O2k-FluoRespirometer from Oroboros Instruments which requires trypsinized cells for measurement. It can not be excluded that the trypzination interrupted the effect that had set in during the 96-hours incubation. Therefore, it may be that the H₂O₂ measured does not reflect the effect of the long-time treatment.

A clear dependency of H₂O₂ production on O₂ pressure is described in literature (Stepanova and Galkin 2020). Komlodi et al. showed that upon decreasing the O₂ concentration the rate of H₂O₂ formation was reduced as compared to the normoxic (21% O₂) H₂O₂ production in the LEAK but not in the OXPHOS state. In addition, after re-oxygenation, the rate of H₂O₂ generation increased again. Therefore, the discrepancy between our results concerning the impact of AA, Myx and S3QEL-2 on H₂O₂ production and the results published in literature could be due to the lower and more physiological O₂ pressures (30 – 60 μ M) that we used while performing the measurements with the O2k-Fluorespirometer.

To summarize, our results show that the inhibition of mitochondrial complex III by targeting either the CIII Qi or the Qo site may have potential for cancer therapy. Yeh et al. suggested in 2013 to combine AA with gefitinib to combat drug resistance in lung cancer patients since AA was able to suppress the formation of A549 tumor spheroids and downregulate the β -catenin signaling cascade (Yeh et al. 2013).

Table 16. Summary table showing the impact of the mitochondrial CIII inhibitors AA, Myx and S3QEL-2 on PC-3 cell metabolism at 21% and 1.5% O₂.

	Antimycin A (vs Et-OH control)		Myxothiazol (vs DMSO control)		S3QEL-2 (vs DMSO control)		
	21% O ₂	1.5% O ₂	21% O ₂	1.5% O ₂	21% O ₂	1.5% O ₂	
Metabolic conversion rates	Glucose consumption	↑	=	↑	↑	↑	↑
	Lactate production	↑	↑	↑	↑	↑	=
	Pyruvate production	=	=	↓	↓	=	↓
	Alanine production	↑	↑	=	↑	↑	=
	Serine consumption	=	=	↑	↑	=	=
	Glutamate production	↑	↑	↑	↑	=	↑
Enzymes	Glutamine consumption	=	=	↓	=	=	=
	LDH, GOT, MDH isoenzymes	=	Not measured	=	Not measured	=	Not measured
Oroboros	O ₂ consumption	↓	Not measured	↓	Not measured	↓	Not measured
	H ₂ O ₂ production	=	Not measured	=	Not measured	=	Not measured

7 Conclusions

Targeting of both mG3PDH and CIII induced a dose dependent inhibition of PC-3 cell proliferation.

Our experiments revealed that the nutrient composition of the cultivation medium and the oxygen pressure may have an influence on the inhibitory effect of mG3PDH and complex III inhibitors on cell proliferation.

Inhibition of cell proliferation by the mG3PDH inhibitor iGP-1 and RH02211 was weakened by supplementation of extracellular pyruvate in the cultivation medium whereas the oxygen pressure did not have any impact. Extracellular pyruvate had a severe impact on the metabolism of PC-3 cells since they shifted from pyruvate production when cultivated in pyruvate starved conditions to pyruvate consumption when cultivated in pyruvate supplemented medium. The pyruvate concentration in the blood is around 0.1 mM, therefore low pyruvate concentrations in the cultivation medium better simulate the physiological conditions.

Inhibition of cell proliferation by CIII inhibition was weakened by hypoxia when Q_i site was inhibited (AA). In the case of CIII Q_o site inhibition (Myx and S3QEL-2) hypoxia did not have any impact. Low oxygen pressure better simulates the oxygen concentrations of solid tumors.

Measurement of the metabolic conversion rates revealed a shift to glycolysis with all 5 inhibitors (iGP-1, RH02211 in pyruvate starved medium, AA, Myx and S3QEL-2).

For none of the five inhibitors the increase of glycolysis was linked with changes in the tetramer : dimer ration of M2-PK or the isoenzyme pattern of lactate dehydrogenase.

Measurement of glutamine and glutamate conversion rates points to an inhibition of glutaminolysis in AA and Myx treated PC-3 cells in presence of 21% and 1.5% O_2 while in S3QEL-2 treated cells glutaminolysis was impaired only at 1.5% O_2 . In the case of the published mG3PDH inhibitors, RH02211 inhibited glutaminolysis at both low and high pyruvate cultivation conditions while iGP-1 seemed to activate glutaminolysis.

In pyruvate starved RH02211 cells the increase in glycerol 3-P and decrease of DHAP concentrations together with the increase in H_2O_2 production and the increase in oxygen consumption rather indicate an activation of mG3PDH which is in contrast to the first description of the inhibitor by Singh in 2014. In the experiments of Singh PC-3 cells were cultivated in presence of extracellular pyruvate. When we cultivated PC-3 cells in pyruvate supplemented medium DHAP levels dropped which is in accordance to Singh and point to an inhibition of mG3PDH. As already assumed by Singh in 2014 besides targeting mG3PDH other modes of actions of RH02211 can not be excluded. In future experiments it will be interesting to characterize the impact of RH02211 on proliferation and metabolism of cells with low mG3PDH activity.

8 Abbreviations

AA	Antimycin A
AC	Aconitase
ADP	Adenosine diphosphate
ALDO	Aldolase
ALT	Alanine-Aminotransferase
ATP	Adenosine triphosphate
AUC	Area under the curve
cG3PDH	Cytosolic glycerol 3-phosphate dehydrogenase
CIII	Mitochondrial complex III
CoQ	Coenzyme Q
Cyt	Cytochrome
DHAP	Dihydroxyacetone phosphate
EDTA-Na ₄	Ethylene Diamine Tetra acetic Acid Tetra sodium
EN	Enolase
FAD ⁺	Flavin adenine dinucleotide (oxidized)
FADH	Flavin adenine dinucleotide (reduced)
FBP	Fructose 2,6-bisphosphate
G6PDH	Glucose 6-phosphate dehydrogenase
GAPDH	Glyceraldehyde 3-phosphate dehydrogenase
GDP	Guanosine diphosphate
GLDH	Glutamate dehydrogenase
GLS	Glutaminase
Glut-1	Glucose transporter 1
GOT	Glutamate oxaloacetate transaminase
GPI	Glucose 6-phosphate isomerase
GPT	Glutamate pyruvate transaminase
GTP	Guanosine triphosphate
HIF-1	Hypoxia inducible factor 1
HK	Hexokinase
HK	Hexokinase
HRE	Hypoxia-responsive-elements
LDH	Lactate dehydrogenase
MDH	Malate dehydrogenase
MDH	Malate dehydrogenase
mG3PDH	Mitochondrial glycerol 3-phosphate dehydrogenase
Myx	Myxothiazol
NAD ⁺	Nicotinamide adenine dinucleotide (oxidized)
NADH	Nicotinamide adenine dinucleotide (reduced)

NADP ⁺	Nicotinamide adenine dinucleotide phosphate (oxidized)
NADPH	Nicotinamide adenine dinucleotide phosphate (reduced)
OAA	Oxaloacetate
PEP	Phosphoenolpyruvate
PFK	Phosphofructokinase
PGK	Phosphoglycerate kinase
PGM	Phosphoglycerate mutase
PHD	Pyruvate dehydrogenase
PHD	Prolyl hydroxylases
PK	Pyruvate kinase
Q	Semiquinone
Q ^{·-}	Semiquinone radical
QH ₂	Quinol
ROS	Reactive oxygen species
SOD	Superoxide dismutase
TDP	Thymidine 5'-diphosphate trisodium salt
TIM	Triose phosphate isomerase
TRA	Triethanolamine hydrochloride
Ub	Ubiquitin
VEGF	Vascular endothelial growth factor
VHL	Von Hippel-Lindau tumor suppressor protein
α -KG	α -ketoglutarate
3-PG	3-phosphoglycerate
2/3-PG	2-phosphoglycerate plus 3-phosphoglycerate
1,3-BPG	1,3-biphosphoglycerate

9 List of tables

Table 1. List of enzymatic reactions used to determine the metabolites concentrations	26
Table 2. Composition of the solutions used for the IEF.....	28
Table 3. List of enzymatic reactions used to measure enzyme activities.	29
Table 4. IC ₅₀ and IC ₉₀ values of RH02211 in PC-3 cells depending upon oxygen pressure and pyruvate concentrations in the medium.....	41
Table 5. Impact of extracellular pyruvate and RH02211 (16 μM) on the isoenzyme equipment of lactate dehydrogenase (LDH), malate dehydrogenase (MDH) and glutamate oxaloacetate transaminase (GOT) as measured by free flow isoelectric focusing.....	47
Table 6. Isoelectric points (IEP) of glycolytic enzymes in pyruvate starved cells as determined by free flow isoelectric focusing.....	49
Table 7. Impact of 7 μM RH02211 on intracellular metabolic intermediates in pyruvate starved and pyruvate supplemented PC-3 cells cultivated at 21% O ₂	54
Table 8. IC ₅₀ (A) and IC ₉₅ (B) values of Antimycin A, Myxothiazol and S3QEL-2 at 21% and 1.5% O ₂	55
Table 9. Impact of 1.5% O ₂ on the Vmax activities of the glycolytic enzymes.....	63
Table 10. Impact of 1.5% O ₂ on the isoenzyme equipment of lactate dehydrogenase (LDH), malate dehydrogenase (MDH) and glutamate oxaloacetate transaminase (GOT) measured by isoelectric focusing.....	63
Table 11. Impact of Antimycin A on the isoenzyme equipment of lactate dehydrogenase (LDH), malate dehydrogenase (MDH) and glutamate oxaloacetate transaminase (GOT) as measured by free flow isoelectric focusing.	64
Table 12. Impact of Myxothiazol on the isoenzyme equipment of lactate dehydrogenase (LDH), malate dehydrogenase (MDH) and glutamate oxaloacetate transaminase (GOT) as measured by free flow isoelectric focusing.	64
Table 13. Impact of S3QEL-2 on the isoenzyme equipment of lactate dehydrogenase (LDH), malate dehydrogenase (MDH) and glutamate oxaloacetate transaminase (GOT) as measured by free flow isoelectric focusing.....	64
Table 14. Summary tables showing the impact of the mG3PDH inhibitors on the metabolic conversion rates of PC-3 cells cultivated in the presence of 0.015 mM pyruvate and 21% O ₂	86
Table 16. Summary table showing the impact of extracellular pyruvate (2 mM) on the metabolism of control PC-3 cells as well as on RH02211-inhibited PC-3 cells cultivated at 21% O ₂	87
Table 17. Summary table showing the impact of the mitochondrial CIII inhibitors AA, Myx and S3QEL-2 on PC-3 cell metabolism at 21% and 1.5% O ₂	99

10 List of figures

Figure 1. Schematic representation of glycolysis.....	6
Figure 2. Role of pyruvate kinase isoenzyme type M2 (M2-PK) in glycolysis.....	8
Figure 3. Schematic representation of glutaminolysis.....	11
Figure 4. Metabolic scheme of glycolysis with the metabolic reactions involved in the regeneration of cytosolic NAD ⁺ : lactate dehydrogenase (LDH), glycerol phosphate shuttle and malate-aspartate shuttle.....	12
Figure 5. The OXPHOS system consisting of CI, CII, CIII, CIV and the ATP synthase (CV)..	14
Figure 6. Mitochondrial respiratory chain with a representative scheme of the CIII with the Q-cycle.....	16
Figure 7. Mitochondrial complex III as source of ROS and target of the inhibitors Antimycin A, Myxothiazol and S3QEL-2.....	18
Figure 8. Mitochondrial glycerol 3-phosphate dehydrogenase as source of ROS and target of the inhibitors iGP-1 and RH02211.....	20
Figure 9. Schematic representation of the oxygen-dependent regulation of the hypoxia inducible factor 1 (HIF-1).....	22
Figure 10. Cell cultivation scheme.....	25
Figure 11. Design of the flux experiments.....	25
Figure 12. Representative traces of PC-3 cells using the O2k-FluoRespirometer.....	35
Figure 13. Inhibition of PC-3 cell proliferation by iGP-1.....	39
Figure 14. Cell density dependencies of the metabolic turnover rates in mock-treated control and iGP-1 inhibited PC-3 cells using the example of glutamine, pyruvate and lactate.....	40
Figure 15. Metabolic conversion rates measured in the cultivation supernatants of mock-treated control and iGP-1-treated PC-3 cells.....	40
Figure 16. Impact of 0.015 mM and 2 mM pyruvate on PC-3 cell proliferation at 21% O ₂ (A) and 1.5% O ₂ (B).....	42
Figure 17. Inhibition of PC-3 cell proliferation by iGP-1 in the presence of 2 mM pyruvate.....	42
Figure 18. Reversibility of RH02211 induced inhibition of cell proliferation.....	43
Figure 19. Dose dependent impact of RH02211 on the glycolytic and glutaminolytic conversion rates in pyruvate starved PC-3 cells cultivated at 21% O ₂	44
Figure 20. Metabolic flux rates of PC-3 cells depending upon the pyruvate concentration in the medium.....	45
Figure 21. Impact of 7 μM RH02211 on the glycolytic and glutaminolytic conversion rates in PC-3 cells depending upon the presence or absence of pyruvate in the medium.....	46
Figure 22. Glycolytic enzyme complex of pyruvate starved PC-3 cells treated with 0.008% DMSO.....	48
Figure 23. Impact of RH02211 on the tetramer : dimer ratio of M2PK.....	49
Figure 24. Impact of 16 μM RH02211 on O ₂ consumption in pyruvate starved PC-3 cells cultivated at 21% O ₂	51
Figure 25. Impact of 16 μM RH02211 on O ₂ consumption in pyruvate supplemented PC-3 cells cultivated at 21% O ₂	52
Figure 26. Impact of 16 μM RH02211 on H ₂ O ₂ production in pyruvate-starved PC-3 cells cultivated at 21% O ₂	52
Figure 27. Impact of 16 μM RH02211 on H ₂ O ₂ production in pyruvate supplemented PC-3 cells cultivated at 21% O ₂	53
Figure 28. Reversibility of AA induced inhibition of PC-3 cell proliferation.....	56

Figure 29. Reversibility of Myx induced inhibition of PC-3 cell proliferation.	57
Figure 30. Impact of Antimycin A on the glycolytic and glutaminolytic conversion rates in PC-3 cells cultivated at 21% and 1.5% O ₂	59
Figure 31. Impact of Myxothiazol on the glycolytic and glutaminolytic conversion rates in PC-3 cells cultivated at 21% and 1.5% O ₂	60
Figure 32. Impact of S3QEL-2 on the glycolytic and glutaminolytic conversion rates in PC-3 cells cultivated at 21% and 1.5% O ₂	61
Figure 33. Comparison of the glycolytic enzyme complex of PC-3 cells at 21% O ₂ (A) and 1.5% O ₂ (B).	62
Figure 34. Impact of CIII inhibitors on H ₂ O ₂ production in PC-3 cells cultivated on presence of 21% O ₂	65
Figure 35. Comparison of the impact of AA, Myx and S3QEL-2 IC ₅₀ concentrations on ROUTINE and OXPHOS respiration.	67
Figure 36. Impact of S3QEL-2 on O ₂ consumption in PC-3 cells cultivated at 21% O ₂	68
Figure 37. O ₂ concentration and O ₂ flow per cell of control and S3QEL-2 treated PC-3 cells measured by high-resolution respirometry.	68
Figure 38. Impact of 2 mM pyruvate on the glycolytic and glutaminolytic conversion rates in PC-3 cells.	75
Figure 39. Metabolic schemes of the impact of RH02211 on the glycolytic and glutaminolytic conversion rates in pyruvate starved PC-3 cells.	79
Figure 40. Impact of 7 μM RH02211 on the glycolytic and glutaminolytic conversion rates in PC-3 cells depending upon the pyruvate concentration in the medium.	81
Figure 41. Impact of 300 μM iGP-1 on the glycolytic and glutaminolytic conversion rates in PC-3 cells.	82
Figure 42. Impact of RH02211 on mG3PDH activity and on the glycerol 3-P shuttle in pyruvate starved and pyruvate supplemented PC-3 cells.	85
Figure 43. Impact of the IC ₅₀ concentrations of Antimycin A at both 21% and 1.5% O ₂ on the glycolytic and glutaminolytic conversion rates in PC-3 cells.	93
Figure 44. Impact of the IC ₅₀ concentrations of Myxothiazol at both 21% and 1.5% O ₂ on the glycolytic and glutaminolytic conversion rates in PC-3 cells.	94
Figure 45. Impact of the IC ₅₀ concentrations of S3QEL-2 at both 21% and 1.5% O ₂ on the glycolytic and glutaminolytic conversion rates in PC-3 cells.	95
Figure 46. Electron flows through the mitochondrial respiratory complexes and sites of ROS production during oxidation of different substrates.	97

References

- Abusalamah, Hazar; Reel, Jessica M.; Lupfer, Christopher R. (2020): Pyruvate affects inflammatory responses of macrophages during influenza A virus infection. In *Virus research* 286, p. 198088. DOI: 10.1016/j.virusres.2020.198088.
- Altman, Brian J.; Stine, Zachary E.; Dang, Chi V. (2016): From Krebs to clinic: glutamine metabolism to cancer therapy. In *Nature reviews. Cancer* 16 (10), pp. 619–634. DOI: 10.1038/nrc.2016.71.
- Anastasiou, Dimitrios; Poulgiannis, George; Asara, John M.; Boxer, Matthew B.; Jiang, Jian-kang; Shen, Min et al. (2011): Inhibition of pyruvate kinase M2 by reactive oxygen species contributes to cellular antioxidant responses. In *Science (New York, N.Y.)* 334 (6060), pp. 1278–1283. DOI: 10.1126/science.1211485.
- Ansell, R.; Granath, K.; Hohmann, S.; Thevelein, J. M.; Adler, L. (1997): The two isoenzymes for yeast NAD⁺-dependent glycerol 3-phosphate dehydrogenase encoded by GPD1 and GPD2 have distinct roles in osmoadaptation and redox regulation. In *The EMBO journal* 16 (9), pp. 2179–2187. DOI: 10.1093/emboj/16.9.2179.
- Babich, H.; Liebling, E. J.; Burger, R. F.; Zuckerbraun, H. L.; Schuck, A. G. (2009): Choice of DMEM, formulated with or without pyruvate, plays an important role in assessing the in vitro cytotoxicity of oxidants and prooxidant nutraceuticals. In *In vitro cellular & developmental biology. Animal* 45 (5-6), pp. 226–233. DOI: 10.1007/s11626-008-9168-z.
- Becker, W. F.; Jagow, G. von; Anke, T.; Steglich, W. (1981): Oudemansin, strobilurin A, strobilurin B and myxothiazol: new inhibitors of the bc 1 segment of the respiratory chain with an E- β -methoxyacrylate system as common structural element. In *FEBS Letters* 132 (2), pp. 329–333. DOI: 10.1016/0014-5793(81)81190-8.
- Bénit, Paule; Lebon, Sophie; Rustin, Pierre (2009): Respiratory-chain diseases related to complex III deficiency. In *Biochimica et biophysica acta* 1793 (1), pp. 181–185. DOI: 10.1016/j.bbamcr.2008.06.004.
- Bereiter-Hahn, J.; Regen, M.; Nüch, Angela; Woiteneck, P. (1998): Dependence of Energy Metabolism on the Density of Cells in Culture. In *Cell Structure and Function* 23 (2), pp. 85–93. DOI: 10.1247/csf.23.85.
- Bergmeyer, Hans Ulrich (1974): Methoden der enzymatischen Analyse. Weinheim/Bergstr.: Verlag Chemie.
- Boitier, Eric; Merad-Boudia, Mansouria; Guguen-Guillouzo, Christiane; Defer, Nicole; Ceballos-Picot, Irène; Leroux, Jean-Paul; Marsac, Cécile (1995): Impairment of the Mitochondrial Respiratory Chain Activity in Diethylnitrosamine-induced Rat Hepatomas: Possible Involvement of Oxygen Free Radicals. In *Cancer Research* 55 (14), p. 3028.
- Borsi, Enrica; Terragna, Carolina; Brioli, Annamaria; Tacchetti, Paola; Martello, Marina; Cavo, Michele (2014): Therapeutic targeting of hypoxia and hypoxia-inducible factor 1 alpha in multiple myeloma. In *Translational research : the journal of laboratory and clinical medicine* 165. DOI: 10.1016/j.trsl.2014.12.001.
- Brand, Martin D. (2010): The sites and topology of mitochondrial superoxide production. In *Experimental gerontology* 45 (7-8), pp. 466–472. DOI: 10.1016/j.exger.2010.01.003.

- Brunelle, Joslyn K.; Bell, Eric L.; Quesada, Nancy M.; Vercauteren, Kristel; Tiranti, Valeria; Zeviani, Massimo et al. (2005): Oxygen sensing requires mitochondrial ROS but not oxidative phosphorylation. In *Cell metabolism* 1 (6), pp. 409–414. DOI: 10.1016/j.cmet.2005.05.002.
- Bunn, H. F.; Poyton, R. O. (1996): Oxygen sensing and molecular adaptation to hypoxia. In *Physiological Reviews* 76 (3), pp. 839–885. DOI: 10.1152/physrev.1996.76.3.839.
- Burgaud, Caroline; Clifton, Michael J.; Sanchez, Victor (1992): The relative importance of transport phenomena in recycling isoelectric focusing. In *ELECTROPHORESIS* 13 (1), pp. 128–135. DOI: 10.1002/elps.1150130127.
- Cai, Hongshi; Li, Jiabin; Zhang, Yadong; Liao, Yan; Zhu, Yue; Wang, Cheng; Hou, Jinsong (2019): LDHA Promotes Oral Squamous Cell Carcinoma Progression Through Facilitating Glycolysis and Epithelial-Mesenchymal Transition. In *Frontiers in oncology* 9, p. 1446. DOI: 10.3389/fonc.2019.01446.
- Carmeliet, P.; Dor, Y.; Herbert, J. M.; Fukumura, D.; Brusselmans, K.; Dewerchin, M. et al. (1998): Role of HIF-1 α in hypoxia-mediated apoptosis, cell proliferation and tumour angiogenesis. In *Nature* 394 (6692), pp. 485–490. DOI: 10.1038/28867.
- Chandel, N. S.; McClintock, D. S.; Feliciano, C. E.; Wood, T. M.; Melendez, J. A.; Rodriguez, A. M.; Schumacker, P. T. (2000): Reactive oxygen species generated at mitochondrial complex III stabilize hypoxia-inducible factor-1 α during hypoxia: a mechanism of O₂ sensing. In *The Journal of biological chemistry* 275 (33), pp. 25130–25138. DOI: 10.1074/jbc.M001914200.
- Chowdhury, Subir K. R.; Gemin, Adam; Singh, Gurmit (2005): High activity of mitochondrial glycerophosphate dehydrogenase and glycerophosphate-dependent ROS production in prostate cancer cell lines. In *Biochemical and biophysical research communications* 333 (4), pp. 1139–1145. DOI: 10.1016/j.bbrc.2005.06.017.
- Cochrane, Charles G. (1991): Cellular injury by oxidants. In *The American Journal of Medicine* 91 (3, Supplement 3), S23-S30. DOI: 10.1016/0002-9343(91)90280-B.
- Cockrell, Chase; Axelrod, David E. (2019): Optimization of Dose Schedules for Chemotherapy of Early Colon Cancer Determined by High-Performance Computer Simulations. In *Cancer informatics* 18, 1176935118822804. DOI: 10.1177/1176935118822804.
- Cole, E. S.; Lepp, C. A.; Holohan, P. D.; Fondy, T. P. (1978): Isolation and characterization of flavin-linked glycerol-3-phosphate dehydrogenase from rabbit skeletal muscle mitochondria and comparison with the enzyme from rabbit brain. In *The Journal of biological chemistry* 253 (21), pp. 7952–7959.
- Conradt, P.; Dittmar, K. E.; Schliephacke, H.; Trowitzsch-Kienast, W. (1989): Myxothiazol: a reversible blocker of the cell cycle. In *The Journal of antibiotics* 42 (7), pp. 1158–1162. DOI: 10.7164/antibiotics.42.1158.
- Cottingham, I. R.; Ragan, C. I. (1980): The reconstitution of L-3-glycerophosphate-cytochrome c oxidoreductase from L-3-glycerophosphate dehydrogenase, ubiquinone-10 and ubiquinol-cytochrome c oxidoreductase. In *Biochem J* 192 (1), pp. 19–31. DOI: 10.1042/bj1920019.
- Curthoys, Norman P.; Watford, Malcolm (1995): Regulation of Glutaminase Activity and Glutamine Metabolism. In *Annual Review of Nutrition* 15 (1), pp. 133–159. DOI: 10.1146/annurev.nu.15.070195.001025.

- Dawson, T. L.; Gores, G. J.; Nieminen, A. L.; Herman, B.; Lemasters, J. J. (1993): Mitochondria as a source of reactive oxygen species during reductive stress in rat hepatocytes. In *The American journal of physiology* 264 (4 Pt 1), C961-7. DOI: 10.1152/ajpcell.1993.264.4.C961.
- DeBerardinis, R. J.; Cheng, T. (2010): Q's next: the diverse functions of glutamine in metabolism, cell biology and cancer. In *Oncogene* 29 (3), pp. 313–324. DOI: 10.1038/onc.2009.358.
- DeBerardinis, Ralph J.; Sayed, Nabil; Ditsworth, Dara; Thompson, Craig B. (2008): Brick by brick: metabolism and tumor cell growth. In *Current Opinion in Genetics & Development* 18 (1), pp. 54–61. DOI: 10.1016/j.gde.2008.02.003.
- Deffieu, Maika; Bhatia-Kiššová, Ingrid; Salin, Bénédicte; Klionsky, Daniel J.; Pinson, Benoît; Manon, Stéphen; Camougrand, Nadine (2013): Increased levels of reduced cytochrome b and mitophagy components are required to trigger nonspecific autophagy following induced mitochondrial dysfunction. In *Journal of cell science* 126 (Pt 2), pp. 415–426. DOI: 10.1242/jcs.103713.
- Dewhirst, Mark W.; Cao, Yiting; Moeller, Benjamin (2008): Cycling hypoxia and free radicals regulate angiogenesis and radiotherapy response. In *Nature reviews. Cancer* 8 (6), pp. 425–437. DOI: 10.1038/nrc2397.
- Di Magno, Laura; Manni, Simona; Di Pastena, Fiorella; Coni, Sonia; Maccone, Alberto; Cairoli, Sara et al. (2020): Phenformin Inhibits Hedgehog-Dependent Tumor Growth through a Complex I-Independent Redox/Corepressor Module. In *Cell reports* 30 (6), 1735-1752.e7. DOI: 10.1016/j.celrep.2020.01.024.
- Di Xia; Esser, Lothar; Tang, Wai-Kwan; Zhou, Fei; Zhou, Yihui; Yu, Linda; Yu, Chang-An (2013): Structural analysis of cytochrome bc1 complexes: implications to the mechanism of function. In *Biochimica et biophysica acta* 1827 (11-12), pp. 1278–1294. DOI: 10.1016/j.bbabi.2012.11.008.
- Diebold, Lauren; Chandel, Navdeep S. (2016): Mitochondrial ROS regulation of proliferating cells. In *Free radical biology & medicine* 100, pp. 86–93. DOI: 10.1016/j.freeradbiomed.2016.04.198.
- Diers, Anne R.; Broniowska, Katarzyna A.; Chang, Ching-Fang; Hogg, Neil (2012): Pyruvate fuels mitochondrial respiration and proliferation of breast cancer cells: effect of monocarboxylate transporter inhibition. In *Biochem J* 444 (3), pp. 561–571. DOI: 10.1042/bj20120294.
- Dröse, Stefan; Brandt, Ulrich (2008): The mechanism of mitochondrial superoxide production by the cytochrome bc1 complex. In *The Journal of biological chemistry* 283 (31), pp. 21649–21654. DOI: 10.1074/jbc.M803236200.
- Eales, K. L.; Hollinshead, K. E. R.; Tennant, D. A. (2016): Hypoxia and metabolic adaptation of cancer cells. In *Oncogenesis* 5, e190. DOI: 10.1038/oncsis.2015.50.
- Eigenbrodt, E.; Kallinowski, F.; Ott, M.; Mazurek, S.; Vaupel, P. (1998): Pyruvate kinase and the interaction of amino acid and carbohydrate metabolism in solid tumors. In *Anticancer research* 18 (5A), pp. 3267–3274.
- Eigenbrodt, E.; Mazurek, S.; Friis, R. R. (1997): Double role of pyruvate kinase type M2 in the regulation of phosphometabolite pools. In Peter Bannasch, Darja Kanduc, Sergio Papa, J. M. Tager (Eds.): *Cell Growth and Oncogenesis*. Basel: Birkhäuser Basel, pp. 15–30.
- Eigenbrodt, E.; Reinacher, M.; Scheefers-Borchel, U.; Scheefers, H.; Friis, R. (1992): Double role for pyruvate kinase type M2 in the expansion of phosphometabolite pools found in tumor cells. In *Critical reviews in oncogenesis* 3 (1-2), pp. 91–115.

- Eigenbrodt, Erich; Glossmann, Hartmut (1980): Glycolysis—one of the keys to cancer? In *Trends in Pharmacological Sciences* 1 (2), pp. 240–245. DOI: 10.1016/0165-6147(80)90009-7.
- Elia, Ilaria; Rossi, Matteo; Stegen, Steve; Broekaert, Dorien; Doglioni, Ginevra; van Gorsel, Marit et al. (2019): Breast cancer cells rely on environmental pyruvate to shape the metastatic niche. In *Nature* 568 (7750), pp. 117–121. DOI: 10.1038/s41586-019-0977-x.
- Epstein, A. C.; Gleadle, J. M.; McNeill, L. A.; Hewitson, K. S.; O'Rourke, J.; Mole, D. R. et al. (2001): *C. elegans* EGL-9 and mammalian homologs define a family of dioxygenases that regulate HIF by prolyl hydroxylation. In *Cell* 107 (1), pp. 43–54. DOI: 10.1016/s0092-8674(01)00507-4.
- Fang, Jingqi; Wong, Hoi-Shan; Brand, Martin D. (2020): Production of superoxide and hydrogen peroxide in the mitochondrial matrix is dominated by site IQ of complex I in diverse cell lines. In *Redox biology* 37, p. 101722. DOI: 10.1016/j.redox.2020.101722.
- Feng, Yangbo; Xiong, Yanlu; Qiao, Tianyun; Li, Xiaofei; Jia, Lintao; Han, Yong (2018): Lactate dehydrogenase A: A key player in carcinogenesis and potential target in cancer therapy. In *Cancer medicine* 7 (12), pp. 6124–6136. DOI: 10.1002/cam4.1820.
- Fernandez-Gomez, F. J.; Pastor, M. D.; Garcia-Martinez, E. M.; Melero-Fernandez de Mera, R.; Gou-Fabregas, M.; Gomez-Lazaro, M. et al. (2006): Pyruvate protects cerebellar granular cells from 6-hydroxydopamine-induced cytotoxicity by activating the Akt signaling pathway and increasing glutathione peroxidase expression. In *Neurobiology of Disease* 24 (2), pp. 296–307. DOI: 10.1016/j.nbd.2006.07.005.
- Formosa, Luke E.; Ryan, Michael T. (2018): Mitochondrial OXPHOS complex assembly lines. In *Nature cell biology* 20 (5), pp. 511–513. DOI: 10.1038/s41556-018-0098-z.
- Garcia, Christine Kim; Goldstein, Joseph L.; Pathak, Ravindra K.; Anderson, Richard G.W.; Brown, Michael S. (1994): Molecular characterization of a membrane transporter for lactate, pyruvate, and other monocarboxylates: Implications for the Cori cycle. In *Cell* 76 (5), pp. 865–873. DOI: 10.1016/0092-8674(94)90361-1.
- Genova, Maria Luisa; Lenaz, Giorgio (2015): The Interplay Between Respiratory Supercomplexes and ROS in Aging. In *Antioxidants & Redox Signaling* 23 (3), pp. 208–238. DOI: 10.1089/ars.2014.6214.
- Ghosh, A. K.; Slovirer, H. A. (1973): Glycolysis and pasteur effect in rat reticulocytes. In *The Journal of biological chemistry* 248 (9), pp. 3035–3040.
- Gnaiger, Erich (2008): Polarographic Oxygen Sensors, the Oxygraph, and High-Resolution Respirometry to Assess Mitochondrial Function. In James A. Dykens, Yvonne Will (Eds.): *Drug-Induced Mitochondrial Dysfunction*. Hoboken, NJ, USA: John Wiley & Sons, Inc, pp. 325–352.
- Gnaiger, Erich (2020): *Mitochondrial Pathways and Respiratory Control*. With assistance of Erich Gnaiger.
- Gu, Xia; Ma, Yuan; Liu, Yi; Wan, Qiang (2021): Measurement of mitochondrial respiration in adherent cells by Seahorse XF96 Cell Mito Stress Test. In *STAR Protocols* 2 (1), p. 100245. DOI: 10.1016/j.xpro.2020.100245.
- Halestrap, A. P.; Price, N. T. (1999): The proton-linked monocarboxylate transporter (MCT) family: structure, function and regulation. In *The Biochemical journal* 343 Pt 2, pp. 281–299. DOI: 10.1042/bj3430281.

- Hamanaka, Robert B.; Chandel, Navdeep S. (2010): Mitochondrial reactive oxygen species regulate cellular signaling and dictate biological outcomes. In *Trends in biochemical sciences* 35 (9), pp. 505–513. DOI: 10.1016/j.tibs.2010.04.002.
- Han, D.; Williams, E.; Cadenas, E. (2001): Mitochondrial respiratory chain-dependent generation of superoxide anion and its release into the intermembrane space. In *Biochem J* 353 (Pt 2), pp. 411–416. DOI: 10.1042/0264-6021:3530411.
- Han, Yong Hwan; Kim, Sun Hee; Kim, Sung Zoo; Park, Woo Hyun (2008): Antimycin A as a mitochondria damage agent induces an S phase arrest of the cell cycle in HeLa cells. In *Life sciences* 83 (9-10), pp. 346–355. DOI: 10.1016/j.lfs.2008.06.023.
- Han, Yong Hwan; Park, Woo Hyun (2009): Growth inhibition in antimycin A treated-lung cancer Calu-6 cells via inducing a G1 phase arrest and apoptosis. In *Lung cancer (Amsterdam, Netherlands)* 65 (2), pp. 150–160. DOI: 10.1016/j.lungcan.2008.11.005.
- Han, Yong Hwan; Park, Woo Hyun (2010): The effects of MAPK inhibitors on antimycin A-treated Calu-6 lung cancer cells in relation to cell growth, reactive oxygen species, and glutathione. In *Molecular and cellular biochemistry* 333 (1-2), pp. 211–219. DOI: 10.1007/s11010-009-0222-2.
- Han, Yong Whan; Kim, Sung Zoo; Kim, Sun Hee; Park, Woo Hyun (2007): The changes of intracellular H₂O₂ are an important factor maintaining mitochondria membrane potential of antimycin A-treated A549 juxtaglomerular cells. In *Biochemical Pharmacology* 73 (6), pp. 863–872. DOI: 10.1016/j.bcp.2006.11.017.
- Han, Yong, Hwan; Kim, Sun, Hee; Kim, Sung, Zoo; Park, Woo, Hyun (2008): Antimycin A as a mitochondrial electron transport inhibitor prevents the growth of human lung cancer A549 cells. In *Oncol Rep* 20 (3), pp. 689–693. DOI: 10.3892/or_00000061.
- Hanse, E. A.; Ruan, C.; Kachman, M.; Wang, D.; Lowman, X. H.; Kelekar, A. (2017): Cytosolic malate dehydrogenase activity helps support glycolysis in actively proliferating cells and cancer. In *Oncogene* 36 (27), pp. 3915–3924. DOI: 10.1038/onc.2017.36.
- Harada, Kikuko; Saheki, Shuichi; Wada, Keishiro; Tanaka, Takehiko (1978): Purification of four pyruvate kinase isozymes of rats by affinity elution chromatography. In *Biochimica et Biophysica Acta (BBA) - Enzymology* 524 (2), pp. 327–339. DOI: 10.1016/0005-2744(78)90169-9.
- Hatefi, Y.; Haavik, A. G.; Griffiths, D. E. (1962): Studies on the electron transfer system. XLI. Reduced coenzyme Q (QH₂)-cytochrome c reductase. In *The Journal of biological chemistry* 237, pp. 1681–1685.
- Hu, Hongxia; Takano, Naoharu; Xiang, Lisha; Gilkes, Daniele M.; Luo, Weibo; Semenza, Gregg L. (2014): Hypoxia-inducible factors enhance glutamate signaling in cancer cells. In *Oncotarget* 5 (19), pp. 8853–8868. DOI: 10.18632/oncotarget.2593.
- Hussain, Rashid; Shaikat, Zeeshan; Khan, Mahwish; Saint, Robert; Gregory, Stephen L. (2017): Phosphoenolpyruvate Carboxykinase Maintains Glycolysis-driven Growth in Drosophila Tumors. In *Scientific reports* 7 (1), p. 11531. DOI: 10.1038/s41598-017-11613-2.
- Iqbal, Mohd Askandar; Siddiqui, Farid Ahmad; Gupta, Vibhor; Chattopadhyay, Shilpi; Gopinath, Prakasam; Kumar, Bhupender et al. (2013): Insulin enhances metabolic capacities of cancer cells by dual regulation of glycolytic enzyme pyruvate kinase M2. In *Molecular cancer* 12, p. 72. DOI: 10.1186/1476-4598-12-72.

- Janssens, D.; Delaive, E.; Houbion, A.; Eliaers, F.; Remacle, J.; Michiels, C. (2000): Effect of venotropic drugs on the respiratory activity of isolated mitochondria and in endothelial cells. In *Br J Pharmacol* 130 (7), pp. 1513–1524. DOI: 10.1038/sj.bjp.0703461.
- Jeong, Jae Ick; Lee, Young Woo; Kim, Yong Keun (2003): Chemical hypoxia-induced cell death in human glioma cells: role of reactive oxygen species, ATP depletion, mitochondrial damage and Ca²⁺. In *Neurochemical research* 28 (8), pp. 1201–1211. DOI: 10.1023/a:1024280429036.
- Jezeek, Petr; Hlavatá, Lydie (2005): Mitochondria in homeostasis of reactive oxygen species in cell, tissues, and organism. In *The international journal of biochemistry & cell biology* 37 (12), pp. 2478–2503. DOI: 10.1016/j.biocel.2005.05.013.
- Jorjani, Parisa; Ozturk, Sadettin S. (1999): Effects of cell density and temperature on oxygen consumption rate for different mammalian cell lines. In *Biotechnol. Bioeng.* 64 (3), pp. 349–356. DOI: 10.1002/(SICI)1097-0290(19990805)64:3<349::AID-BIT11>3.0.CO;2-V.
- Jurica, Melissa S.; Mesecar, Andrew; Heath, Patrick J.; Shi, Wuxian; Nowak, Thomas; Stoddard, Barry L. (1998): The allosteric regulation of pyruvate kinase by fructose-1,6-bisphosphate. In *Structure* 6 (2), pp. 195–210. DOI: 10.1016/S0969-2126(98)00021-5.
- Jurin, Richard R.; McCune, Sylvia A. (1985): Effect of cell density on metabolism in isolated rat hepatocytes. In *J. Cell. Physiol.* 123 (3), pp. 442–448.
- Kalaiarasan, Ponnusamy; Subbarao, Naidu; Bamezai, Rameshwar (2014): Molecular simulation of Tyr105 phosphorylated pyruvate kinase M2 to understand its structure and dynamics. In *Journal of molecular modeling* 20, p. 2447. DOI: 10.1007/s00894-014-2447-6.
- Kilbride, Seán M.; Gluchowska, Sonia A.; Telford, Jayne E.; O'Sullivan, Catherine; Davey, Gavin P. (2011): High-level inhibition of mitochondrial complexes III and IV is required to increase glutamate release from the nerve terminal. In *Molecular neurodegeneration* 6 (1), p. 53. DOI: 10.1186/1750-1326-6-53.
- Kladna, Aleksandra; Marchlewicz, Mariola; Piechowska, Teresa; Kruk, Irena; Aboul-Enein, Hassan Y. (2015): Reactivity of pyruvic acid and its derivatives towards reactive oxygen species. In *Luminescence : the journal of biological and chemical luminescence* 30 (7), pp. 1153–1158. DOI: 10.1002/bio.2879.
- Klingenberg, M. (1970): Localization of the glycerol-phosphate dehydrogenase in the outer phase of the mitochondrial inner membrane. In *European journal of biochemistry* 13 (2), pp. 247–252. DOI: 10.1111/j.1432-1033.1970.tb00924.x.
- Komlódi, Tímea; Sobotka, Ondrej; Krumschnabel, Gerhard; Bezuidenhout, Nicole; Hiller, Elisabeth; Doerrier, Carolina; Gnaiger, Erich (2018): Comparison of Mitochondrial Incubation Media for Measurement of Respiration and Hydrogen Peroxide Production. In *Methods in molecular biology (Clifton, N.J.)* 1782, pp. 137–155. DOI: 10.1007/978-1-4939-7831-1_8.
- Krebs, H. A. (1972): The Pasteur effect and the relations between respiration and fermentation. In *Essays in biochemistry* 8, pp. 1–34.
- Krumschnabel, Gerhard; Fontana-Ayoub, Mona; Sumbalova, Zuzana; Heidler, Juliana; Gauper, Kathrin; Fasching, Mario; Gnaiger, Erich (2015): Simultaneous high-resolution measurement of mitochondrial respiration and hydrogen peroxide production. In *Methods in molecular biology (Clifton, N.J.)* 1264, pp. 245–261. DOI: 10.1007/978-1-4939-2257-4_22.

- Le, Anne; Lane, Andrew N.; Hamaker, Max; Bose, Sminu; Gouw, Arvin; Barbi, Joseph et al. (2012): Glucose-independent glutamine metabolism via TCA cycling for proliferation and survival in B cells. In *Cell metabolism* 15 (1), pp. 110–121. DOI: 10.1016/j.cmet.2011.12.009.
- Lenaz, Giorgio; Genova, Maria Luisa (2009): Structure and Organization of Mitochondrial Respiratory Complexes: A New Understanding of an Old Subject. In *Antioxidants & Redox Signaling* 12 (8), pp. 961–1008. DOI: 10.1089/ars.2009.2704.
- Li, Nianyu; Oquendo, Elisa; Capaldi, Roderick A.; Robinson, J. Paul; He, Yudong D.; Hamadeh, Hisham K. et al. (2014a): A systematic assessment of mitochondrial function identified novel signatures for drug-induced mitochondrial disruption in cells. In *Toxicological sciences: an official journal of the Society of Toxicology* 142 (1), pp. 261–273. DOI: 10.1093/toxsci/kfu176.
- Li, Qi; Liu, Xue; Yin, Yu; Zheng, Ji-Tai; Jiang, Cheng-Fei; Wang, Jing et al. (2014b): Insulin regulates glucose consumption and lactate production through reactive oxygen species and pyruvate kinase M2. In *Oxidative medicine and cellular longevity* 2014, p. 504953. DOI: 10.1155/2014/504953.
- Li, S. S.; Fitch, W. M.; Pan, Y. C.; Sharief, F. S. (1983): Evolutionary relationships of vertebrate lactate dehydrogenase isozymes A4 (muscle), B4 (heart), and C4 (testis). In *The Journal of biological chemistry* 258 (11), pp. 7029–7032.
- Long, Lee Hua; Halliwell, Barry (2009): Artefacts in cell culture: pyruvate as a scavenger of hydrogen peroxide generated by ascorbate or epigallocatechin gallate in cell culture media. In *Biochemical and biophysical research communications* 388 (4), pp. 700–704. DOI: 10.1016/j.bbrc.2009.08.069.
- Luo, Weibo; Hu, Hongxia; Chang, Ryan; Zhong, Jun; Knabel, Matthew; O'Meally, Robert et al. (2011): Pyruvate kinase M2 is a PHD3-stimulated coactivator for hypoxia-inducible factor 1. In *Cell* 145 (5), pp. 732–744. DOI: 10.1016/j.cell.2011.03.054.
- Ma, Rui; Wu, Yinsheng; Zhai, Yansheng; Hu, Bicheng; Ma, Wei; Yang, Wenqiang et al. (2019): Exogenous pyruvate represses histone gene expression and inhibits cancer cell proliferation via the NAMPT–NAD⁺–SIRT1 pathway. In *Nucleic Acids Res* 47 (21), pp. 11132–11150. DOI: 10.1093/nar/gkz864.
- Makowska, Agnieszka; Zablocki, Krzysztof; Duszyński, Jerzy (2000): The role of mitochondria in the regulation of calcium influx into Jurkat cells. In *European journal of biochemistry* 267 (3), pp. 877–884. DOI: 10.1046/j.1432-1327.2000.01066.x.
- Markert, C. L.; Shaklee, J. B.; Whitt, G. S. (1975): Evolution of a gene. Multiple genes for LDH isozymes provide a model of the evolution of gene structure, function and regulation. In *Science (New York, N.Y.)* 189 (4197), pp. 102–114. DOI: 10.1126/science.1138367.
- Mary C. McKenna; Helle S. Waagepetersen; Arne Schousboe; Ursula Sonnewald (2006): Neuronal and astrocytic shuttle mechanisms for cytosolic-mitochondrial transfer of reducing equivalents: Current evidence and pharmacological tools. In *Biochemical Pharmacology* 71 (4), pp. 399–407. DOI: 10.1016/j.bcp.2005.10.011.
- Matés, José M.; Di Paola, Floriana J.; Campos-Sandoval, José A.; Mazurek, Sybille; Márquez, Javier (2020): Therapeutic targeting of glutaminolysis as an essential strategy to combat cancer. In *Seminars in cell & developmental biology* 98, pp. 34–43. DOI: 10.1016/j.semcdb.2019.05.012.
- Mathioudakis, D.; Engel, J.; Welters, I. D.; Dehne, M. G.; Matejec, R.; Harbach, H. et al. (2011): Pyruvate: immunonutritional effects on neutrophil intracellular amino or alpha-keto acid profiles

- and reactive oxygen species production. In *Amino acids* 40 (4), pp. 1077–1090. DOI: 10.1007/s00726-010-0731-z.
- Maxwell, P. H.; Wiesener, M. S.; Chang, G. W.; Clifford, S. C.; Vaux, E. C.; Cockman, M. E. et al. (1999): The tumour suppressor protein VHL targets hypoxia-inducible factors for oxygen-dependent proteolysis. In *Nature* 399 (6733), pp. 271–275. DOI: 10.1038/20459.
- Mazurek, S.; Eigenbrodt, E.; Failing, K.; Steinberg, P. (1999): Alterations in the glycolytic and glutaminolytic pathways after malignant transformation of rat liver oval cells. In *J. Cell. Physiol.* 181 (1), pp. 136–146. DOI: 10.1002/(SICI)1097-4652(199910)181:1<136::AID-JCP14>3.0.CO;2-T.
- Mazurek, S.; Grimm, H.; Boschek, C. B.; Vaupel, P.; Eigenbrodt, E. (2002): Pyruvate kinase type M2: a crossroad in the tumor metabolome. In *Br J Nutr* 87 (S1), S23. DOI: 10.1079/BJN2001454.
- Mazurek, S.; Hugo, F.; Failing, K.; Eigenbrodt, E. (1996): Studies on associations of glycolytic and glutaminolytic enzymes in MCF-7 cells: Role of P36. In *J. Cell. Physiol.* 167 (2), pp. 238–250. DOI: 10.1002/(SICI)1097-4652(199605)167:2<238::AID-JCP7>3.0.CO;2-Q.
- Mazurek, S.; Michel, A.; Eigenbrodt, E. (1997): Effect of extracellular AMP on cell proliferation and metabolism of breast cancer cell lines with high and low glycolytic rates. In *The Journal of biological chemistry* 272 (8), pp. 4941–4952. DOI: 10.1074/jbc.272.8.4941.
- Mazurek, S.; Zwerschke, W.; Jansen-Dürr, P.; Eigenbrodt, E. (2001): Effects of the human papilloma virus HPV-16 E7 oncoprotein on glycolysis and glutaminolysis: role of pyruvate kinase type M2 and the glycolytic-enzyme complex. In *The Biochemical journal* 356 (Pt 1), pp. 247–256. DOI: 10.1042/0264-6021:3560247.
- Mazurek, Sybille (2011): Pyruvate kinase type M2: a key regulator of the metabolic budget system in tumor cells. In *The international journal of biochemistry & cell biology* 43 (7), pp. 969–980. DOI: 10.1016/j.biocel.2010.02.005.
- Mazurek, Sybille; Boschek, C. Bruce; Hugo, Ferdinand; Eigenbrodt, Erich (2005): Pyruvate kinase type M2 and its role in tumor growth and spreading. In *Seminars in Cancer Biology* 15 (4), pp. 300–308. DOI: 10.1016/j.semcancer.2005.04.009.
- McKeown, S. R. (2014): Defining normoxia, physoxia and hypoxia in tumours—implications for treatment response. In *The British Journal of Radiology* 87 (1035), p. 20130676. DOI: 10.1259/bjr.20130676.
- Meléndez-Rodríguez, Florinda; Urrutia, Andrés A.; Lorendeau, Doriane; Rinaldi, Gianmarco; Roche, Olga; Böggürcü-Seidel, Nuray et al. (2019): HIF1 α Suppresses Tumor Cell Proliferation through Inhibition of Aspartate Biosynthesis. In *Cell reports* 26 (9), 2257–2265.e4. DOI: 10.1016/j.celrep.2019.01.106.
- Metallo, Christian M.; Gameiro, Paulo A.; Bell, Eric L.; Mattaini, Katherine R.; Yang, Juanjuan; Hiller, Karsten et al. (2012): Reductive glutamine metabolism by IDH1 mediates lipogenesis under hypoxia. In *Nature* 481 (7381), pp. 380–384. DOI: 10.1038/nature10602.
- Metallo, Christian M.; Vander Heiden, Matthew G. (2013): Understanding metabolic regulation and its influence on cell physiology. In *Molecular cell* 49 (3), pp. 388–398. DOI: 10.1016/j.molcel.2013.01.018.
- Mitchell, Alice Rose; Yuan, Meng; Morgan, Hugh P.; McNae, Iain W.; Blackburn, Elizabeth A.; Le Bihan, Thierry et al. (2018): Redox regulation of pyruvate kinase M2 by cysteine oxidation and S-nitrosation. In *The Biochemical journal* 475 (20), pp. 3275–3291. DOI: 10.1042/BCJ20180556.

- Mitchell, P. (1976): Possible molecular mechanisms of the protonmotive function of cytochrome systems. In *Journal of theoretical biology* 62 (2), pp. 327–367. DOI: 10.1016/0022-5193(76)90124-7.
- Mitchell, Peter (1961): Coupling of Phosphorylation to Electron and Hydrogen Transfer by a Chemi-Osmotic type of Mechanism. In *Nature* 191 (4784), pp. 144–148. DOI: 10.1038/191144a0.
- Miwa, Satomi; St-Pierre, Julie; Partridge, Linda; Brand, Martin D. (2003): Superoxide and hydrogen peroxide production by *Drosophila* mitochondria. In *Free Radical Biology and Medicine* 35 (8), pp. 938–948. DOI: 10.1016/S0891-5849(03)00464-7.
- Mohd Askandar Iqbal; Farid Ahmad Siddiqui; Vibhor Gupta; Shilpi Chattopadhyay; Prakasam Gopinath; Bhupender Kumar et al.: Insulin enhances metabolic capacities of cancer cells by dual regulation of glycolytic enzyme pyruvate kinase M2.
- Mráček, Tomáš; Drahot, Zdeněk; Houštek, Josef (2013): The function and the role of the mitochondrial glycerol-3-phosphate dehydrogenase in mammalian tissues. In *Biochimica et Biophysica Acta (BBA) - Bioenergetics* 1827 (3), pp. 401–410. DOI: 10.1016/j.bbabi.2012.11.014.
- Mráček, Tomáš; Holzerová, Eliška; Drahot, Zdeněk; Kovářová, Nikola; Vrbacký, Marek; Ješina, Pavel; Houštek, Josef (2014): ROS generation and multiple forms of mammalian mitochondrial glycerol-3-phosphate dehydrogenase. In *Biochimica et Biophysica Acta (BBA) - Bioenergetics* 1837 (1), pp. 98–111. DOI: 10.1016/j.bbabi.2013.08.007.
- Mullarky, Edouard; Cantley, Lewis C. (2015): Diverting Glycolysis to Combat Oxidative Stress. In Kazuwa Nakao, Nagahiro Minato, Shinji Uemoto (Eds.): *Innovative Medicine: Basic Research and Development*. Tokyo, pp. 3–23.
- Mullen, Andrew R.; Wheaton, William W.; Jin, Eunsook S.; Chen, Pei-Hsuan; Sullivan, Lucas B.; Cheng, Tzuling et al. (2011): Reductive carboxylation supports growth in tumour cells with defective mitochondria. In *Nature* 481 (7381), pp. 385–388. DOI: 10.1038/nature10642.
- Muller, Florian L.; Liu, Yuhong; van Remmen, Holly (2004): Complex III releases superoxide to both sides of the inner mitochondrial membrane. In *The Journal of biological chemistry* 279 (47), pp. 49064–49073. DOI: 10.1074/jbc.M407715200.
- Muller, Florian L.; Roberts, Arthur G.; Bowman, Michael K.; Kramer, David M. (2003): Architecture of the Qo site of the cytochrome bc1 complex probed by superoxide production. In *Biochemistry* 42 (21), pp. 6493–6499. DOI: 10.1021/bi0342160.
- Murphy, Michael P. (2009): How mitochondria produce reactive oxygen species. In *Biochem J* 417 (1), pp. 1–13. DOI: 10.1042/BJ20081386.
- Nagy, E.; Rigby, W. F. (1995): Glyceraldehyde-3-phosphate dehydrogenase selectively binds AU-rich RNA in the NAD(+)-binding region (Rossmann fold). In *The Journal of biological chemistry* 270 (6), pp. 2755–2763. DOI: 10.1074/jbc.270.6.2755.
- Nakayama, K.; Okamoto, F.; Harada, Y. (1956): Antimycin A: isolation from a new *Streptomyces* and activity against rice plant blast fungi. In *The Journal of antibiotics* 9 (2), pp. 63–66.
- Nath, K. A.; Enright, H.; Nutter, L.; Fischereder, M.; Zou, J. N.; Hebbel, R. P. (1994): Effect of pyruvate on oxidant injury to isolated and cellular DNA. In *Kidney international* 45 (1), pp. 166–176. DOI: 10.1038/ki.1994.20.
- Noguchi, T.; Inoue, H.; Tanaka, T. (1986): The M1- and M2-type isozymes of rat pyruvate kinase are produced from the same gene by alternative RNA splicing. In *Journal of Biological Chemistry* 261 (29), pp. 13807–13812.

- Orr, Adam L.; Ashok, Deepthi; Sarantos, Melissa R.; Ng, Ryan; Shi, Tong; Gerencser, Akos A. et al. (2014): Novel inhibitors of mitochondrial sn-glycerol 3-phosphate dehydrogenase. In *PloS one* 9 (2), e89938. DOI: 10.1371/journal.pone.0089938.
- Orr, Adam L.; Quinlan, Casey L.; Perevoshchikova, Irina V.; Brand, Martin D. (2012): A refined analysis of superoxide production by mitochondrial sn-glycerol 3-phosphate dehydrogenase. In *The Journal of biological chemistry* 287 (51), pp. 42921–42935. DOI: 10.1074/jbc.M112.397828.
- Orr, Adam L.; Vargas, Leonardo; Turk, Carolina N.; Baaten, Janine E.; Matzen, Jason T.; Dardov, Victoria J. et al. (2015): Suppressors of superoxide production from mitochondrial complex III. In *Nature chemical biology* 11 (11), pp. 834–836. DOI: 10.1038/nchembio.1910.
- Park, Sang-Youel; Billiar, Timothy R.; Seol, Dai-Wu (2002): Hypoxia inhibition of apoptosis induced by tumor necrosis factor-related apoptosis-inducing ligand (TRAIL). In *Biochemical and biophysical research communications* 291 (1), pp. 150–153. DOI: 10.1006/bbrc.2002.6421.
- Park, Woo Hyun; Han, Yong Whan; Kim, Sun Hee; Kim, Sung Zoo (2007a): An ROS generator, antimycin A, inhibits the growth of HeLa cells via apoptosis. In *Journal of cellular biochemistry* 102 (1), pp. 98–109. DOI: 10.1002/jcb.21280.
- Park, Woo Hyun; You, Bo Ra (2016): Antimycin A induces death of the human pulmonary fibroblast cells via ROS increase and GSH depletion. In *International journal of oncology* 48 (2), pp. 813–820. DOI: 10.3892/ijo.2015.3276.
- Park, Woo-Hyun; Han, Yong-Whan; Kim, Sang-Wook; Kim, Sun-Hee; Cho, Kyung-Woo; Kim, Sung-Zoo (2007b): Antimycin A induces apoptosis in As4.1 juxtglomerular cells. In *Cancer Letters* 251 (1), pp. 68–77. DOI: 10.1016/j.canlet.2006.11.002.
- Potter, Pamela E.; Detwiler, Paul; Thorne, Beverley; Moskal, Joseph R. (1991): Diphenylhydantoin attenuates hypoxia-induced release of [3H]glutamate from rat hippocampal slices. In *Brain Research* 558 (1), pp. 127–130. DOI: 10.1016/0006-8993(91)90728-E.
- Prakasam, Gopinath; Iqbal, Mohammad Askandar; Bamezai, Rameshwar N. K.; Mazurek, Sybille (2018): Posttranslational Modifications of Pyruvate Kinase M2: Tweaks that Benefit Cancer. In *Frontiers in oncology* 8, p. 22. DOI: 10.3389/fonc.2018.00022.
- Quinlan, Casey L.; Perevoshchikova, Irina V.; Hey-Mogensen, Martin; Orr, Adam L.; Brand, Martin D. (2013): Sites of reactive oxygen species generation by mitochondria oxidizing different substrates. In *Redox biology* 1, pp. 304–312. DOI: 10.1016/j.redox.2013.04.005.
- Ramos-Ibeas, Priscila; Barandalla, Maria; Colleoni, Silvia; Lazzari, Giovanna (2017): Pyruvate antioxidant roles in human fibroblasts and embryonic stem cells. In *Molecular and cellular biochemistry* 429 (1-2), pp. 137–150. DOI: 10.1007/s11010-017-2942-z.
- Salceda, Susana; Caro, Jaime (1997): Hypoxia-inducible Factor 1 α (HIF-1 α) Protein Is Rapidly Degraded by the Ubiquitin-Proteasome System under Normoxic Conditions. In *The Journal of biological chemistry* 272 (36), pp. 22642–22647. DOI: 10.1074/jbc.272.36.22642.
- Sand, T.; Condie, R.; Rosenberg, A. (1977): Metabolic crowding effect in suspension of cultured lymphocytes. In *Blood* 50 (2), pp. 337–346.
- SAS® Institute Inc. (2013): Base SAS® 9.4 Procedures Guide: Statistical Procedures. 2nd edition. Cary, NC, USA: Statistical Analysis System Institute Inc.

- Sazanov, Leonid A. (2015): A giant molecular proton pump: structure and mechanism of respiratory complex I. In *Nature reviews. Molecular cell biology* 16 (6), pp. 375–388. DOI: 10.1038/nrm3997.
- Schmidt, G.; Gross, J.; Necas, E.; Neuwirt, J. (1977): Changes of erythrocyte criteria of the guinea pig under hypoxia. In *Acta biologica et medica Germanica* 36 (2), pp. 205–211.
- Semenza, G. L. (2010a): Defining the role of hypoxia-inducible factor 1 in cancer biology and therapeutics. In *Oncogene* 29 (5), pp. 625–634. DOI: 10.1038/onc.2009.441.
- Semenza, G. L.; Jiang, B. H.; Leung, S. W.; Passantino, R.; Concordet, J. P.; Maire, P.; Giallongo, A. (1996): Hypoxia response elements in the aldolase A, enolase 1, and lactate dehydrogenase A gene promoters contain essential binding sites for hypoxia-inducible factor 1. In *The Journal of biological chemistry* 271 (51), pp. 32529–32537. DOI: 10.1074/jbc.271.51.32529.
- Semenza, G. L.; Wang, G. L. (1992): A nuclear factor induced by hypoxia via de novo protein synthesis binds to the human erythropoietin gene enhancer at a site required for transcriptional activation. In *Molecular and Cellular Biology* 12 (12), p. 5447. DOI: 10.1128/MCB.12.12.5447.
- Semenza, Gregg L. (2003): Targeting HIF-1 for cancer therapy. In *Nature reviews. Cancer* 3 (10), pp. 721–732. DOI: 10.1038/nrc1187.
- Semenza, Gregg L. (2010b): HIF-1: upstream and downstream of cancer metabolism. In *Current Opinion in Genetics & Development* 20 (1), pp. 51–56. DOI: 10.1016/j.gde.2009.10.009.
- Sena, Laura A.; Chandel, Navdeep S. (2012): Physiological roles of mitochondrial reactive oxygen species. In *Molecular cell* 48 (2), pp. 158–167. DOI: 10.1016/j.molcel.2012.09.025.
- Simon, M.; Spahr, P.-F.; Dainous, F. (1989): The proteins associated with the soluble form of p36, the main target of the src oncogene product in chicken fibroblasts, are glycolytic enzymes. In *Biochemistry and Cell Biology* 67 (10), pp. 740–748. DOI: 10.1139/o89-111.
- Singh, Gurmit (2014): Mitochondrial FAD-linked Glycerol-3-phosphate Dehydrogenase: A Target for Cancer Therapeutics. In *Pharmaceuticals (Basel, Switzerland)* 7 (2), pp. 192–206. DOI: 10.3390/ph7020192.
- Starkov, Anatoly A.; Fiskum, Gary (2001): Myxothiazol Induces H₂O₂ Production from Mitochondrial Respiratory Chain. In *Biochemical and biophysical research communications* 281 (3), pp. 645–650. DOI: 10.1006/bbrc.2001.4409.
- Stekhoven, F.; Gorissen, Marnix; Flik, Gert (2008): The isoelectric point, a key to understanding a variety of biochemical problems: A minireview. In *Fish physiology and biochemistry* 34, pp. 1–8. DOI: 10.1007/s10695-007-9145-6.
- Stepanova, Anna; Galkin, Alexander (2020): Chapter 11 - Measurement of mitochondrial H₂O₂ production under varying O₂ tensions. In Liza A. Pon, Eric A. Schon (Eds.): *Methods in Cell Biology : Mitochondria*, 3rd Edition, vol. 155: Academic Press, pp. 273–293. Available online at <http://www.sciencedirect.com/science/article/pii/S0091679X19301633>.
- Sullivan, S. G.; Stern, A. (1983): Effects of physiologic concentrations of lactate, pyruvate and ascorbate on glucose metabolism in unstressed and oxidatively stressed human red blood cells. In *Biochemical Pharmacology* 32 (19), pp. 2891–2902. DOI: 10.1016/0006-2952(83)90393-3.
- Sumida, K. D.E.N.; Frisch, Frank; Donovan, Casey M. (1995): Training suppresses hepatic lactate dehydrogenase activity without altering the isoenzyme profile. In *Medicine & Science in Sports &*

- Exercise* 27 (4). Available online at https://journals.lww.com/acsm-msse/Fulltext/1995/04000/Training_suppresses_hepatic_lactate_dehydrogenase.7.aspx.
- Szalárdy, Levente; Zádori, Dénes; Klivényi, Péter; Toldi, József; Vécsei, László (2015): Electron Transport Disturbances and Neurodegeneration: From Albert Szent-Györgyi's Concept (Szeged) till Novel Approaches to Boost Mitochondrial Bioenergetics. In *Oxidative medicine and cellular longevity* 2015, p. 498401. DOI: 10.1155/2015/498401.
- Szatrowski, T. P.; Nathan, C. F. (1991): Production of large amounts of hydrogen peroxide by human tumor cells. In *Cancer Research* 51 (3), pp. 794–798.
- Takakusagi, Yoichi; Matsumoto, Shingo; Saito, Keita; Matsuo, Masayuki; Kishimoto, Shun; Wojtkowiak, Jonathan W. et al. (2014): Pyruvate induces transient tumor hypoxia by enhancing mitochondrial oxygen consumption and potentiates the anti-tumor effect of a hypoxia-activated prodrug TH-302. In *PloS one* 9 (9), e107995-e107995. DOI: 10.1371/journal.pone.0107995.
- Taylor, R. W.; Birch-Machin, M. A.; Bartlett, K.; Lowerson, S. A.; Turnbull, D. M. (1994): The control of mitochondrial oxidations by complex III in rat muscle and liver mitochondria. Implications for our understanding of mitochondrial cytopathies in man. In *Journal of Biological Chemistry* 269 (5), pp. 3523–3528. DOI: 10.1016/S0021-9258(17)41894-1.
- Thierbach, G.; Reichenbach, H. (1981): Myxothiazol, a new antibiotic interfering with respiration. In *Antimicrob Agents Chemother* 19 (4), pp. 504–507. DOI: 10.1128/aac.19.4.504.
- Thomas, Douglas D.; Liu, Xiaoping; Kantrow, Stephen P.; Lancaster, Jack R. (2001): The biological lifetime of nitric oxide: Implications for the perivascular dynamics of NO and O₂. In *Proceedings of the National Academy of Sciences* 98 (1), p. 355. DOI: 10.1073/pnas.98.1.355.
- Tiefenthaler, Martin; Amberger, Albert; Bacher, Nicole; Hartmann, Bernd L.; Margreiter, Raimund; Kofler, Reinhard; Konwalinka, Günther (2001): Increased lactate production follows loss of mitochondrial membrane potential during apoptosis of human leukaemia cells. In *British Journal of Haematology* 114 (3), pp. 574–580. DOI: 10.1046/j.1365-2141.2001.02988.x.
- Turrens, J. F. (1997): Superoxide production by the mitochondrial respiratory chain. In *Bioscience reports* 17 (1), pp. 3–8. DOI: 10.1023/a:1027374931887.
- Vadlakonda, L; Dash, A; Pasupuleti, M; Anil Kumar, K; Reddanna, P. (2013): Did We Get Pasteur, Warburg, and Crabtree on a Right Note? In *Frontiers in oncology* 3, p. 186. DOI: 10.3389/fonc.2013.00186.
- Wallace, Douglas C.; Fan, Weiwei (2010): Energetics, epigenetics, mitochondrial genetics. In *Mitochondrion* 10 (1), pp. 12–31. DOI: 10.1016/j.mito.2009.09.006.
- Wang, G. L.; Jiang, B. H.; Rue, E. A.; Semenza, G. L. (1995): Hypoxia-inducible factor 1 is a basic-helix-loop-helix-PAS heterodimer regulated by cellular O₂ tension. In *Proceedings of the National Academy of Sciences of the United States of America* 92 (12), pp. 5510–5514. DOI: 10.1073/pnas.92.12.5510.
- Wang, G. L.; Semenza, G. L. (1995): Purification and characterization of hypoxia-inducible factor 1. In *The Journal of biological chemistry* 270 (3), pp. 1230–1237. DOI: 10.1074/jbc.270.3.1230.
- Wang, Xiaofei; Perez, Evelyn; Liu, Ran; Yan, Liang-Jun; Mallet, Robert T.; Yang, Shao-Hua (2007): Pyruvate protects mitochondria from oxidative stress in human neuroblastoma SK-N-SH cells. In *Brain Research* 1132, pp. 1–9. DOI: 10.1016/j.brainres.2006.11.032.

- Warburg, Otto (1956): On the Origin of Cancer Cells. In *Science (New York, N.Y.)* 123 (3191), p. 309. DOI: 10.1126/science.123.3191.309.
- Ward, Patrick S.; Patel, Jay; Wise, David R.; Abdel-Wahab, Omar; Bennett, Bryson D.; Collier, Hilary A. et al. (2010): The common feature of leukemia-associated IDH1 and IDH2 mutations is a neomorphic enzyme activity converting alpha-ketoglutarate to 2-hydroxyglutarate. In *Cancer cell* 17 (3), pp. 225–234. DOI: 10.1016/j.ccr.2010.01.020.
- Waypa Gregory B.; Chandel Navdeep S.; Schumacker Paul T. (2001): Model for Hypoxic Pulmonary Vasoconstriction Involving Mitochondrial Oxygen Sensing. In *Circulation Research* 88 (12), pp. 1259–1266. DOI: 10.1161/hh1201.091960.
- Wohlpert, Dave; Kirwan, Donald; Gainer, John (1990): Effects of cell density and glucose and glutamine levels on the respiration rates of hybridoma cells. In *Biotechnol. Bioeng.* 36 (6), pp. 630–635. DOI: 10.1002/bit.260360611.
- Wyatt, C. N.; Buckler, K. J. (2004): The effect of mitochondrial inhibitors on membrane currents in isolated neonatal rat carotid body type I cells. In *The Journal of Physiology* 556 (1), pp. 175–191. DOI: 10.1113/jphysiol.2003.058131.
- Xia, D.; Yu, C. A.; Kim, H.; Xia, J. Z.; Kachurin, A. M.; Zhang, L. et al. (1997): Crystal structure of the cytochrome bc1 complex from bovine heart mitochondria. In *Science (New York, N.Y.)* 277 (5322), pp. 60–66. DOI: 10.1126/science.277.5322.60.
- Xia, Sha; Chen, Gan; Wang, Bo; Yin, Yujing; Sun, Zhenwei; Zhao, Jingxiang et al. (2016): Addition of Sodium Pyruvate to Stored Red Blood Cells Attenuates Liver Injury in a Murine Transfusion Model. In *Mediators of inflammation* 2016, p. 3549207. DOI: 10.1155/2016/3549207.
- Yamada, K.; Noguchi, T. (1999): Regulation of pyruvate kinase M gene expression. In *Biochemical and biophysical research communications* 256 (2), pp. 257–262. DOI: 10.1006/bbrc.1999.0228.
- Yeh, Chi-Tai; Su, Chun-Li; Huang, Chi-Ying F.; Lin, Justin Kung-Yi; Lee, Wei-Hwa; Chang, Peter M-H et al. (2013): A preclinical evaluation of antimycin a as a potential antilung cancer stem cell agent. In *Evidence-based complementary and alternative medicine : eCAM* 2013, p. 910451. DOI: 10.1155/2013/910451.
- Yin, Chengqian; He, Dan; Chen, Shuyang; Tan, Xiaoling; Sang, Nianli (2016): Exogenous pyruvate facilitates cancer cell adaptation to hypoxia by serving as an oxygen surrogate. In *Oncotarget* 7 (30), pp. 47494–47510. DOI: 10.18632/oncotarget.10202.
- Young, Tracey A.; Cunningham, Carol C.; Bailey, Shannon M. (2002): Reactive oxygen species production by the mitochondrial respiratory chain in isolated rat hepatocytes and liver mitochondria: studies using myxothiazol. In *Archives of Biochemistry and Biophysics* 405 (1), pp. 65–72. DOI: 10.1016/S0003-9861(02)00338-7.
- Yu, Tzu-Jung; Hsieh, Che-Yu; Tang, Jen-Yang; Lin, Li-Ching; Huang, Hurng-Wern; Wang, Hui-Ru et al. (2020): Antimycin A shows selective antiproliferation to oral cancer cells by oxidative stress-mediated apoptosis and DNA damage. In *Environmental toxicology* 35 (11), pp. 1212–1224. DOI: 10.1002/tox.22986.
- Zanchetta, Luciene M.; Kirk, David; Lyng, Fiona; Walsh, James; Murphy, James E. J. (2010): Cell-density-dependent changes in mitochondrial membrane potential and reactive oxygen species production in human skin cells post sunlight exposure. In *Photodermatology, photoimmunology & photomedicine* 26 (6), pp. 311–317. DOI: 10.1111/j.1600-0781.2010.00551.x.

Zhang, Mingming; Pan, Yida; Tang, Dehua; Dorfman, Robert Gregory; Xu, Lei; Zhou, Qian et al. (2019): Low levels of pyruvate induced by a positive feedback loop protects cholangiocarcinoma cells from apoptosis. In *Cell Commun Signal* 17 (1), p. 23. DOI: 10.1186/s12964-019-0332-8.

Ziółkowska-Suchanek, Iwona (2021): Mimicking Tumor Hypoxia in Non-Small Cell Lung Cancer Employing Three-Dimensional In Vitro Models. In *Cells* 10 (1). DOI: 10.3390/cells10010141.

Zwerschke, W.; Mazurek, S.; Massimi, P.; Banks, L.; Eigenbrodt, E.; Jansen-Dürr, P. (1999): Modulation of type M2 pyruvate kinase activity by the human papillomavirus type 16 E7 oncoprotein. In *Proceedings of the National Academy of Sciences of the United States of America* 96 (4), pp. 1291–1296. DOI: 10.1073/pnas.96.4.1291.

Acknowledgements

Firstly, I would like to thank the European Union's Horizon 2020 research and innovation programme since my Ph.D. was supported by the EU H2020 Marie Curie project TRANSMIT GA 722605.

In addition, I want to express my gratitude to my advisor Prof. Sybille Mazurek for her assistance at every stage of my research project.

Besides my advisor, I would like to thank the rest of my Ph.D. disputation committee: Prof. Martin Diener, Prof. Thomas Linn and Prof. Leoni Kunz-Schughard for their insightful comments and suggestions.

A huge thanks to Prof. Anna Maria Porcelli (TRANSMIT project coordinator) as well as to all professors, management team and researchers involved in the 'TRANSMIT' project, which funded my Ph.D.

Thanks to the several training and dissemination activities organized within the framework of the ITN-TRANSMIT – Marie Skłodowska Curie project I grew in science and I built up a strong scientific network.

I would like to thank all the Oroboros Instrument team, especially Dr. Erich Gnaiger and Dr. Luiza Cardoso for helping me in the respirometry experiments design during my secondment at the Oroboros company, Innsbruck, Austria.

In addition, I want to thank Dr. Christian Frezza and his laboratory team for helping me in the mass spectrometry experiments design as well as for carrying out the measurements in their laboratory at the Medical Research Council Cancer Unit, University of Cambridge, Cambridge, United Kingdom.

My sincere thanks also go to Dr. Klaus Faling, Dr. Kathrin Buttner and Mrs Marion Sparenberg for their support in the statistical analysis of my data.

I would like to express my gratitude to my family: my parents, my sister, my brother-in-law and my niece. Without their understanding and encouragement in the past few years, it would have been impossible for me to complete my Ph.D.

A special thanks to my boyfriend for his unwavering support and belief in me especially during the thesis writing process.

Lastly, I would like to thank all my friends and colleagues for their support all through my studies.

Declaration

I declare that I have completed this dissertation single-handedly without the unauthorized help of a second party and only with the assistance acknowledged therein. I have appropriately acknowledged and referenced all text passages that are derived literally from or are based on the content of published or unpublished work of others, and all information that relates to verbal communications. I have abided by the principles of good scientific conduct laid down in the charter of the Justus Liebig University of Giessen in carrying out the investigations described in the dissertation.

Bologna, February 14th 2022



Ph.D. Candidate: Floriana Jessica Di Paola